ANALYSIS OF THE ROLE OF IRON UPTAKE MECHANISMS AND ADDITION OF IRON-DOPED APATITE NANOPARTICLES IN PHAGE INFECTIONS IN *STAPHYLOCOCCUS AUREUS* AND *MYCOBACTERIUM SMEGMATIS*

by

Linda Christina Rost

A professional paper submitted in partial fulfillment
of the requirements for the degree

of

Master of Science

in

Science Education

MONTANA STATE UNIVERSITY
Bozeman, Montana

July 2018

DEDICATION

I would like to dedicate this to my parents, Dr. William and Emma Mackay. Now that I have children, I can remember that while they were pouring love and validation into my life, they were also pouring knowledge and yearning to learn. Now I can watch them do the same with their grandchildren. Their curiosity and zest for life is contagious. They always had a sincere and genuine desire for not only my sister and I to succeed, but also for every student they encountered and mentored. They instilled in me a profound love of the wonder and discipline of science and the natural world, and I hope to do the same with my children and students. They have accomplished so much in their lifetimes and the extent of their legacy they may never fully realize. Their love and support during this project was unwavering and absolute. I couldn't have done it without them.

ACKNOWLEDGMENTS

The materials for my research were funded by the Bringing Research into the Classroom grant from the National Institutes of Health (Grant code: R25 OD 16533-1) obtained by Dr. Marisa Pedulla and the Clark Fork Watershed Education Program (CFWEP) team at Montana Tech, directed by Rayelynn Brandl. Dr. Jessica Gregory from Montana Tech also provided experimental training and expertise and helped me design my experiments. Dr. John Graves from MSU- Bozeman was my project advisor and reader, and his help was critical along the way. My student Bo Rost was also very helpful in developing procedures for the *Mycobacterium smegmatis* experiments. He also lent an extra hand in the lab and was there for moral support when overcoming obstacles. My husband, Jay Rost, provided support through my struggles and frustrations, watched our kids during my long evenings and weekends at school, and helped troubleshoot and fix equipment as needed.

TABLE OF CONTENTS

TABLE OF CONTENTS - CONTINUED

LIST OF TABLES

LIST OF TABLES - CONTINUED

LIST OF FIGURES

LIST OF FIGURES - CONTINUED

LIST OF FIGURES - CONTINUED

LIST OF EQUATIONS

(1) $r = 10 \cdot (D/L)^{½}$

where D = virion diffusion rate and L = phage latent period.

(2) $7\ Ca(OH)_2 + 3FeCl_3 + 6KH_2PO_4 \xrightarrow{\text{Citric Acid}} Ca_7Fe_3(PO_4)_6(OH)_2 + 6KOH + 12\ H_2O + 9Cl^-$

(3) $y = 236x + 1.13$

where y = plaque counts standardized to control and x = iron concentration

ABSTRACT

Antibiotic resistance has become a significant global public health issue, and phage therapy could serve as an adjuvant to traditional antibiotics. Phages are viruses that kill bacteria and produce more phages. Iron-doped apatite nanoparticles (IDANPs) have been shown to increase phage killing of bacteria. However, the mechanism of JB and Yodasoda infection of bacteria, and mechanism by which IDANPs increase phage infections, is unknown. Based on the iron composition of the IDANP, as well as extensive literature describing *Staphylococcus aureus* having aggressive iron uptake systems, it was hypothesized that IDANPs may affect such systems, and thereby be involved in the subsequent increase of phage-mediated bacterial death. In this work, the relationship between bacterial exposure to iron and subsequent phage infectivity was established, and IDANP effect on plaque size was determined. *S. aureus* cells were grown in various iron treatments, plaque assays were performed. There was a strong, positive relationship between iron treatments and plaque counts. The plaque counts were 29% higher in the 0.0004g/L iron treatment, 34% higher in 0.0008g/L, 60% higher in 0.0016 g/L and 82% higher in 0.0032g/L. When *S. aureus* and *M. smegmatis* cells were treated with IDANPs, plaque sizes were significantly larger, which may indicate increased infection in adjacent cells. Plaque sizes from IDANP-treated cells continued to increase in size as plates were incubated over 24, 48 and 96 hours. Plaque sizes also increased in size in the control cells in some time frames. *S. aureus* cells were also grown in 0.0016g/L iron treatment and treated with IDANPs, and there was a 65% increase in plaque counts. In higher iron treatments, it was difficult to achieve a lawn of cells to perform plaque assays. Cell growth was measured by performing serial dilutions and determining CFU/mL. There was no significant difference between cells grown in M9 minimal media or treated with IDANPs. Cells were also grown in the different iron treatments over three hours, with or without IDANPs. Less growth was observed in high iron treatments, but the differences were not significant. Cell growth was relatively slower in high iron levels in overnight treatments, and the results were significantly different. These data can be used to elucidate the relationship of iron uptake and phage killing, and therefore allow conjectures as to whether or not iron uptake mechanisms may be involved in the IDANP effect. Further research in this field can provide opportunities to develop reliable alternatives to antibiotics to treat bacterial infections.

Keywords: Iron-doped apatite nanoparticles, *Staphylococcus aureus*, *Mycobacterium smegmatis*, JB Phage, Yodasoda Phage, iron uptake mechanism, phage infection mechanism, antibiotic resistance, phage therapy

INTRODUCTION AND BACKGROUND

The rise of antibiotic resistant bacteria, referred to as *superbugs*, has created significant health concerns in many regions of the world, especially developing countries. Every year 480,000 people around the world are infected with multi-drug resistant tuberculosis (TB). The range of pathogens has also grown to include not only bacteria, but also viruses, and eukaryotes such as fungi and parasites (Antimicrobial resistance, 2017).

According to the Centers for Disease Control and Prevention, antibiotics have been used heavily for the past 70 years, and while they do significantly reduce illness and mortality, some pathogens have developed resistance to these treatments. New and better drugs are being developed and tested, but around two million people are infected with resistant bacteria every year in the U.S., and 23,000 die due to the infections (Antibiotic/Antimicrobial resistance, 2017). Research of alternatives to traditional antibiotics is therefore critical, and recent advancements have been made in the field of bacteriophages (phages), which are viruses that infect bacteria. Phage therapy refers to the use of phages to infect and kill pathogenic bacteria. Phage therapy was first introduced in the 1920s (Loc-Carrillo & Abedon, 2011). While some antibiotics are bacteriostatic (stop bacteria from reproducing), obligately lytic phages (those that never show a lysogenic cycle) have been shown to be bactericidal (Carlton, 1999). This is an advantage over traditional antibiotics (Tan & Tatsumura, 2015). Chemicals that stop reproduction of bacteria can lead to resistance mechanisms (Stratton, 2003). However, phages can evolve to counteract the defenses of the bacteria. Additionally, phages can respond to higher numbers of bacteria in hosts because more phages will be produced,

called “auto *dosing”* (Abedon & Thomas-Abedon, 2010). Phages work by injecting their DNA into a host cell, which can lead to the lysogenic cycle, in which the bacteria integrate the phage genome into theirs, or the lytic cycle, in which the cell expresses the virus’s DNA and builds new phages. The cell will eventually lyse and release phages to infect more cells. If the cell is in the lysogenic cycle, it can enter into the lytic cycle under certain conditions, or remain as a lysogen (Bonnain, Breitbart & Buck, 2016).

Phages are host specific and typically infect one or few bacterial strains (Hyman & Abedon, 2010). Therefore, phages are unlikely to significantly affect the normal flora of the host, unlike chemical antibiotics which can have a broad effect on the normal flora and lead to other infections of opportunistic pathogens (Carlton, 1999). In addition, narrow virulence limits the potential for bacteria to become resistant. If they do develop resistance, these mechanisms will be different from the mechanisms that develop during antibiotic resistance because the mechanism of action in the phage is different (Fischbach & Walsh, 2009) and phages may evolve. In antibiotics, bacterial metabolic processes are inhibited, while in lytic phages, the cell is lysed and viruses are released (Kohanski, Dwyer & Collins, 2010). Additionally, phages can be used to treat biofilms by penetrating layers of the film and lysing bacteria (Abedon, 2011).

Other benefits of phage therapy as antimicrobial agents include the use of a single low dose, as well as the potential to transfer phages between patients (Abedon & Thomas-Abedon, 2010; Alisky, Iczkowski, Rapoport & Troitsky, 1998; Capparelli et al, 2010). Phage therapy has other advantages, including a potentially positive acceptance from the public, as a natural alternative to chemical, “synthetic” antibiotics. Phage

therapies also are low cost, especially when purification procedures are optimized, and other methods are used to amplify their effects (Skurnik, Pajunen & Kilijunen, 2007).

Research into adjuvants which enhance phage therapy could further its potential as an antibiotic alternative. Iron-doped apatite nanoparticles (IDANPs), for instance, have been shown to increase the number of bacterial deaths by phage. In this study, the relationship between iron uptake mechanisms and bacterial death by phage was investigated.

Some of this study was completed in Dr. Marisa Pedulla's lab at Montana Tech in Butte, Montana. The focus of her research involves the discovery and description of mycobacteriophages. I became involved in this research through the Bringing Research into the Classroom program via a grant funded by the National Institutes of Health Science Education Partnership Award. This program joined efforts between the Montana Tech Phage Discovery Program and Cfwep.org (Clark Fork Watershed Education Program). Middle school and high school teachers are recruited from across Montana to participate in the project, which brings scientists into the classroom for students to participate in phage discovery. Participating teachers also attend two summer research academies at the Butte campus and complete two online graduate courses.

CONCEPTUAL FRAMEWORK

Nanoparticles (NPs) are defined as having all three dimensions less than 100 nm. NPs are currently being studied for many applications in medicine and industry (Pinto-Alphandary, Andremont & Couvreur, 2000). Studies have shown that NPs have unique antimicrobial properties, particularly with certain pathogenic bacteria. NPs are being used to inhibit or stop bacterial growth while not harming surrounding tissue. Nanosized

carriers have been used to deliver antibiotics to cells which then uptake the particle filled with antibiotic. NPs also exhibit unique characteristics, including a high surface area to volume ratio, as well as other physical and chemical properties associated with a majority of the particles' atoms being placed at the surface of the particle (Hajipour et al., 2012).

Bacteria possess different types of cell walls. Gram positive (+) bacteria contain a thick layer of peptidoglycan external to the cell membrane, while gram negative (-) bacteria contain two phospholipid membranes, with a thinner peptidoglycan layer in between (Coico, 2005). Antibiotics work differently on these two cell wall types, and thus NPs may also interact differently with these types of cells. For example, *Escherichia coli* (-) are more affected by CuO-NPs than gram-positive bacteria such as *Staphylococcus aureus* and *Bacillis subtilis* (Hajipour et.al., 2012).

The mechanism explaining NP microbial toxicity is not well understood, and recent reports have been contradictory. It has been observed that NPs adhere to the cell membrane of bacterial cells (Hajipour et al., 2012). The attachment is caused by an electrostatic interaction, which may affect the integrity or permeability of the cell membrane. It has also been observed that some NPs cause the formation of free radicals by causing oxidative stress, resulting in cell death. Some NPs even exhibit a mutagenic effect on the bacteria, such as TiO_2 and ZnO-NPs.

Several hypotheses have been proposed by Prabhu and Poulose (2012) for the mechanism of action of Ag-NPs antibiotic activity. According to one hypothetical mechanism, Ag-NPs adhere to the bacterial cell wall and enter the cell (Zhao & Stevens, 1998). This results in permeability changes to the cell wall, causing NPs to collect around the resulting pits. Another mechanism proposes that free radicals can also be produced by

Ag-NPs, which can also cause damage to the cell membrane (Danilcauk, Lund, Saldo, Yamada & Michalik, 2006; Kim, et al., 2007). Silver ions could also be released and could interact with cellular enzymes, in their thiol group, and inactivate them (Feng, Wu, Chen, Cui, Kim & Kim, 2008); Matsumara, Yoshikata, Kunisaki & Tsuchido, 2003). Reactive oxygen species formation has also been posited as a mechanism when the silver ions inhibit a respiratory enzyme. Finally, another group of mechanisms involve the action of the Ag-NPs on DNA, or on the sulfur and phosphorus components of cells (Hatchett & Henry, 1996).

Dar, Ingle & Rai (2013) evaluated the enhanced effect that Ag-NPs have when used in conjunction with antibiotics. Findings indicated that Ag-NPs increased the bacteriostatic effects of the antibiotic in *S. aureus*, *Salmonella typhi* and *E.coli*, but not the eukaryotic *Candida albicans*. Another study confirmed this, showing enhanced effects with *S. aureus* and *E. coli* when using Penicillin G-10, Amoxicillin 10, Erythromycin 5, Vancomycin 30, and Clindamycin 2, to a lesser extent (Shahverdi, Fakhimi, Shahverdi & Minaian, 2007). Hwang, Hwang, Choi, Kim & Lee (2012) investigated the mechanism of NP toxicity in bacteria, as well as the synergistic effects of NPs and antibiotics. It was found that the activity of the NPs was influenced by the ATPase inhibition, but not by permeability of the cell membrane. The NPs also produced high levels of hydroxyl radicals, and moreover, when the NPs were used with antibiotics, some produced higher hydroxyl radicals than without the NPs.

Current Iron-doped Nanoparticle Phage Research

Recently, antibiotic resistance has promoted research into alternatives (Wittebole, De Roock & Opal, 2014). Puck & Lee (1954) were among some of the first investigators

to study the mechanism of phage infection. They found one mechanism that involves the splitting of cell proteins by viral amino acid groups in the cell surface, thereby allowing the DNA to penetrate the cell. They measured the leakage of radioactively marked phosphorus and sulfur from the cell into the medium over time and they found that the leakage is not from complete cell lysis of a few cells, but from changes in permeability from many cells. Increasing the concentration of phages did not change the amount of leakage produced. They also found that DNA was not contained in the leakage.

A recent study on the mechanism of infection shows that the T4 phage adsorbs into a specific cell membrane receptor, and penetration of DNA follows (Rakhuba, Kolomiets, Szwajcer Dey & Novik, 2010). At the point of adsorption, there are irreversible changes to the virus and bacterial cell wall. Since then, a wide variety of iron-cell interactions have been characterized, and therefore, it is unlikely that a universal model can be developed for phage infection.

While many biomedical applications of NPs have been investigated, one intriguing application involves a synergism with phages (Nickel, 2010; Nickel, Pedulla & Kasinath, 2010). When a lawn of bacteria is grown that was infected with phages, a clear spot will form, which is known as a plaque. An increase in viral plaques has been observed when phages were allowed to infect bacteria in the presence of specific iron-doped NPs. One study showed that plaque counts were increased with NPs in five different phages: Mycobacteriophages Macho, Second, Bxzl, infecting *Mycobacterium smegmatis* (+) and Coliphages MS2 and T4, infecting *E. coli* (-). These phages included RNA- and DNA- genome phages and had a variety of morphologies, including non-contractile and contractile tails, and an icosahedron structure. On average, IDANPs

increased phage plaques by 11.4%. When a t-test was performed on total plaque counts, there was a significant difference in the treatment with IDANPs compared to the control ($p = 0.002$). The results showed a consistent increase in phage plaque counts, with the contractile tail phages showing a larger increase, compared to non-contractile phages. The tail structure could be investigated further to determine a mechanism. IDANPs accumulate near the ends of the cells, as seen with electron microscopy, and this could be related to the mechanism (Gregory, 2017). Also, the nanoparticles may cause changes to the outer membrane of the cell, making it more susceptible to infection.

In a subsequent study, IDANPs with 30% Fe were investigated to enhance phage infection in staphylococcal bacteria were also tested in vitro (Kasineth, McConnell, Voyich & Pedulla, 2013). Only the 30% Fe IDANPs increased infection rate. These particles were also studied in vivo, to determine how well they could be used to treat skin methicillin-resistant *Staphylococcus aureus* (MRSA) infections in mice. The Fe-doped NPs increased mice recovery by 30% compared to the control. The result of that study indicate IDANPs could therefore possibly be used to enhance the effects of phage infections as an adjuvant to phage therapy (Moody, 2014).

IDANPs added to bacterial hosts prior to phage exposure increased phage infections in some species; however, the mechanism is unknown (Andriolo et al., 2014). When *S. aureus* were pre-exposed to IDANPs prior to phage introduction, bacterial death by phage increased 128%. In the same study, it was determined that the IDANPs that were synthesized at 25 degrees Celsius with 30% Fe and citrate functionalization work best for promoting phage infections. The JB phage used has a Siphoviridae morphology (non-contractile tail) (Figures 1 & 2). JB phage was isolated in the Dr. Jovanka Voyich

lab at Montana State University, by Dr. Tyler Nygaard, from dairy cow hair samples. They used *S. aureus* USA300 to isolate and purify the phage. It can also infect MRSA (Andriolo, et al., 2014).

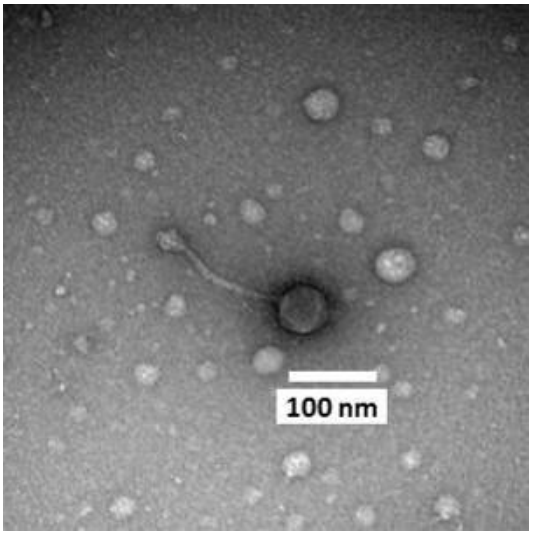

Figure 1. JB phage viewed under TEM. JB phage was determined to have Siphoviridae morphology, with an icosahedral head approximately 75 nm in width, and a long, non-contractile tail 160 nm in length. Reprinted from Doped Apatite Nanoparticles: Characterization and Biomedical Relevance by Jessica Andriolo Gregory, 2017, Doctoral dissertation. Reprinted with permission.

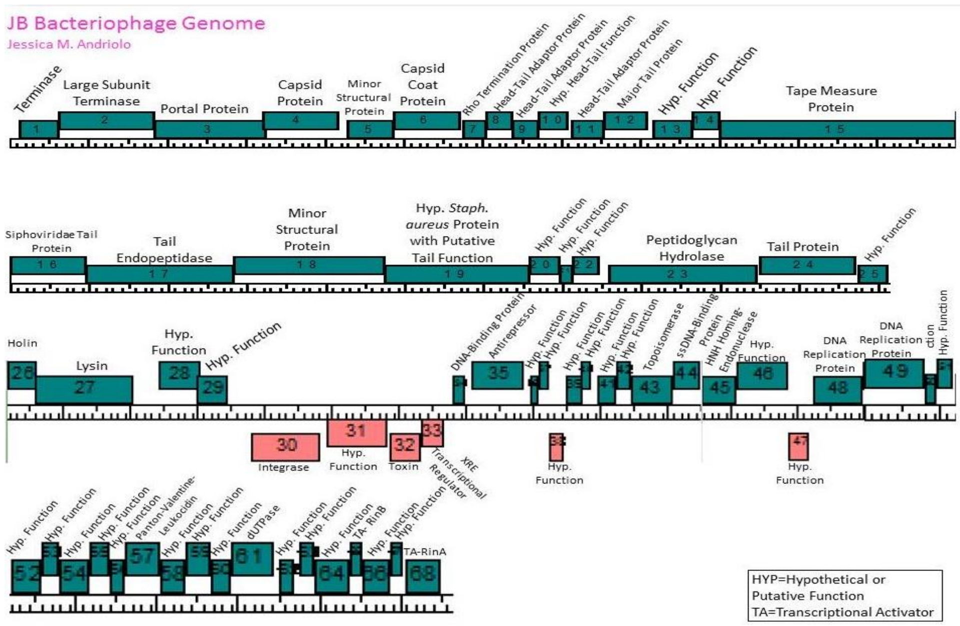

Figure 2. Predicted JB phage genome. The predicted genome contained 68 genes, 42,683 bp, and a GC content of 35.2%. Also discovered during bioinformatics analysis, is a short section of reverse transcribed genes (30-33) which contain integrase and toxin proteins. Such a section must be removed prior to the use of JB phage for therapeutic purposes to prevent any enhanced toxicity of a bacterial host in a eukaryotic organism. Reprinted from Doped Apatite Nanoparticles: Characterization and Biomedical Relevance by Jessica Andriolo Gregory, 2017, Doctoral dissertation. Reprinted with permission.

When NPs interact with a biological environment, a protein corona is formed around the NP, and the composition of the corona could be due to the surface charge of the NP. The protein corona could affect how the NP interacts with the cell. The surface charge of IDANPs was found to be positive (Gregory, 2017), while the surface charge on bacterial cell walls is negative (Corpe, 1970). The charge of some phage tails is positive, while the head is generally negative (Serwer & Hayes, 1982), although the surface charges of JB phage are unknown. A difference in surface charge and the formation of a protein corona could reveal the mechanism of the NPs in increasing phage infections.

The use of IDANPs to enhance virulence of phages appears to be promising, especially in the field of medicine (Andriolo et al., 2016). However, the effects of

IDANPs on eukaryotic organisms and their viruses must also be investigated before introducing them as a possible treatment. Hydroxyapatite, a component of IDANPs, is similar to the compound in bones and teeth, and has been shown to be biocompatible, not eliciting any significant immune response. The host cell *Chlorella variabilis* was used, along with the phage *Paramecium bursaria* chlorella Virus 1 (PBCV-1), to demonstrate the interaction of IDANPs with a eukaryotic host. *S. aureus*, a gram-positive pathogen, was also infected with JB phage and IDANPs. In both cases with these infectious agents, clumping of nanoparticles was observed on cell surfaces. However, in the eukaryotic *C. variabilis* system, there was no statistically significant difference in plaque counts between the IDANP treatment and the control. As found in other studies, the IDANPs did have a marked effect on the infections of the JB phage in *S. aureus* host cells. These results indicate that the use of IDANPs may be safe if used to treat bacterial infections in eukaryotic organisms, as they may be used safely to enhance a phage therapy without increasing mammalian-virus infections.

The micronutrient iron is essential for bacteria, and some have evolved protein structures called siderophores that act as a receptor on the membrane surface to bind iron (Bonnain, Breitbart & Buck 2016). It has been shown that some phages also use the same receptor to infect the cell, providing the possibility that when the cell is uptaking iron, it is more vulnerable to infection. The “Ferrojan Horse Hypothesis” (Figure 4) posits an explanation whereby phage tails have iron ions that provide an advantage in infecting a host cell. The theory states that siderophores strongly attract iron ions, so the iron in the phage tail presumably allows the phage to attach more readily, puncture the cell membrane and infect the host. The newly assembled phages have iron integrated into

their tails from the iron present in the host cell (Figure 3).

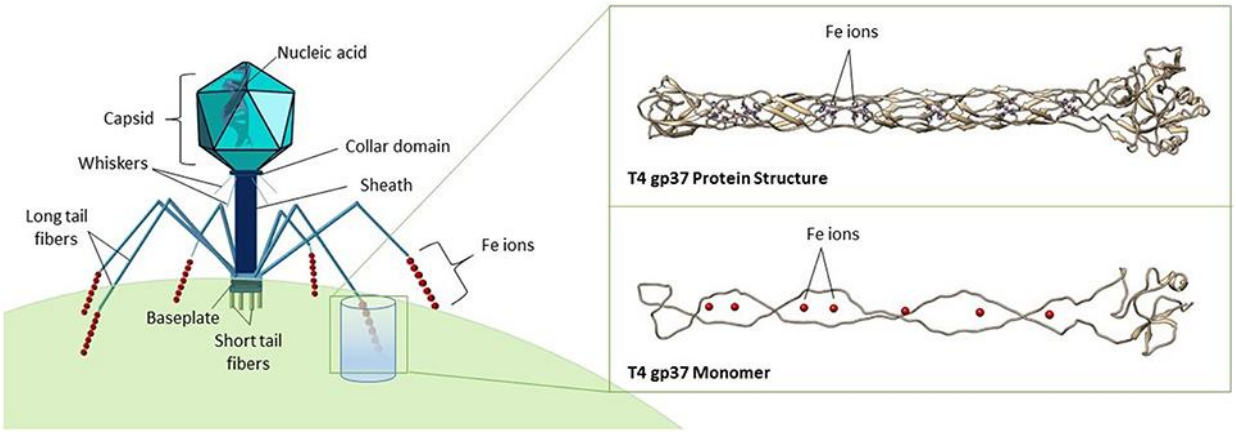

Figure 3. Structure of a typical bacteriophage belonging to the Myoviridae family. The expanded inset shows a model of the gp37 tail fiber protein of phage T4 (PDB ID code 2XGF), visualized in Chimera (Pettersen et al., 2004), and VMD (Humphrey et al., 1996). Seven iron ions (red spheres) are coordinated octahedrally by histidine residues, forming a trimer as shown in the top image, while the bottom image shows a gp37 monomer. Reprinted from The Ferrojan Horse Hypothesis: Iron-Virus Interactions in the Ocean by Chelsea Bonnain, Mya Breitbart and Kristen Buck, 2016, Frontiers in Marine Science, (3). Reprinted with permission.

Iron ions in phage tails have been seen in both the Siphoviridae family (non-contractile tails) in an iron sulfur cluster, and Myoviridae family (contractile tail) with an iron-loaded spike. Non-tailed phages could also possibly adsorb iron into their capsids and utilize some adaptation for increased virulence (Bonnain, Breitbart & Buck, 2016) (Figure 4).

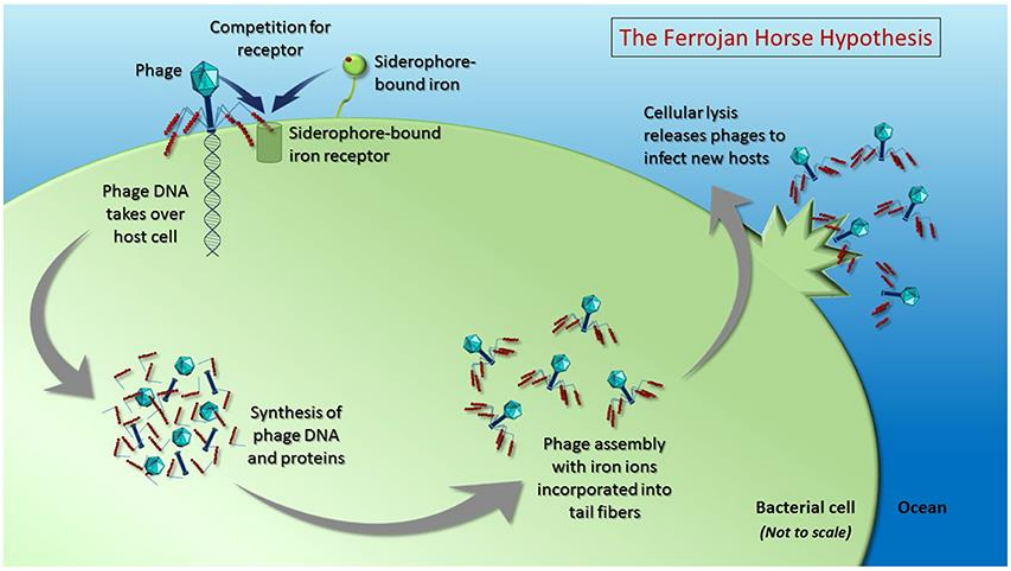

Figure 4. The Ferrojan Horse Hypothesis depicts the use of iron ions (red spheres) within phage tail fibers to compete with siderophore-bound iron for access to the same receptor on the surface of the host cell. Once a phage docks on the cell surface, it can pierce the cell membrane and inject its nucleic acid, which takes over the host cell, instructing the cell to produce phage DNA and proteins. Cellular mechanisms are used to fold the proteins and assemble them into progeny phages, with iron from within the cell incorporated into the tail fibers. Upon cell lysis, new phages are released to infect hosts using the iron that has been pre-packaged within their tail fibers. This proposed recycling of cellular iron during phage production results in a depletion of the amount of iron available for remineralization upon lysis (i.e., via the viral shunt). Figure is not drawn to scale. Reprinted from The Ferrojan Horse Hypothesis: Iron-Virus Interactions in the Ocean by Chelsea Bonnain, Mya Breitbart and Kristen Buck, 2016, Frontiers in Marine Science, (3). Reprinted with permission.

Phage Plaque Counts and Sizes

Plaque assays are experiments where bacteria are infected with phages in a broth culture and grown on a plate, usually with a semisolid agar (Abedon & Yin, 2009). This affords the phages motility. Phages infect the bacteria, which in turn undergo lysis and release more phages. These phages continue to infect more bacteria in the near vicinity, and as the top agar is solidifying, a clear spot in the lawn, or a solid mat of bacteria grown in a petri dish, forms as the bacteria grow over a 24-hour period. Plaque development is characterized by four steps: “(i) the primary adsorption event; (ii) the first

round or first few rounds of viral multiplication; (iii) the enlargement phase; and (iv) the final phase, in which viral replication ceases" (Koch, 1964). These clear areas are called plaques.

Researchers have found many factors that affect plaque counts, size and morphologies. Gallet, Kannoly & Wang (2011) determined how adsorption rate, timing of lysis and phage morphology, influenced plaque formation. First, they found the rate at which the phages were adsorbed positively impacted phage concentration, size and progeny productivity. In other words, if the phages were adsorbed quickly, those three measures would be higher since infection would occur sooner. Further, lysis time had an effect on plaque size. Plaque size peaked for phages that lyse at 50-55 minutes and was lower before and after. However, the opposite was true of burst size and lysis time, which was lowest around 50 minutes of lysis time and higher before and after.

Phage adsorption can occur while the bacteria are still in the liquid broth, or after the semisolid top agar has been added, and even after the agar is solid (Abedon & Yin, 2009). Therefore, the timing of phage infection and the pouring of the top agar are critical, since adsorption rate plays such a large role in plaque size and count. The timing of phage adsorption is directly related to the density of bacterial cells and the adsorption rate constant, which is the rate of one phage adsorbing to one cell. Phage adsorption is inversely related to agar concentration, which delays phage adsorption. A delayed adsorption can cause smaller plaques, and more variation in plaque size (Abedon & Yin, 2009).

Plaque size can also be influenced by phage diffusion, which can be a function of intrinsic properties of the individual phage type (Abedon & Yin, 2009). Phages diffuse,

or move passively, more readily than bacteria in semisolid agar and some phages diffuse better than others. Further, plaque size can be dependent on phage latent period, which is the time span from cell membrane adsorption of the phage to bacterial cell lysis. If the latent period is shorter, the phages spend more time diffusing through the agar and infecting more cells.

Koch (1964) developed a model to characterize the rate of plaque enlargement, *r*.

$$r = 10 \cdot (D/L)^{½} \quad (1)$$

where D = virion diffusion rate and L = phage latent period.

Other authors have developed models with other conditions, including burst size, density of bacterial lawn, even bacterial shape, and other parameters (Abedon & Yin, 2009).

There are many factors that can influence plaque size and count, and both are coveted characteristics of a phage used in phage therapy. An increase in phage size alone may even be as important as an increase in plaque count, in terms of phage virulence (Abedon & Yin, 2009).

Mechanism of Iron Uptake in *S. aureus* Bacteria

S. aureus is a gram-positive coccus shaped bacterium that is non-motile (Kuehnert et al., 2006; Noble, Valkenburg & Wolters, 1967). If it gains access inside the mammalian epithelium, it can cause a large gamut of life-threatening illnesses. *S. aureus* is a leading cause of many conditions, including heart, skin, soft tissue, and hospital acquired infections. Additionally, it is a primary cause of bacterial pneumonia (Hammer & Skaar, 2011). Some strains have also developed resistance to many antibiotics, including Methicillin, yielding Methicillin-resistant *S. aureus* (MRSA), which results in a

serious threat to public health. As part of its pathogenicity, it has evolved complex methods to rob iron from its host. Studies have shown that patients with problems of iron homeostasis have more severe *S. aureus* infections.

Iron metabolism is critical in the survival of bacteria, particularly pathogenic species. It is used for growth and propagation, including its role in reducing a precursor of DNA and oxygen reduction prior to ATP synthesis (Hammer & Skaar, 2011; Neilands, 1995). At minimum, at least 1 μM of iron is needed in the growth medium to maintain reproduction and metabolism of the cell (Neilands, 1995).

Humans respond to pathogenic bacterial infections by limiting iron and using a protein to synthesize a reactive oxygen species that can cause cell death (Ratledge & Dover, 2000). Some bacteria respond by sending out iron chelators "siderophores" (Greek: "iron carriers") to steal iron from their hosts (Neilands, 1995). This response can happen in many bacterial species whenever there is low iron. There are also many bacterial genes that are controlled by the ferric uptake regulator (Fur protein) or equivalent (Ratledge & Dover, 2000). Siderophores can be detected best in iron-limited conditions (Neilands, 1995). In mammals, most of the intracellular and extracellular iron is typically not available because it is bound in proteins called transferrin and lactoferrin (Drabkin, 1951). *S. aureus* uses siderophores to steal the iron from these binding proteins. Once the siderophore is bound to iron, the bacterial cell surface recognizes the siderophore-iron complex. Iron is also found in the heme molecule, a tetrapyrrole ring, and holds 80% of the iron in the host (Skaar, Humayan, Bae, DeBord & Schneewind, 2004). This is the preferred source for *S. aureus* to fulfill its iron requirement (Drabkin, 1951). In vertebrates, four heme molecules are contained in one hemoglobin protein,

which is a major component of an erythrocyte. *S. aureus* lyses erythrocytes using hemolysins to free the iron in the hemoglobin (Torres, Pishchany, Humayan, Schneedwind & Skaar, 2006). In response, the vertebrate produces haptoglobin, which is a protein that binds to free hemoglobin, forming a hemoglobin- haptoglobin complex that is then processed by the liver. However, *S. aureus* is capable of accessing the iron in this complex. If heme is released from the erythrocyte, a hemopexin protein binds to the heme and is processed in the liver (Tolosano & Altruda, 2002). This hemopexin-heme complex is unusable by *S. aureus.*

In iron-limited conditions, *S. aureus* responds by expressing specific proteins. The Fur protein is a regulatory protein that acts as a repressor (Friedman, Stauff, Pishchany, Whitwell, Torres & Skaar, 2006; Torres et al., 2006). It binds to a portion of DNA named the *fur* box, in the presence of iron. In limited iron, Fur is released and a gene is transcribed. Some of the genes that are regulated by Fur include "iron acquisition, iron utilization, iron transport, and transcription regulator" (Zhang, Ma, Zang, Song & Lui, 2011). Another response in iron-limiting conditions is the formation of lactate, produced when the bacteria undergo fermentative metabolism. This lowers the pH, which enables it to access iron from host proteins (Friedman et al., 2006).

S. aureus produce two siderophores, staphyloferrin A and staphyloferrin B, which are regulated by Fur, and thus respond in low iron environments (Hammer & Skaar, 2011). Both are formed via the non-ribosomal peptide synthetase independent pathway. A third siderophore in *S. aureus* has been suggested but not characterized and is named aureochelin. However, mutants without staphyloferrin A or B are unable to grow in iron-depleted media, which shows that the hypothetical aureochelin may not be important

(Courcol, Trivier, Bissinger, Martin & Brown, 1997). The primary method of *S. aureus* to obtain iron from transferrin is via the staphyloferrin A and B, which suggests that *S. aureus* does not have a transferrin receptor.

Staphyloferrin A is composed of D-ornithine linking two molecules of citrate (Konetschny-Rapp, Jung, Meiwes & Zahner, 1990). ABC transporters for siderophores are present on the cell membrane and their genes are located on the chromosome near siderophore genes (Beasley, et al., 2009). One transporter, HtsBC, is required to bring in staphyloferrin A, but also may transport other iron sources. The receptor of staphyloferrin A is HtsA, a lipoprotein. When staphyloferrin A binds, there is a conformational change resulting in ligand entrapment, and this is not likely the place for heme transport.

Staphyloferrin B is also part of the carboxylate family, like staphyloferrin A, and is "composed of L-2,3-diaminopropionic acid, 1,2-diaminoethane and ⟨-ketoglutaric acid" (Hammer & Skaar, 2011, p. 5). There are a series of molecules (staphylococcal *i*ron *r*egulated transporter, *sirABC*) involved in the import of staphyloferrin B (Dale, Sebulksy & Heinrichs, 2004). One, the SirBC, is probably the permease in the membrane, and SirA is the lipoprotein receptor, similar to HtsA in staphyloferrin A. This molecule also experiences a change in conformation to trap the staphyloferrin B (Grigg, Cheung, Heinrichs & Murphy, 2010). These two siderophores may perform different functions in terms of iron acquisition, depending on the host or site of colonization (Hammer & Skaar, 2011).

In order to fuel the import of staphyloferrin A and B, ATP is needed, but the operons for *sirABC* and *htsABC* do not code ATPase (Beasley et al., 2009). Instead, the

*f*erric *h*ydroxymate *u*ptake operon *fhuCBG* does code a putative ATPase, *fhuC*, which is involved in transport.

S. aureus also has the ability to steal iron from other bacteria via hydroxymate siderophores known as xenosiderophores. Similar to the other siderophores, uptake depends on the *fhuCBG* operon, and also to lipoprotein receptors, FhuD1 and FhuD2 are used (Sebulsky, Hothstein, Hunter, Heinrichs, 2000). These receptors undergo less of a shape change compared to the receptors for the staphyloferrins, so this may provide more binding possibilities for a variety of molecules (Sebulsky, Shilton, Speziali & Heinrichs, 2003; Sebulsky, Speziali, Shilton, Edgell & Heinrichs, 2004).

Another mechanism of iron acquisition, depicted in Figure 5, involves the heme molecule itself. A transpeptidase known as Sortase B (SrtB) may be involved in importing heme into the cell and is now called the *i*ron-regulated *s*urface *d*eterminant (Isd) system (Hammer & Skaar, 2011). There are five operons (*isdA, isdB, isdCDEF, srtBisdG, isdH, or fXisdI*), involved in the Isd system and they are all iron-regulated. These code for cell membrane receptors involved in binding heme. Another transpeptidase, Sortase A (SrtA) is also involved and anchors some of these receptors to the cell wall. Heme is passed from receptor to receptor through the cell membrane. Each receptor contains regions called *NEA*r iron *T*ransporter (NEAT) domains, and each receptor binds one heme molecule (Andrade, Ciccarelli, Perez-Iratxeta & Bork, 2002). As mentioned before, *S. aureus* can also use the haptoglobin-hemoglobin complex, and this is accessed by IsdH, which has three NEAT domains (Dryla, Gelbmann, Von Gabain & Nagy, 2003). By doing this, heme is removed from this complex and transferred to the

other receptors (Dryla, Hoffmann, Gelmann, Giefing & Hanner, 2007; Pilpa, Robson, Villareal, Wong, Phillips & Clubb, 2009).

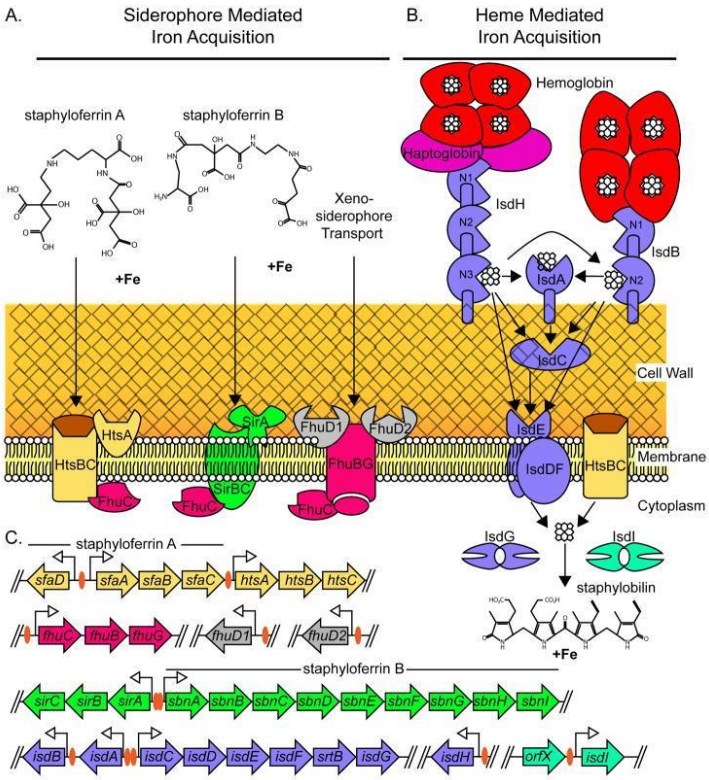

Figure 5. A model of *S. aureus* iron acquisition pathways.

A. *S. aureus* produces two siderophores, staphyloferrin A and staphyloferrin

B. Staphyloferrin A import is mediated by the HtsA lipoprotein and HtsBC permease. The SirA lipoprotein is the receptor for staphyloferrin B and the SirBC permease mediates the translocation of staphyloferrin B across the membrane. *S. aureus* imports xenosiderophores produced by other bacteria through the binding activity of FhuD1 and FhuD2 receptor lipoproteins and the FhuBG permease. The energy needed for siderophore uptake is provided by the FhuC ATPase. B. Heme acquisition is mediated by the Isd system. IsdH binds hemoglobin-haptoglobin and IsdB binds hemoglobin. Heme is passed through the NEAT domains of IsdH (N1-N3) IsdB (N1-N2), IsdA, and IsdC. Heme can also be passed from IsdH or IsdB directly to the IsdE heme-receptor lipoprotein. Heme transport across the membrane occurs through either the IsdDF or HtsBC permeases. Once in the cytoplasm heme is a substrate for the heme-degrading enzymes IsdG and IsdI. *S. aureus* degradation of heme leads to the release of iron and the production of staphylobilin.

C. Genetic loci involved in *S. aureus* iron acquisition pathways. The *sfa* operon encodes the genes required for staphyloferrin A biosynthesis, while the genes within the *sbn* operon encode the staphyloferrin B synthesis genes. Promoter regions containing a consensus *fur* box are indicated with an orange oval. Genes are not drawn

to scale. Reprinted from Molecular mechanisms of *S. aureus* iron acquisition by N.D. Hammer and E.P. Skaar, 2011, *Annual Review of Microbiology, 65,* 129-147. Reprinted with permission.

Mechanism of Iron Uptake in *M. smegmatis* Bacteria

M. smegmatis is a gram-positive bacterium that is related to the pathogens *Mycobacterium tuberculosis* and *Mycobacterium leprae.* It is a common, fast-growing soil bacterium and is considered non-pathogenic (Akinola, Mazandu & Mulder, 2013). It has also been studied as a model for tuberculosis since it has certain similar cellular processes to these pathogenic relatives. Specifically, many of the iron uptake mechanisms are similar in the different species of the *Mycobacterium* genus. *M. smegmatis* colonies have a unique off-white color with a wrinkly, dry appearance when grown on agar. They are easily maintained in 7H9 broth at room temperature.

According to the phagesdb.org website, 13059 phages have been discovered, with 2547 sequenced. One phage, named Yodasoda (Figure 6), was discovered in a compost pile in rural Willard, MT by then sophomore high school student Bo Rost as part of the Bringing Research into the Classroom program through Montana Tech.

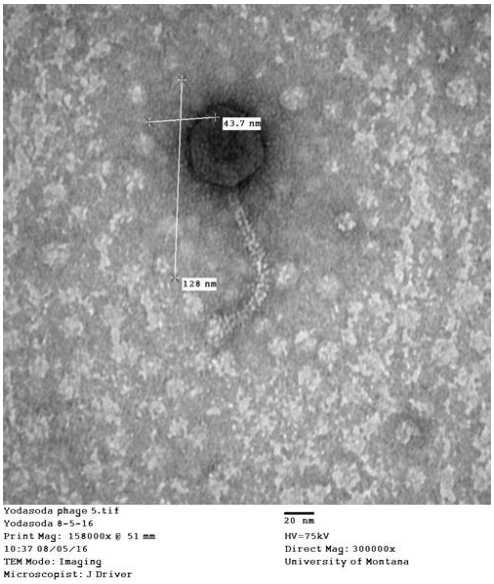

Figure 6. Yodasoda phage viewed under TEM. The bar represents 20 nm.

Gram positive bacteria possess a thick peptidoglycan outer layer, which can make access to nutrients more difficult, while also making antibiotics less effective. Iron is also difficult to access from the environment, even from soil. Furthermore, *Mycobacteria spp.* are in the Actinobacteria class, which have a unique outer membrane that serves as a permeability barrier (Hoffmann, Leis, Niederweis, Plitzko & Engelhardt, 2008; Jones & Niederweis, 2010). To overcome this, *M. smegmatis* produces porins, such as the MspA, which promotes permeability to glucose, phosphate and amino acids (Jones & Niederweis, 2010). It is the most common protein produced, and it was found that the absence of the protein reduced growth.

M. smegmatis also produces siderophores to uptake iron, like many other bacteria (Figure 7). Siderophore production occurs at a lower rate in high iron environments (Middlebrook, Cohn & Schaefer, 1954; Ratledge & Marshall, 1972). The primary type of siderophore that is produced, especially in the presence of low iron, is exochelin, forming

an Fe-Exochelin MS (Fe-ExoMS) complex when bound to iron (Yu, Fiss & Jacobs, 1998). It is also produced earlier and in higher concentrations than the other siderophores. The mechanism of uptake is unknown, even though this is the main siderophore secreted in many *Mycobacteria* species. It is known that the Fe-ExoMS complex does not move across the membrane via porins, so there must be another mechanism to transport it, such as a "yet to be identified Fe-exochelin MS receptor" (Jones & Niederweis, 2012).

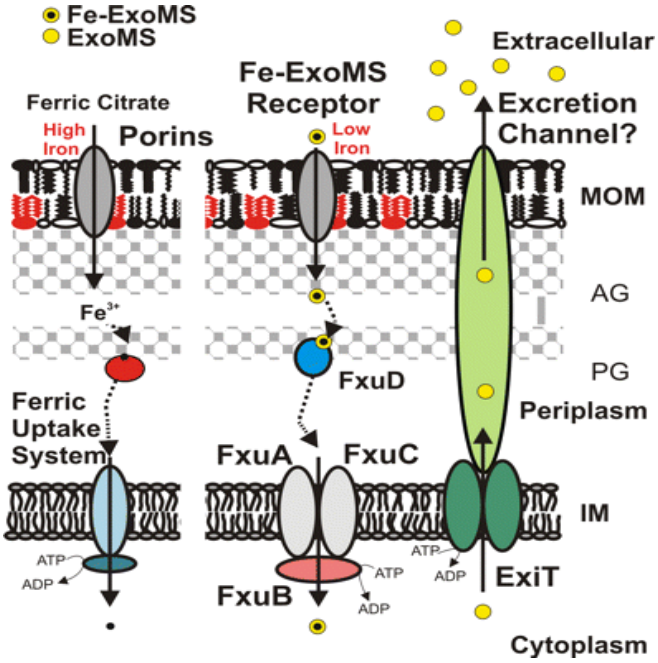

Figure 7. Model of iron transport in *M. smegmatis*.
The model of the mycobacterial cell envelope is based on cryo-electron microscopy. Mycolic acids are depicted in red. Under high-iron conditions ([Fe3+], > 5 µM), the uptake of ferric ions through porins is sufficient to meet the iron requirements of the *M. smegmatis*. When the availability of iron decreases, either by decreasing the number of pores in the outer membrane or by decreasing iron concentrations, *M. smegmatis* compensates for low iron levels by producing siderophores. Exochelin MS (yellow dots) is the main siderophore of *M. smegmatis* and strongly binds iron (black dots). Uptake of iron-loaded exochelin MS probably requires binding to an unknown receptor in the outer membrane and the FxuABC system in the inner membrane. Exochelin MS is secreted by ExiT, probably in combination with a yet-unknown outer membrane channel protein. The uptake of mycobactins depends on the ESX-3 secretion system but was omitted from our model for reasons of clarity. Reprinted from Role of porins in iron uptake by *Mycobacterium smegmatis* by C.M. Jones and M. Niederweis, 2010, *Journal of Bacteriology, 192*(24), pp. 6411-6417. Reprinted with permission.

Additionally, mycobactin is an intracellular siderophore that *M. smegmatis* uses for iron acquisition. Mycobactin is lipid-soluble and has high affinity for iron. It is located within the cell wall, but some distance from the outer envelope (Ratledge, Patel & Mundy, 1982). A third siderophore, carboxymycobactin, is water-soluble and is extracellular. It is modified from a mycobactin molecule with the addition of a carboxylic acid group (Ratledge & Ewing, 1996). Carboxybactin is produced in much higher quantities when cells are grown in glycerol, rather than glucose, but is generally only 10% of all the siderophores produced; most are usually exochelins. It has been found that both carboxymycobactin and mycobactin can be recycled during the process of iron uptake (Jones & Niederweis, 2012).

Since siderophore production is low in high iron environments, other processes are used to uptake iron when siderophores are not present (Jones & Niederweis, 2010). One system involved uptaking iron from ferric citrate, but the mechanism is unknown (Messenger & Ratledge, 1982). A recent study (Jones & Niederweis, 2010) showed that *M. smegmatis* uses porins in a low-affinity iron uptake of ferric citrate, rather than siderophores, in high iron environments when siderophores are not produced. Further, this process happens via diffusion, rather than through a transport mechanism, and the citrate is not taken up into the cell. Evidence shows that Mg^{2+} or Ca^{2+} must be present at a concentration greater than 0.5mM for the cell's citrate uptake mechanism to function, which is less than what is present in 7H9 medium. When the iron diffuses through the porins, it is reduced from Fe^{3+} to Fe^{2+}, when it interacts with the cell surface. This could also explain why citrate was not taken up. Since *M. smegmatis* is non-pathogenic, the

electron donors necessary to reduce iron would have to be supplied by the bacteria itself (Jones & Niederweis, 2010).

Summary

The mechanism of JB phage infection of *S. aureus* has not been characterized, and it could be related to iron uptake, either involving siderophores and/or iron uptake receptors. The mechanism of action of both phenomena should be studied and characterized to increase knowledge on how *S. aureus* and other pathogens can be controlled using phages supplemented with IDANPs.

METHODS

Preparation of Solutions, Media and Cultures

Iron-doped Apatite Nanoparticles 30% Solution

To synthesize nanoparticles, 200 mL of deionized water was placed in a 500 mL flask, held at room temperature. Reagents were added in the following order while stirring: 0.260 g Calcium Hydroxide ($Ca(OH)_2$), 0. 243 g Iron(III) Chloride ($FeCl_3$), 0.263 g Citric Anhydrous ($C_6H_7O_7$), and a solution of 50 mL deionized water with 0.408 g monopotassium phosphate (KH_2PO_4) was added dropwise over one minute. The pH of the solution was brought up from about a 4.5 to approximately 7.5 using 1M NaOH. The solution was stirred for seven days on a magnetic stir plate (25°C), then autoclaved at 121°C for 15 minutes (Fig. 43). The chemical reaction is shown below:

$$7\ Ca(OH)_2 + 3FeCl_3 + 6KH_2PO_4 \xrightarrow{\text{Citric Acid}} Ca_7Fe_3(PO_4)_6(OH)_2 + 6KOH + 12\ H_2O + 9Cl^-$$

(2) (Andriolo et al., 2016).

Iron Treatment Preparation

A 0.016 g/L solution of $FeCl_3$ was prepared by dissolving 0.016 g $FeCl_3$ anhydrous to one liter of deionized water and autoclaved at 121°C for 15 minutes. Dilutions were prepared from this sterile solution.

Dextrose 20% Solution

The solution was prepared by slowly adding 20 g dextrose to 100 mL deionized water and vacuum filtered to sterilize.

0.1M $CaCl_2$ Solution

The solution was prepared by adding 11.10 g $CaCl_2$ with 1 L deionized water and stirring, then autoclaving at 121°C for 15 minutes to sterilize.

M9 Minimal Media (MM++)

An M9 Media was prepared to grow cells in a media free of iron. A solution of M9 salts was made by adding 64 g of $Na_2HPO_4 \cdot 7H_2O$, 15 g KH_2PO_4, 2.5 g NaCl, and 5.0 g NH_4Cl to 800 mL H_2O. The solution was stirred and adjusted to 1000 mL, then autoclaved at 121°C for 15 minutes to sterilize. M9 salts were diluted by combining 200 mL of sterile salts to 700 mL of sterile H_2O, then adding 2 mL of sterile 1M $MgSO_4$, 20 mL of vacuum sterilized 20% glucose and 100 µL of sterile 1M $CaCl_2$, then adjusted to 1000 mL with sterile water.

Tryptic Soy Broth (TSB++)

To prepare, 30.0 grams of medium was added to 800 mL of deionized water until dissolved, then water was added until a volume of one liter was reached. The mixture was heated and stirred to boiling, then autoclaved at 121°C for 15 minutes. The broth was

stored as a liquid at room temperature until use. Just before use, 25 mL/L of a 25% sterile solution of dextrose and 10 mL/L of a 0.1M $CaCl_2$ sterile solution were added, then stored in the refrigerator. With these additions, it was labeled TSB++.

Tryptic Soy Agar (TSA++)

To prepare, 40.0 grams of medium were dissolved into 1 L of deionized water, then heated and stirred to boiling and autoclaved at 121°C for 15 minutes. Once TSA was cooled to touch on a cool stir plate, then 25 mL/L of a 25% sterile solution of dextrose and 10 mL/L of a 0.1M $CaCl_2$ sterile solution was added. This was now labeled TSA++. Agar was placed back on stir plate for one minute to mix and then poured directly into petri dishes.

Tryptic Soy Top Agar (TSTA++)

A 1:1 solution of TSA++:TSB++ was made and the mixture was placed in hot water bath at 50°C to prevent solidification.

7H9 Broth for Liquid Culture (7H9++++)

To prepare, 4.7 g of 7H9 was combined with 900 mL deionized water and 5 mL of 40% sterile glycerol. The solution was stirred on a magnetic stir plate until combined, then autoclaved at 121°C for 15 minutes. After cooling, 100 mL of ADC, 10 mL 0.1 M $CaCl_2$, 1 mL carbenicillin (100 µL/100 mL), 1 mL cycloheximide (100 µL/100 mL) and 2.5 mL Tween 80 (250 µL/100 mL) were added sterilely. This solution was stored at 4°C.

7H9 Broth for Top Agar

To prepare, 4.7 g 7H9 was combined with 900 mL deionized water, with 5 mL of 40% sterile glycerol. The Solution was stirred with a magnetic stir bar on a stir plate until

ingredients were well combined. The solution was autoclaved at 121°C for 15 minutes. After cooling, 2 mL/L of sterile 0.1 M $CaCl_2$ was added.

Middlebrook Top Agar (MBTA)

To 1000 mL deionized water, 4.7 g 7H9 and 7.0 g BactoAgar were added. The solution was stirred with a stir bar on a magnetic stir plate until it boiled. Then, 50 mL of solution was aliquoted into separate bottles and autoclaved at 121°C for 15 minutes. Agar was then diluted at a 1:1 ratio with the 2mL/L of 0.1 $CaCl_2$ 7H9 broth, after the top agar was melted in the microwave. When used in experiments, the solution was shaken to thoroughly mix and poured plates at 55-60°C.

7H10 Agar Plates

Agar was prepared by combining 19 g 7H10 agar to 990 mL of deionized water. The solution was stirred and heated on a magnetic stir plate until boiling, then autoclaved at 121°C for 15 minutes. After cooling to about 55°C, 12.5 mL 40% glycerol, 4.95 mL of 40% dextrose, 10 mL of 0.1M CaCl2, 1 mL carbenicillin (100 µL/100 mL) and 1 mL cycloheximide (100 µL/100 mL) were sterilely added to the solution. The plates were poured, cooled and solidified before being stored in the refrigerator.

Luria Bertani Agar (LBA++)

Agar was prepared by adding 40 g of LB Agar powder to 1 L of water and placed with a magnetic stir bar on a magnetic hot plate until boiling. The solution was autoclaved at 121°C for 15 minutes. Once the solution cooled, 1 mL carbenicillin (100 µL/100 mL) and 1 mL cycloheximide (100 µL/100 mL) were added sterilely and plates were poured, cooled and solidified prior to refrigeration.

Growth of *S. aureus* cells

From a frozen stock culture kept in a liquid nitrogen tank at -200 degrees Celsius, cells were streaked onto TSA++ plates and incubated at 37°C for 24 hours. One colony was picked and transferred into a Falcon tube with 3 mL of TSB++, then placed on a shaker at 225 RPM and incubated at 37°C for 24 hours. Tube was then centrifuged at 3600 RPM (RCF=1500 g) for 10 minutes to form a pellet of cells at the bottom. TSB was drawn off and replaced with M9 minimal medium. Cells were grown in M9 minimal medium at 37°C for 24 hours on a shaker at 225 RPM.

Growth of *M. smegmatis* cells

A 7H9 broth stock culture was kept at room temperature with a stir bar. From this, cells were streaked onto 7H10 plates and incubated for 48 hours. One colony was picked with a sterile inoculation loop, dropped in a 100 mL aliquot solution of 7H9 broth and grown for seven days at room temperature until a turbid culture was achieved.

Amplification of Phage

JB phage was amplified by picking a colony of *S. aureus* and growing it overnight in 3 mL of broth, at 37°C at 225 RPM. Then, 250 µL of bacteria was diluted with 25 mL of media and infected with 100 µL of phage stock. This solution was kept at 37°C for four hours, shaking at 225 RPM, and then filtered with a 0.2-micron filter and stored in a sterile tube in the refrigerator. Titer experiments were performed to determine concentration of phage.

Yodasoda phage was amplified by adding 10 mL of turbid *M. smegmatis* with 100 µL of phage stock for four hours. Then the solution was filtered through a 0.2-micron

filter and stored in the refrigerator. Then titer experiments were performed to determine concentration.

Phage Titer Experiments

Serial dilutions of the JB phage stock were performed from concentrations of 10^{-1} to 10^{-7} by adding 90 µL of TSB++ and 10 µL of each preceding phage concentration. Plaque assays were performed using overnight cultures of *S. aureus*, diluting them to 1:100 and grown for four hours. Then, 250 µL bacteria was added to 250 µL of broth in a tube, one for each titer concentration, and grown in an incubator at 37°C for one hour with gentle agitation from the lab shaker at 225 RPM. Following this, tubes were infected with 10 µL of the different titers of phage for 10 minutes. Then 4.5 mL of heated TSTA was added and poured onto TSB++ plates. These plates were flipped once solidified and incubated at 37°C for 24 hours.

Serial dilutions of Yodasoda phage stock were performed from concentrations of 10^{-1} to 10^{-7} by adding 90 µL of phage buffer and 10 µL of each preceding phage concentration. Plaque assays were performed by adding 500 µL of *M. smegmatis* and 10 µL of phage to tubes, one for each titer concentration, and allowed to infect for 10 minutes. Then 4.5 mL of melted MBTA was added and poured onto LBA++ plates.

Part 1: MM++ *S. aureus* with JB Phage Plaque Assays in Various Iron Treatments

Cells were suspended in a 1:10 dilution of MM++ (250 µL of bacteria and 25 mL of MM++, control or iron supplemented) for three hours in incubator at 37°C on shaker.

Each treatment was then placed in 1:1 dilutions of bacteria and iron supplemented media (250 µL bacteria from flask and 250 µL iron supplemented media), five replicates

of each. Tubes were placed in an incubator at 37°C for one hour with gentle agitation from the lab shaker at 225 RPM.

After one hour, 10 µL of JB phage was added (50 phages per 10 µL determined by titer experiment). The phages were allowed to infect and adhere for 10 minutes. Then 4.5 mL of TSTA, held at 65°C, was added to each tube, one at a time, and then poured onto TSA++ plates. Plates were allowed to solidify for 30 minutes then placed in incubator at 37°C for 24 hours, and plaques were counted. Experiments for each iron treatment were replicated at least five times.

Part 2: Effect of IDANP Treatment in *S. aureus* with JB Phage in MM++

Cells were suspended in a 1:10 dilution of MM++ (250 µL of bacteria and 25 mL of MM++) for three hours in incubator at 37°C on shaker.

The culture was then placed in 1:1 dilutions (250 µL bacteria from flask and 250 µL nanoparticles or 250 µL bacteria from flask and 250 µL MM++), five replicates of each. Tubes were placed in an incubator at 37°C for one hour with gentle agitation from the lab shaker at 225 rpm.

After one hour, 10 µL of JB phage was added (50 phages per 10 µL determined by titer experiment). Phage was allowed to infect and adhere for 10 minutes. Then 4.5 mL of TSTA, held at 65°C, was added to each tube, one at a time, and poured onto TSA++ plates. Plates were allowed to dry for 30 minutes then placed in an incubator at 37°C for 24 hours. Plaques were counted and photographed using high definition photography with a ruler the following day. Ten millimeter measurements from the rulers were calibrated to pixels using Paint® software. Plaques were then measured in pixels

and then converted back to millimeters. Plates were also returned to the incubator for two to four days and photographed each day to observe plaque changes.

Part 3: MM++ *S. aureus* with JB Phage Plaque Assays in Various Iron Treatments Treated with IDANPs

Cells were suspended in a 1:1 dilution (1.5 mL bacteria and 1.2 mL of MM++ with 300 µL of iron) for three hours in incubator at 37°C on shaker.

Each treatment was then placed in 1:1 dilutions of bacteria and nanoparticles (250 µL bacteria from flask and 250 µL nanoparticles or 250 µL of minimal media), five replicates of each. Tubes were placed in incubator at 37°C for one hour with gentle agitation from the lab shaker at 225 RPM.

After one hour, 10 µL of JB phage was added (50 phages per 10 µL determined by titer experiment). Phage was allowed to infect and adhere for 10 minutes. Then 4.5 mL of TSTA, held at 65°C, was added to each tube, one at a time, and poured onto TSA++ plates. Plates were allowed to dry for 30 minutes then placed in incubator at 37°C for 24 hours, and plaques were counted. Experiments for each iron treatment were repeated at least five times.

Part 4: Effect of IDANP Treatment in *M. smegmatis* with YodaSoda Phage

First, 250 µL of *M. smegmatis* in 7H9 broth was added to sterile tubes. To half of the tubes, 250 µL of 7H9 were added, while to the other half 250 µL of IDANPs were added. Tubes were placed in an incubator at 37°C for one hour with gentle agitation from the lab shaker at 225 RPM. They were infected with 10 µL of Yodasoda for ten minutes and then 4.5 mL of melted MBTA at 65°C was added to each tube and they were quickly

poured onto LBA++ plates. Plates were undisturbed for thirty minutes, then flipped and incubated for 24 hours at 37°C. Five plates were done for each experiment, and these experiments were repeated five times. Plaques were counted and photographed using high definition photography with a ruler the following day. Ten millimeter measurements from the rulers were calibrated to pixels using Paint® software. Plaques were then measured in pixels and then converted back to millimeters. Plates were also returned to the incubator for two to four days and photographed each day to observe plaque changes.

Part 5: *S. aureus* cell growth in MM++, Various Iron Treatments with IDANPs

Cell growth in Part 3 was limited and many times not sufficient for a lawn. A question emerged as to whether the combination of treatments of the IDANPs and the iron supplement was affecting cell growth. Cells were first cultured in the various treatments in sterile tubes by inoculating with one colony per tube from a streak plate. Tubes were placed in incubator at 37°C for one hour with gentle agitation from the lab shaker at 225 RPM. The treatments included the following: TSB media, MM++, MM++ with IDANPs, and these iron treatments: 0.0004 g/L, 0.0008 g/L, 0.0016 g/L, 0.0032 g/L and 0.0064 g/L. Tubes were photographed each day for a week to visually assess turbidity.

Growth was also monitored using a colony forming unit (CFU) method. One colony was dropped in a sterile tube with 3 mL of TSB++ grown overnight at 37°C with gentle agitation from the lab shaker at 225 RPM. Then, the tube was centrifuged and replaced with 3 mL of MM++ and grown overnight. Another 3 mL TSB++ culture was also prepared and grown overnight. The next day, tubes were diluted to 1:10 cultures in

the various treatments listed above and grown for three hours at 37°C with gentle agitation from the lab shaker at 225 RPM. At one-hour intervals, cultures were serially diluted in MM++ from 10^{-1} to 10^{-10} and 10 µL of each dilution was dropped three times each on a gridded TSA++. Plates were incubated upright overnight at 37°C. The next day, plates showed which dilution grew a countable number of colonies, which was averaged and used to determine CFU/mL.

Part 6: Scanning Electron Microscopy of *S. aureus* in MM++, Grown in Various Iron Treatments

To determine the effect of various iron treatments on the cell surface, *S. aureus* cells were grown in TSB++ over night from a single colony, centrifuged and replaced with MM++, and then treated with in 1:1 dilution of culture and MM++ with the same concentrations of iron used in experimentation. Cells were treated with iron for three hours, while shaking in an incubator. Following, 100 µL of each culture was placed an aluminum stub. Then, cells were dehydrated with a gradient of ethanol concentrations (10%, 20%, 30%, 40%, 50%, 60%, 70%, 80%, 90% and 100%) and left to evaporate for 10 minutes. The 100% concentration was repeated, and then hexamethyldisilazane (HMDS) was added and left to evaporate overnight. Samples were then sputter coated in gold and imaged using an SEM (Mira 3 Tescan; 15.0 kV).

DATA ANALYSIS LIST

Data were analyzed using Mystat software, a free student version of the statistical package Systat.

1. *S. aureus* were grown in different iron treatments (0 mg/L, 0.4 mg/L, 0.8 mg/L, 1.6 mg/L, 3.2 mg/L) and infected with the JB phage. The number of plaque infections were compared to the control.

   A. Phage plaques in the treatments and control were counted. Plaque counts were standardized to the control by dividing each value by the mean of the control in order to normalize the data.
   B. An Analysis of Variance was performed on the data to detect significant differences.

2. *S. aureus* were treated with IDANPs and infected with the JB phage. The number of infections were compared to the control.

   A. Phage plaques in the treatments and control were counted. Plaque counts were standardized to the control by dividing each value by the mean of the control.
   B. An Analysis of Variance was performed on the data to determine significance.
   C. Photographs were calibrated to a metric ruler and plaques were measured with Paint computer software.
   D. Plaque sizes were analyzed using a two-sample t test to detect statistical differences.

3. *S. aureus* were grown in a 0.0016g/L iron treatment and treated with IDANPs and infected with the JB phage. The number of infections were compared to the control.

   A. Phage plaques in the treatments and control were counted. Plaque counts were standardized to the control by dividing each value by the mean of the control.

B. An Analysis of Variance was performed on the data to detect significant differences.

4. *M. smegmatis* were treated with IDANPs and infected with the Yodasoda phage. The number of plaques were compared to the control.

   A. Phage plaques in the treatments and control were counted. Plaque counts were standardized to the control.

   B. An Analysis of Variance was performed on the data to detect significant differences.

   C. Photographs were calibrated to a metric ruler and plaques were measured with Paint computer software.

   D. Plaque sizes were analyzed using a two-sample t test to determine statistical differences.

5. *S. aureus* was treated with nanoparticles and various iron treatments, and colony forming units per milliliter were determined using serial dilutions. Number of colonies were counted.

   A. Number of colonies were counted and averaged.

   B. A One-Way Analysis of Variance was performed to compare the number of colonies in the control compared to the cells treated with IDANPs.

   C. A Two-Way Analysis of Variance was performed to compare the number of colonies in the control compared to cells in various iron treatments and cells in iron treatments with IDANPs. The XL Miner Analysis Toolpak Add-on to Google Sheets was used to perform this test.

RESULTS

Part 1: MM++ *S. aureus* with JB Phage Plaque Assays in Various Iron Treatments

When *S. aureus* cells were treated with various iron treatments and infected with JB phage, the number of plaques increased with increasing iron concentrations compared to the control (Figures 8 and 10).

There was a positive linear relationship between the iron concentration and the number of plaque infections ($r=0.95$) and the equation of the line was

$$y = 236x + 1.13 \quad (3)$$

where y = standardized plaque counts and x = iron concentration (g/L); The y-intercept was slightly greater than one because the plaque counts were standardized to the control, which was one. Plaque counts were standardized to the mean of the control in each individual experiment because different titers or cell concentrations impact plaque counts, so each experiment could have different plaque counts. These results indicate that the iron promotes phage infections. The two lower concentrations, 0.0004 g/L and 0.0008 g/L, had similar plaque counts at 1.29 and 1.34, respectively. The medium concentration of 0.0016 g/L had an average of 1.6 standardized plaque counts, and the high concentration of 0.0032 g/L had an average standardized plaque count of 1.83. The ANOVA results show the plaque counts were significantly different ($p<0.001$) (Figure 9; Table 1).

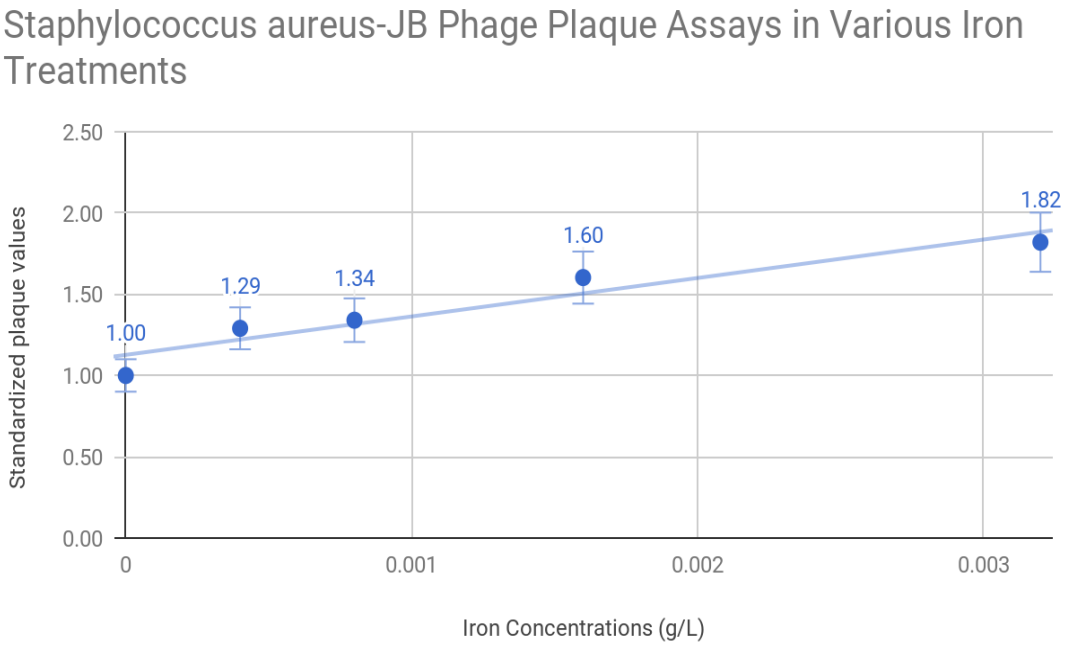

Figure 8. Comparison of plaque assays in various iron treatments of *S. aureus* infected with JB phage. Bars indicate standard error.

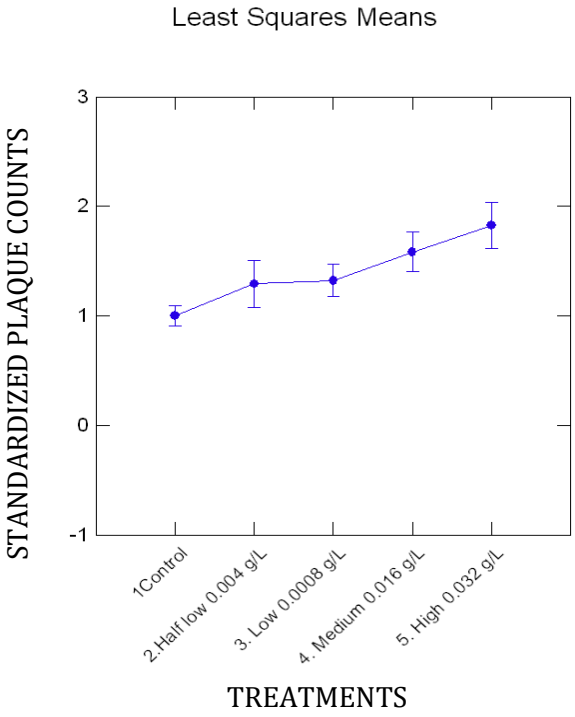

Figure 9. Analysis of variance comparing plaque counts in various iron treatments in *S. aureus* infected with JB phage ($p<0.0001$). Bars indicate standard error.

Table 1

Results From Analysis of Variance Comparing Plaque Counts in Various Iron Treatments in S. aureus Infected with JB Phage

Source	Type III SS	df	Mean Squares	F-ratio	p-value
TREATMENT	12.290	4	3.073	18.084	0.000
Error	26.165	154	0.170		

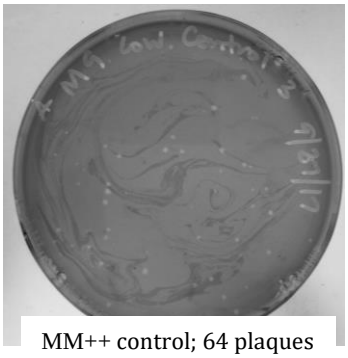

MM++ control; 64 plaques

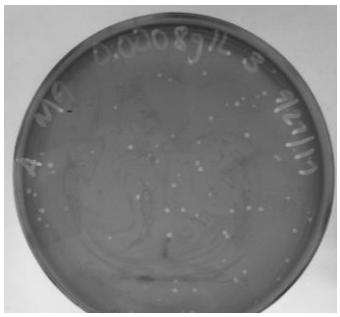

MM++ low iron (0.0008g/L); 91 plaques

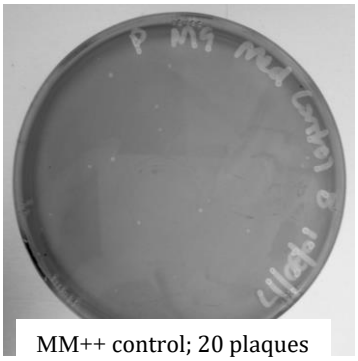

MM++ control; 20 plaques

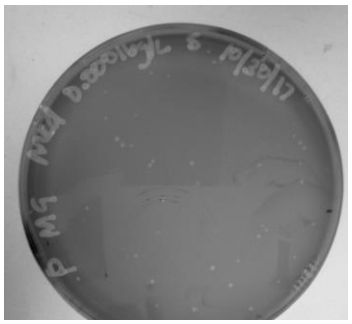

MM++ medium iron (0.0016g/L); 56 plaques

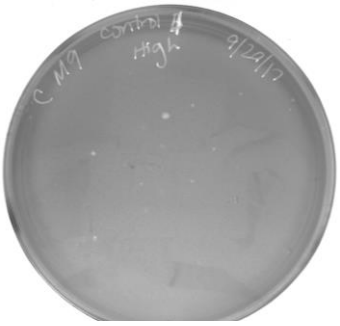

MM++ control; 29 plaques

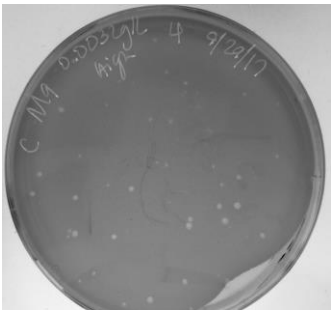

MM++ high iron (0.0032g/L); 67 plaques

Figure 10. S. aureus plaque assays in various iron treatments. Top row: MM++ control vs low iron (0.0008g/L), Middle row: MM++ vs medium iron (0.0016g/L), Bottom row: MM++ vs high iron (0.0032g/L). Negative effect of photograph shown to emphasize plaques. Representative plates are shown.

Part 2: Effect of IDANP Treatment in *S. aureus* Infected with JB Phage in MM++

When *S. aureus* was treated with IDANPs, there was a 15% increase in plaque size when plaques were measured the following day (Figures 11 & 21). This indicates that bacterial cells were infected a further distance from the originally infected cell. The average plaque size for the control was 0.052 cm while the average size of the IDANP-treated *S. aureus* cells was 0.060 cm. There was a significant difference between the control and treatment ($p<0.0001$) (Figure 12; Table 2).

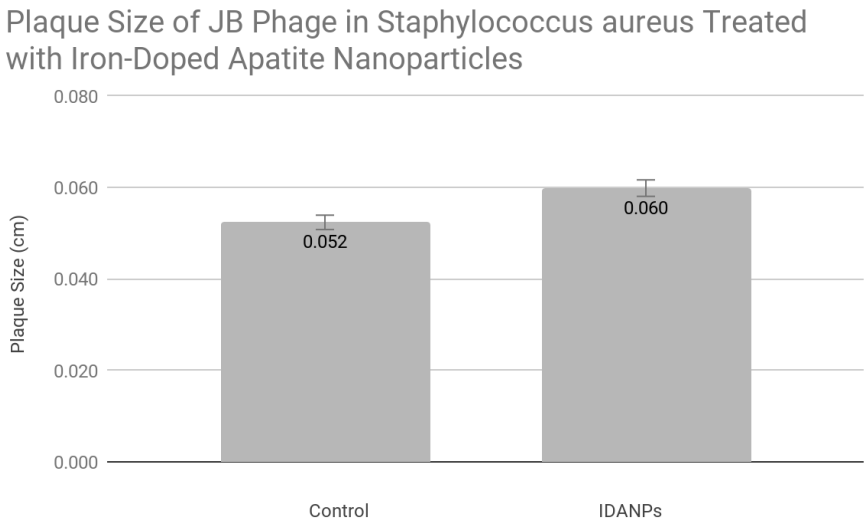

Figure 11. Difference in plaque size between *S. aureus* infected with JB phage and exposed to IDANPs compared to control over 24 hours. Bars indicate standard error.

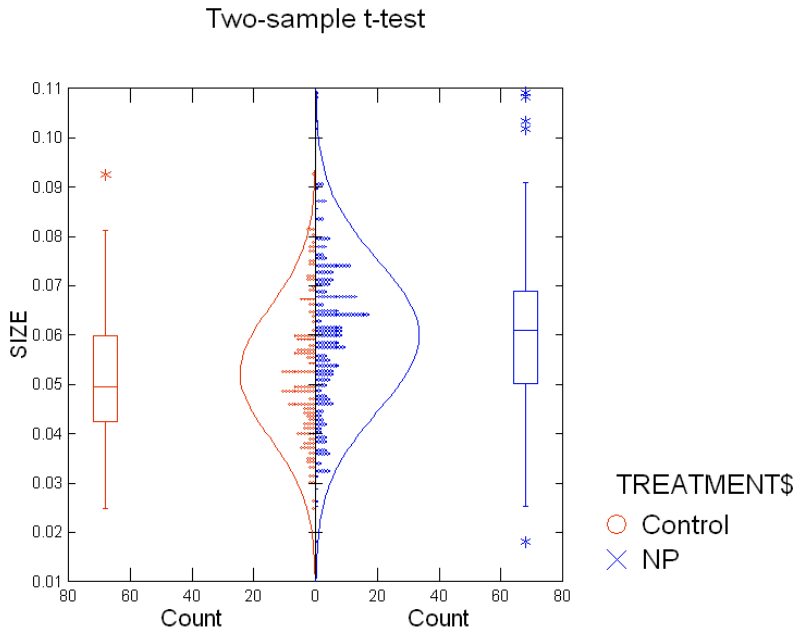

Figure 12. The results from the two-sample t-test comparing plaque size between *S. aureus* infected with JB phage and exposed to IDANPs compared to control over 24 hours ($p<0.0001$). Boxes in box-and-whisker plot indicate first and third quartile, and the whiskers indicate highest and lowest values. The median is indicated with the midline. The distribution of raw data is shown in the normalized curve.

Table 2

Results From Two-sample t-test Comparing Plaque Size Between S. aureus Infected With JB Phage and Exposed to IDANPs Compared to Control Over 24 Hours

GROUP	N	Mean	Standard Deviation
Control	162	0.052	0.013
NP	256	0.060	0.015

Difference in Means	:	-0.007
95.00% Confidence Interval	:	-0.010 to -0.005
t	:	-5.165
df	:	416.000
p-value	:	0.000

Plaque assays were kept in the incubator for an additional 24 hours to determine if the IDANPs had a prolonged effect on the plaque sizes. All of the plaques were photographed, and measured, and there was a 9.2% increase in the size of plaques from 24 hours to 48 hours (Figure 13). This suggests that the effect of the IDANPs on the

increase in plaque size is prolonged over time. Plaque sizes on after 24 hours averaged 0.054 cm and averaged 0.059 cm after 48 hours. There was a significant difference between the 24-hour plaque sizes compared to the 48-hour plaque sizes ($p = 0.021$) (Figure 14; Table 3).

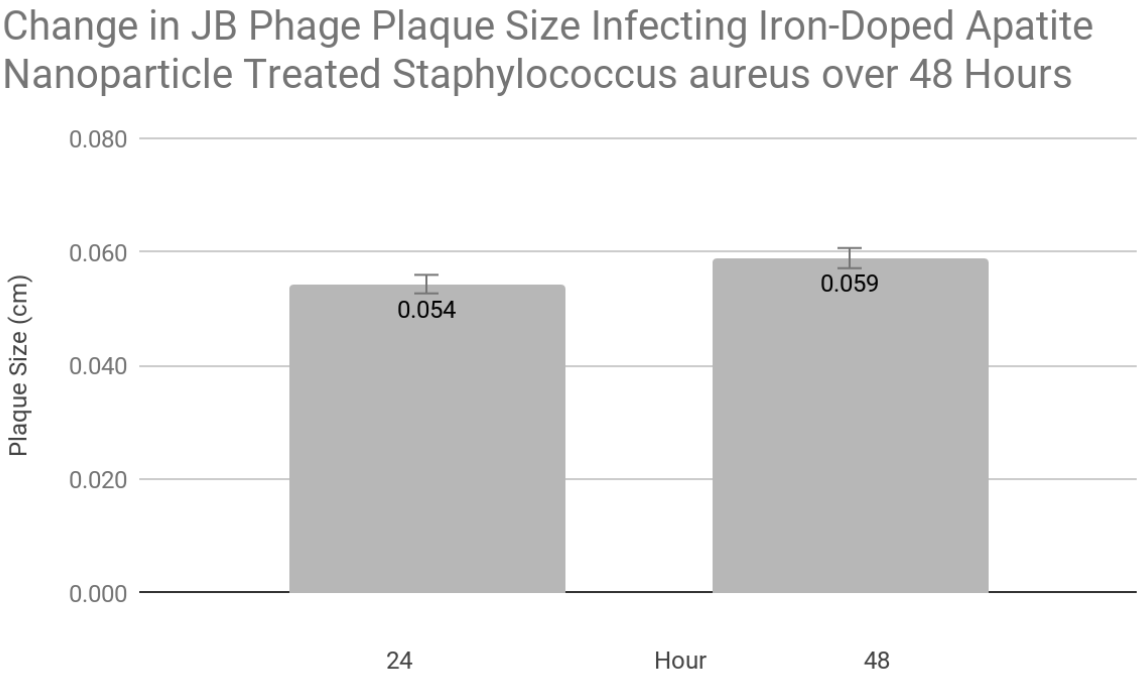

Figure 13. Difference in plaque size of IDANP-treated *S. aureus* infected with JB phage over 48 hours. Bars indicate standard error.
=

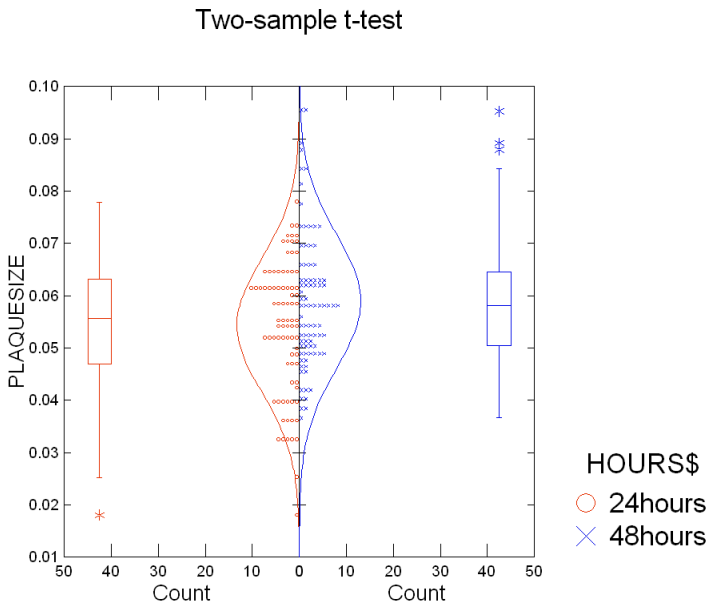

Figure 14. Results of the two-sample t-test comparing plaque size in IDANP-treated *S. aureus* infected with JB phage over 48 hours (p=0.021).

Table 3
Results From Two-sample t-test Comparing Plaque Size in IDANP-treated S. aureus *Infected With JB phage Over 48 Hours*

GROUP	N	Mean	Standard Deviation
24hours	84	0.054	0.013
48hours	84	0.059	0.013

Difference in Means	:	-0.005
95.00% Confidence Interval	:	-0.008 to -0.001
t	:	-2.331
df	:	166.000
p-value	:	0.021

For comparison purposes, an experiment was set up to determine if plaque sizes changed over a 48-hour period in *S. aureus* cells that were not treated with IDANPs. Plaque assays were performed and all of the plaques were photographed and measured at 24 hours and 48 hours. After 24 hours, the average plaque size was 0.051 cm, followed with an average plaque size of 0.047 cm after 48 hours, which yielded a 7.8% decrease (Figure 15). This difference was not significant (p=0.146) (Figure 16; Table 4).

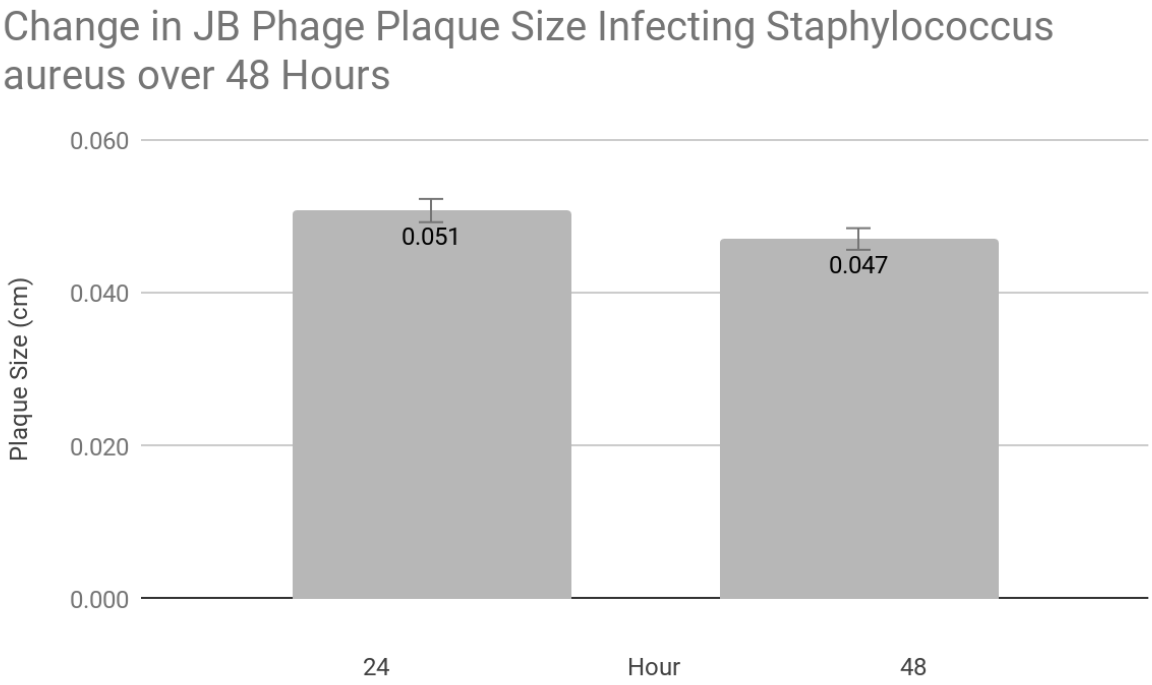

Figure 15. Difference in plaque size *S. aureus* infected with JB phage over 48 hours. Bars indicate standard error.

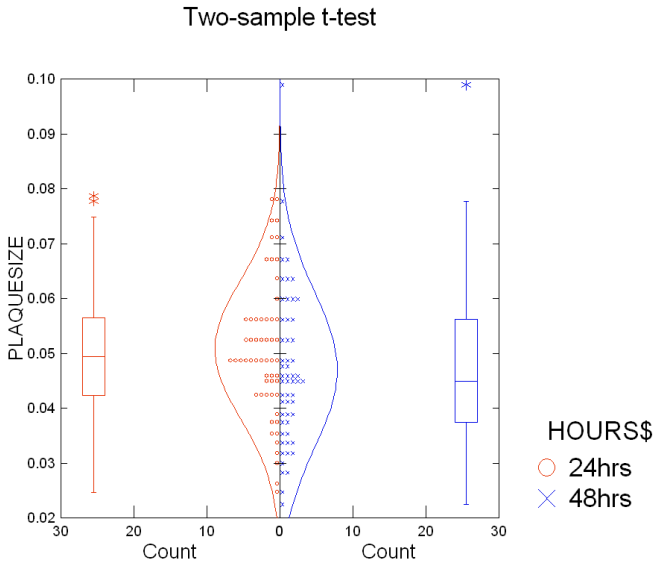

Figure 16. Results of two-sample t-test comparing plaque size in *S. aureus* infected with JB phage over 48 hours (p=0.146).

Table 4
Results From Two-sample t-test Comparing Plaque Size in S. *aureus Infected with JB Phage Over 48 Hours*

GROUP	N	Mean	Standard Deviation
24hrs	56	0.051	0.013
48hrs	56	0.047	0.014

Difference in Means	:	0.004
95.00% Confidence Interval	:	-0.001 to 0.009
t	:	1.464
df	:	110.000
p-value	:	0.146

Plaque assays were again performed with IDANP-treated *S. aureus* and plates were photographed and measured at one day and four days to determine any prolonged effects of the nanoparticles. Over this time period, there was a 50.8% increase in plaque size, with the average size after 24 hours being 0.059 cm and the average size after 96 hours being 0.089 cm (Figure 17). These results were found to be significantly different ($p<0.0001$) (Figure 18; Table 5).

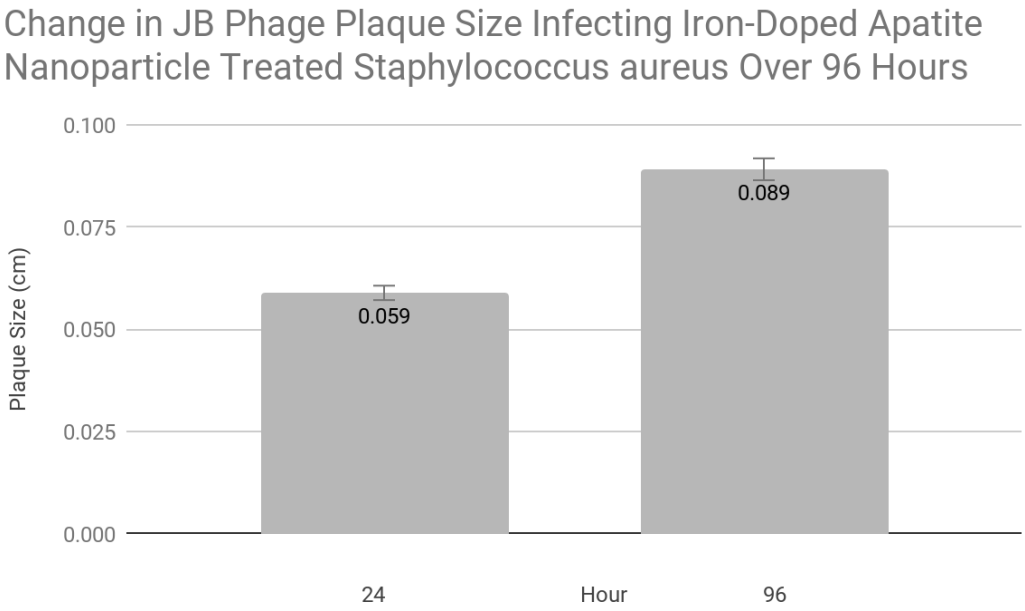

Figure 17. Difference in plaque size in IDANP-treated *S. aureus* infected with JB phage over 96 hours. Bars indicate standard error.

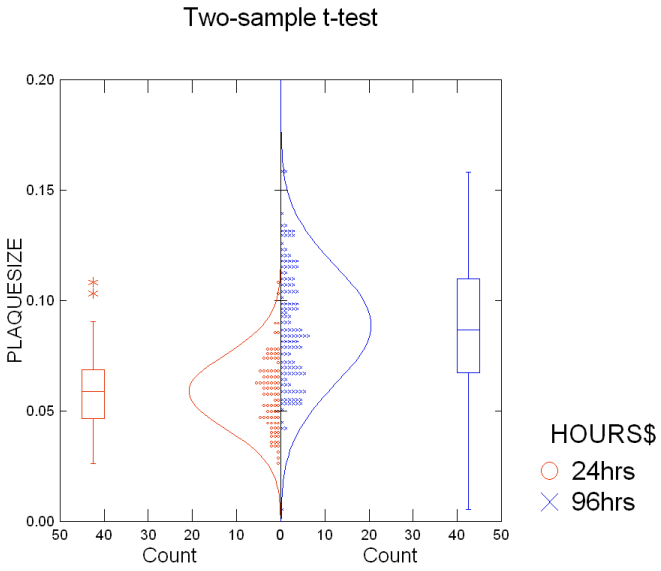

Figure 18. Results of two-sample t-test comparing plaque size in IDANP-treated *S. aureus* infected with JB phage over 96 hours ($p<0.0001$).

Table 5
Results From Two-sample t-test Comparing Plaque Size in IDANP-treated S. *aureus Infected With JB Phage Over 96 Hours*

GROUP	N	Mean	Standard Deviation
24hrs	87	0.059	0.017
96hrs	137	0.089	0.027

Separate Variance

Difference in Means	:	-0.030
95.00% Confidence Interval	:	-0.036 to -0.024
t	:	-10.414
df	:	221.950
p-value	:	0.000

Plaque assays were performed with untreated *S. aureus* cells to determine changes in plaque sizes over 96 hours in cells alone. Plaque size also increased over time in these untreated cells (Figure 19). There was a 39% increase in plaque sizes, with the average plaque size after 24 hours being 0.051 cm and 0.071 cm after 96 hours. The results were significantly different ($p<0.0001$) (Figure 20; Table 6).

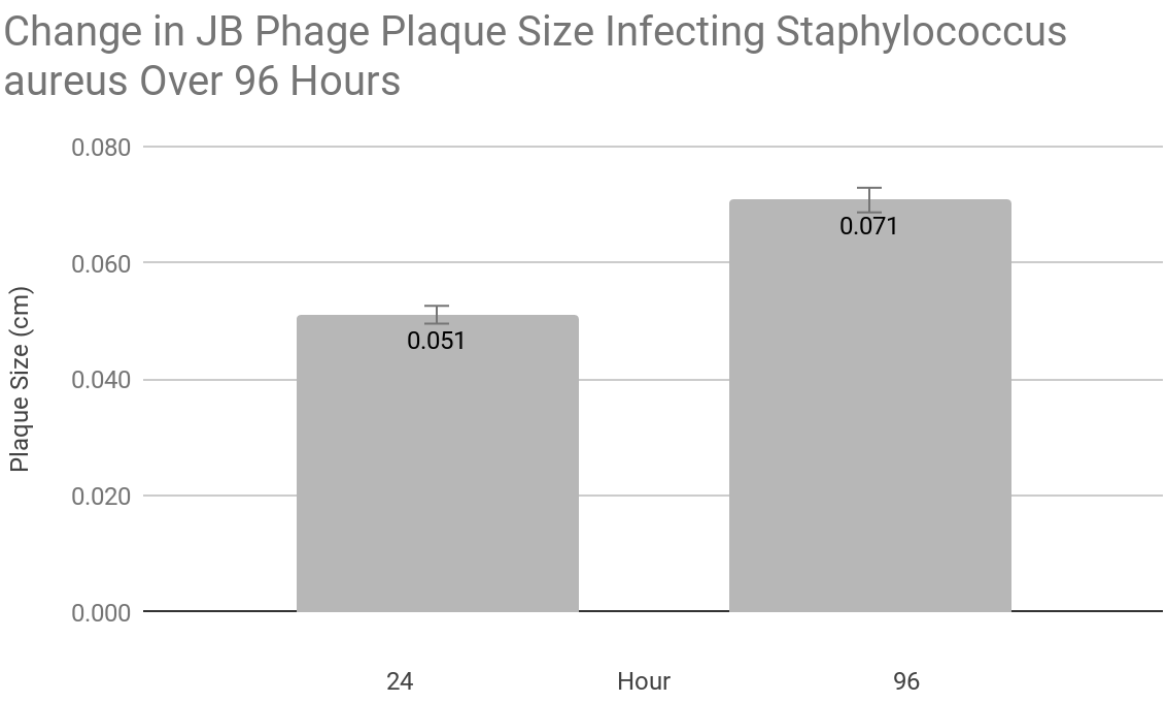

Figure 19. Difference in plaque size in *S. aureus* infected with JB phage over 96 hours. Bars indicate standard error.

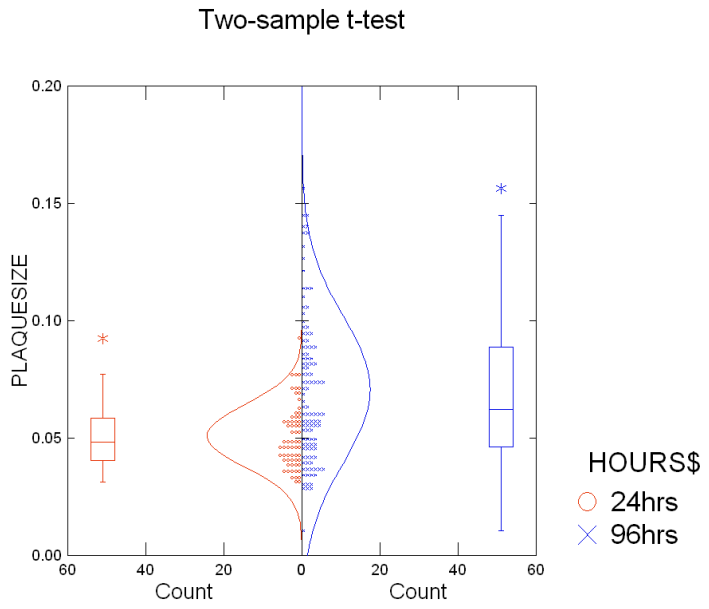

Figure 20. Two-sample t-test comparing plaque size in *S. aureus* infected with JB phage over 96 hours ($p<0.0001$).

Table 6
Results From Two-sample t-test Comparing Plaque Size in S. *aureus Infected With JB Phage Over 96 Hours*

GROUP	N	Mean	Standard Deviation
24hrs	64	0.051	0.013
96hrs	110	0.071	0.031

Separate Variance

Difference in Means	:	-0.020
95.00% Confidence Interval	:	-0.026 to -0.013
t	:	-5.778
df	:	159.516
p-value	:	0.000

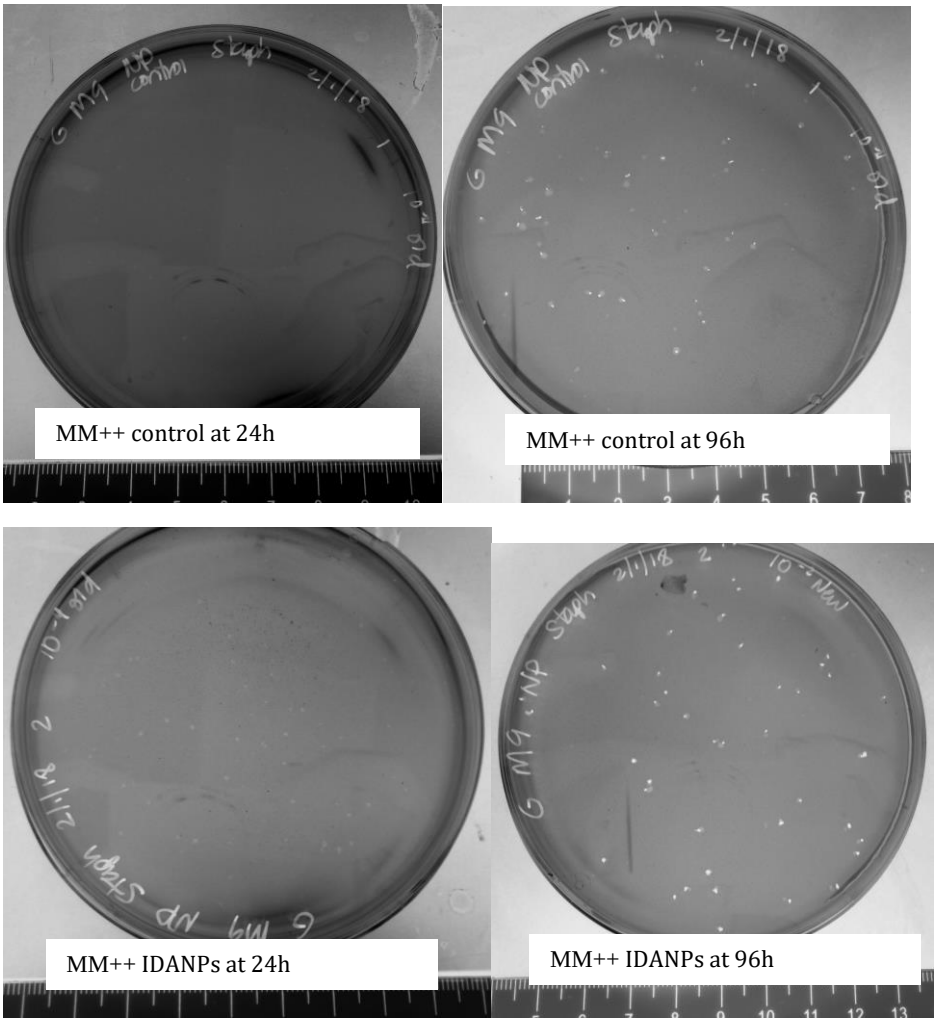

Figure 21. S. aureus plaque assays treated with IDANPs. Top row: MM++ control after 24 hrs and 96 hrs. Bottom row: IDANP-treated after 24 hrs and 96 hrs. Pen dots can be seen on the 96-hr pictures, but plaques are below them. Negative effect of photograph shown to emphasize plaques. Representative plates are shown.

Part 3: MM++ *S. aureus* with JB Phage Plaque Assays in Various Iron Treatments Treated with IDANPs

Cells treated with IDANPs and grown with a 0.0016g/L medium iron treatment were infected with JB phage and were found to have more plaque counts than cells only grown in the iron treatment (Figures 22 & 24). The standardized plaque counts in the IDANP-treated cells was 1.65, compared to 1.00 for the iron control plaque counts, and

the results were significantly different (p=0.001) (Figure 23; Table 7). The increase in plaque counts in the IDANP-treated cells was consistent with the increased plaque counts in other experiments (Gregory, 2017). This shows that there is an additive effect of IDANPs and iron treatments, in terms of increasing plaque counts.

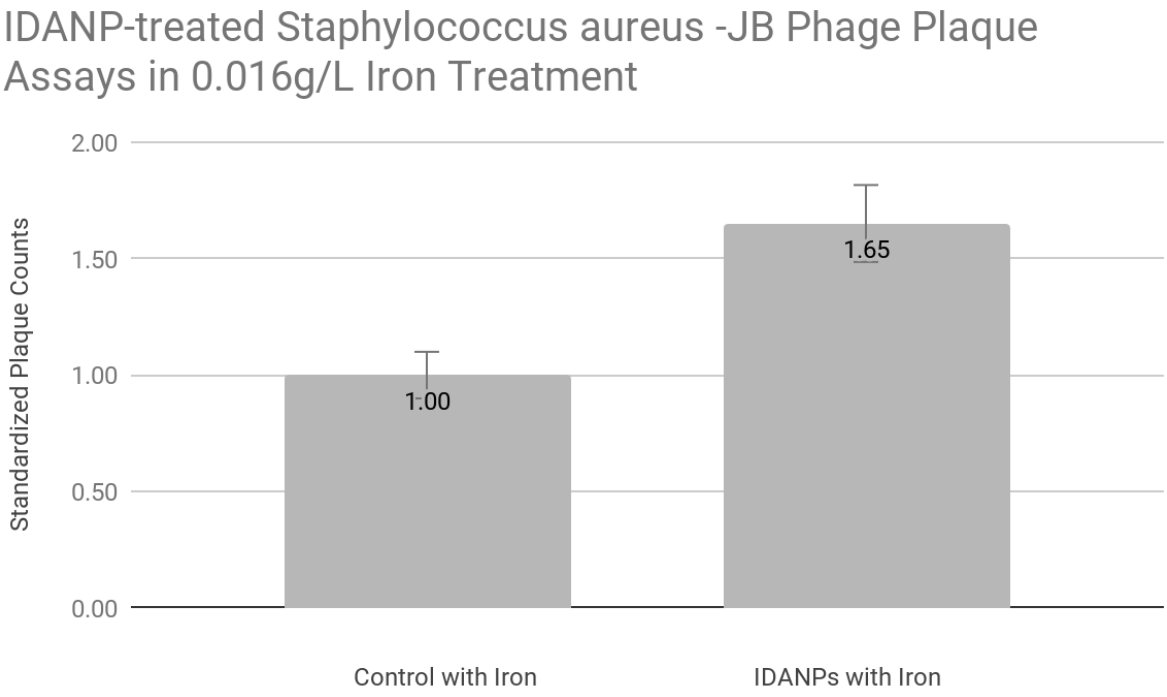

Figure 22. Difference in plaque counts between *S. aureus* cells treated with IDANPs and grown in a 0.0016g/L iron treatment compared to no iron treatment. Bars indicate standard error.

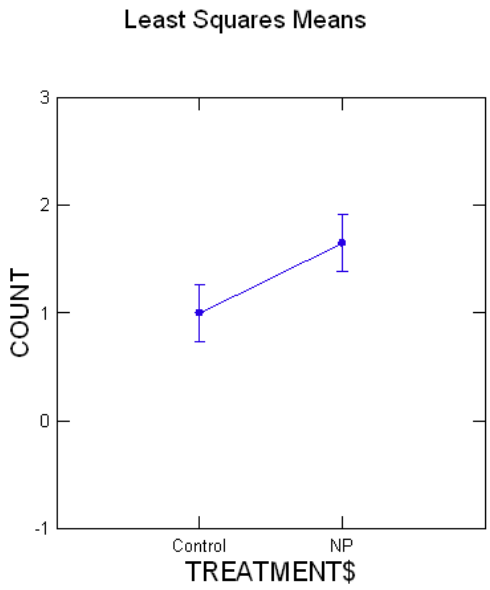

Figure 23. Analysis of variance comparing plaque counts in IDANP-treated *S. aureus* infected with JB phage and grown in 0.0016g/L iron treatments (p=0.001). Bars indicate standard error.

Table 7
Results From Analysis of Variance Comparing Plaque Counts in IDANP-treated S. *aureus Infected With JB Phage and Grown in 0.0016g/L Iron Treatments*

Source	Type III SS	df	Mean Squares	F-ratio	p-value
TREATMENT$	3.813	1	3.813	12.570	0.001
Error	10.314	34	0.303		

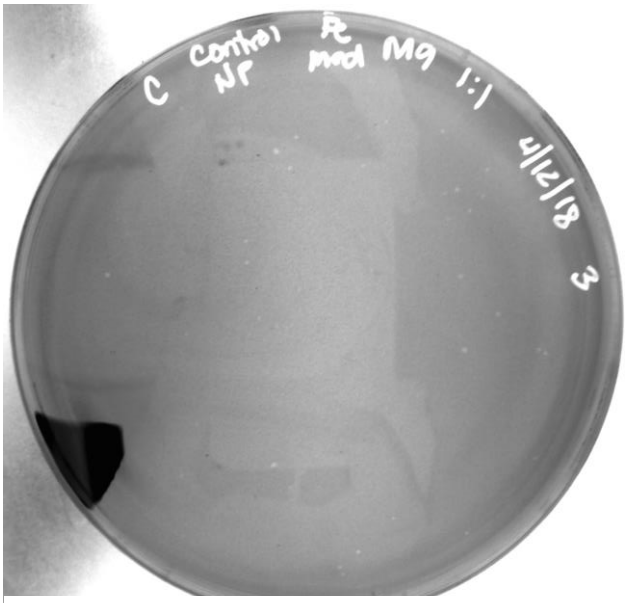

MM++ control with medium iron (0.0016 g/L); 40 plaques

MM++ IDANPs with medium iron (0.0016 g/L); 89 plaques

Figure 24. S. aureus plaque assays treated with IDANPs after being grown in a medium iron treatment (0.0016g/L). Left: control with medium iron; Right: IDANP treatment with medium iron. Negative effect of photograph shown to emphasize plaques. Representative plates are shown.

Part 4: Effect of IDANP Treatment in *M. smegmatis* with Yodasoda Phage

When *M. smegmatis* was treated with IDANPs and a plaque assay was performed, plaque sizes were larger in the IDANP treated plates than the control plates. Plates were photographed and measured after 24 hours. There was a 25% increase in plaque sizes compared to the control. Similar to the *S. aureus* model, the IDANPs prolonged the effect of the increased plaque size over time. The IDANP treated cells showed an average plaque size of 0.19 cm while the control cells had an average plaque size of 0.152 cm (Figures 25 & 31). These were results were significantly different ($p<0.0001$) (Figure 26; Table 8).

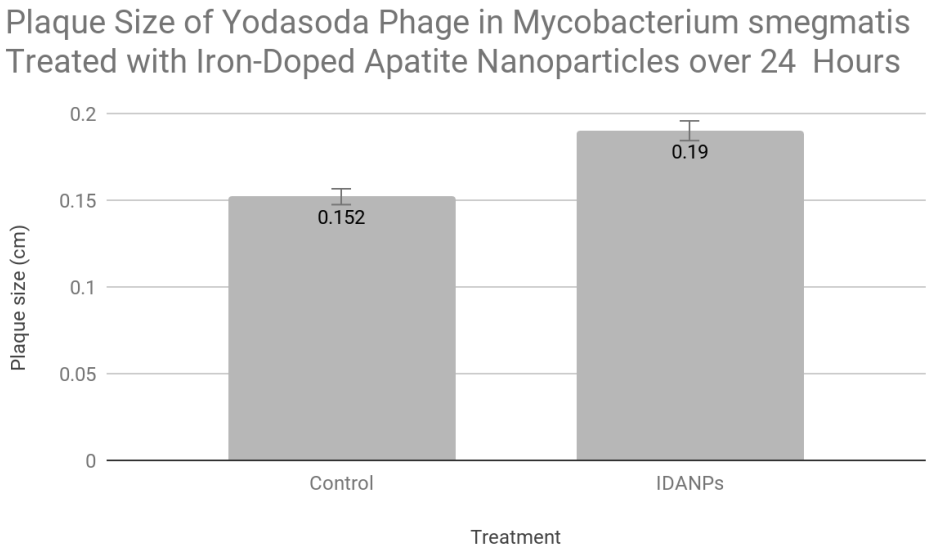

Figure 25. Difference in plaque size between *M. smegmatis* infected with Yodasoda phage and exposed to IDANPs compared to control over 24 hours. Bars indicate standard error.

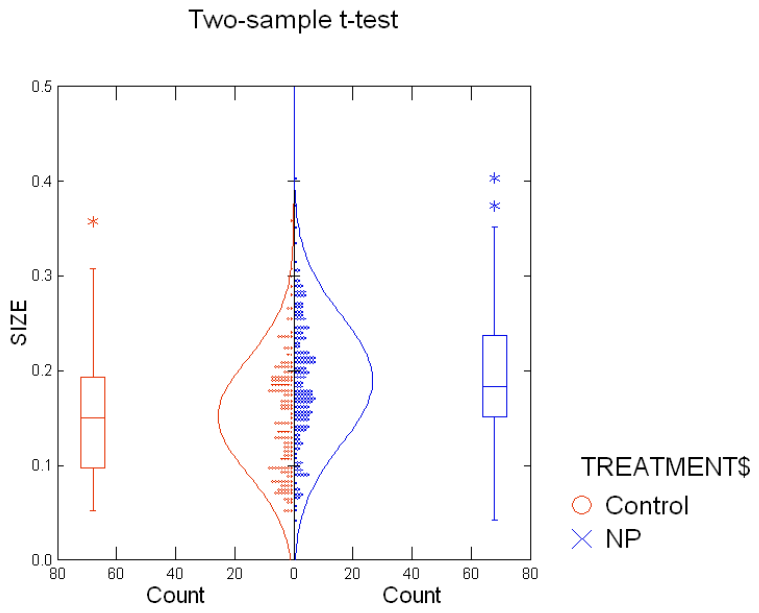

Figure 26. Results of two-sample t-test comparing plaque size in IDANP-treated *M. smegmatis* infected with Yodasoda phage over 24 hours ($p<0.0001$).

Table 8
Results From Two-sample t-test Comparing Plaque Size in IDANP-treated M. smegmatis *Infected with Yodasoda Phage Over 24 Hours.*

GROUP	N	Mean	Standard Deviation
Control	157	0.152	0.061
NP	181	0.190	0.068

Difference in Means	:	-0.039
95.00% Confidence Interval	:	-0.053 to -0.025
t	:	-5.482
df	:	336.000
p-value	:	0.000

Plates of plaque assays of IDANP-treated *M. smegmatis* infected with Yodasoda were photographed and measured at 24 hours, then incubated and photographed again after 48 hours. Similar to the *S. aureus* model, the IDANP-treated cells showed a prolonged effect on plaque size. There was a 57.4% increase in plaque sizes when comparing the 24-hour to the 48-hour plaque sizes (Figure 27). The average plaque size

at 24 hours was 0.19 cm and it increased to 0.299 cm after 48 hours, this difference is statistically significant ($p<0.0001$) (Figure 28; Table 9).

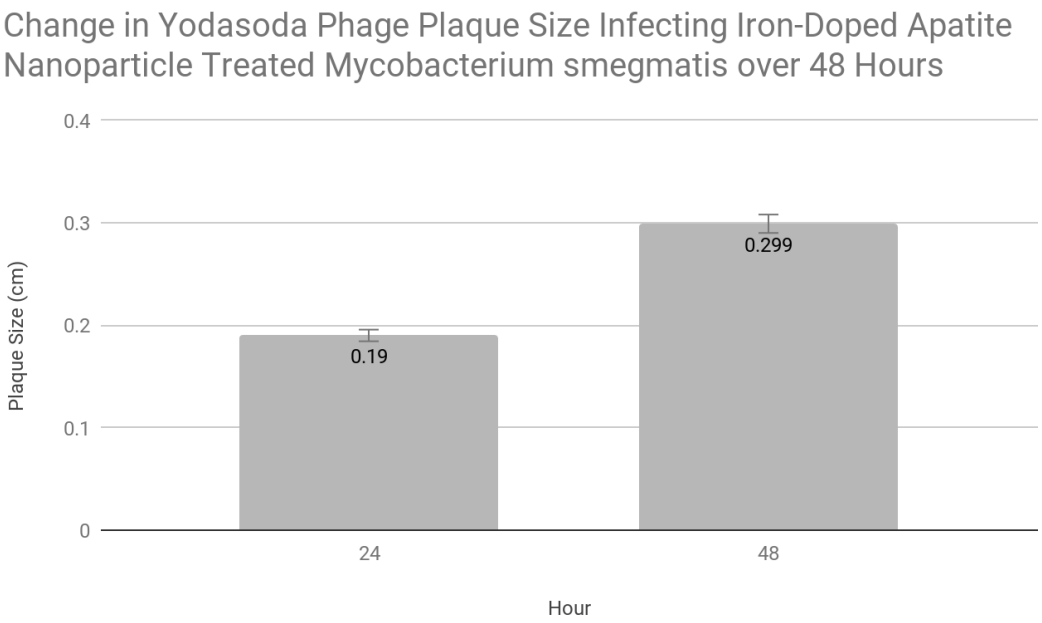

Figure 27. Plaque size in IDANP-treated *M. smegmatis* infected with Yodasoda phage over 48 hours. Bars indicate standard error.

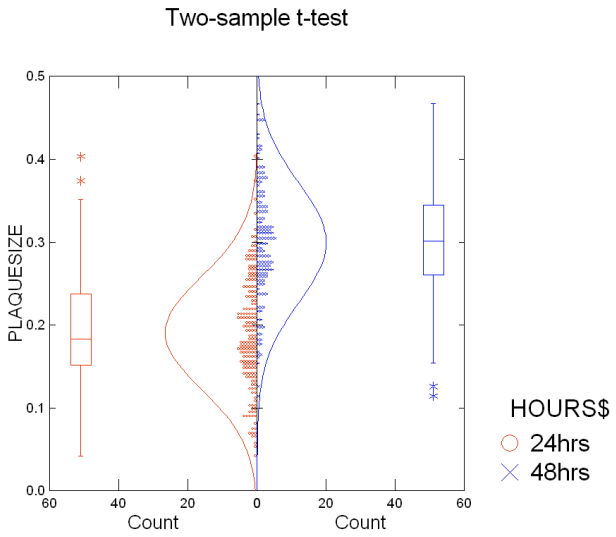

Figure 28. Two-sample t-test comparing plaque size in IDANP-treated *M. smegmatis* infected with Yodasoda phage over 48 hours ($p<0.0001$).

Table 9
Results From Two-sample t-test Comparing Plaque Size in IDANP-treated M. *smegmatis Infected With Yodasoda Phage Over 48 Hours*

GROUP	N	Mean	Standard Deviation
24hrs	181	0.190	0.068
48hrs	144	0.299	0.072

Difference in Means	:	-0.109
95.00% Confidence Interval	:	-0.124 to -0.094
t	:	-14.013
df	:	323.000
p-value	:	0.000

For comparison purposes, plaque assays were also compared to untreated *M. smegmatis* and plaques were measured twice over a 48-hour period. This also shows that plaque size was increasing over time, even in the untreated cells. There was a 64% increase in plaque sizes during this time. After 24 hours, the average plaque size was 0.152 cm, and after 48 hours, they increased to 0.25 cm (Figure 26). The results were statistically significant ($p<0.0001$) (Figure 27; Table 10).

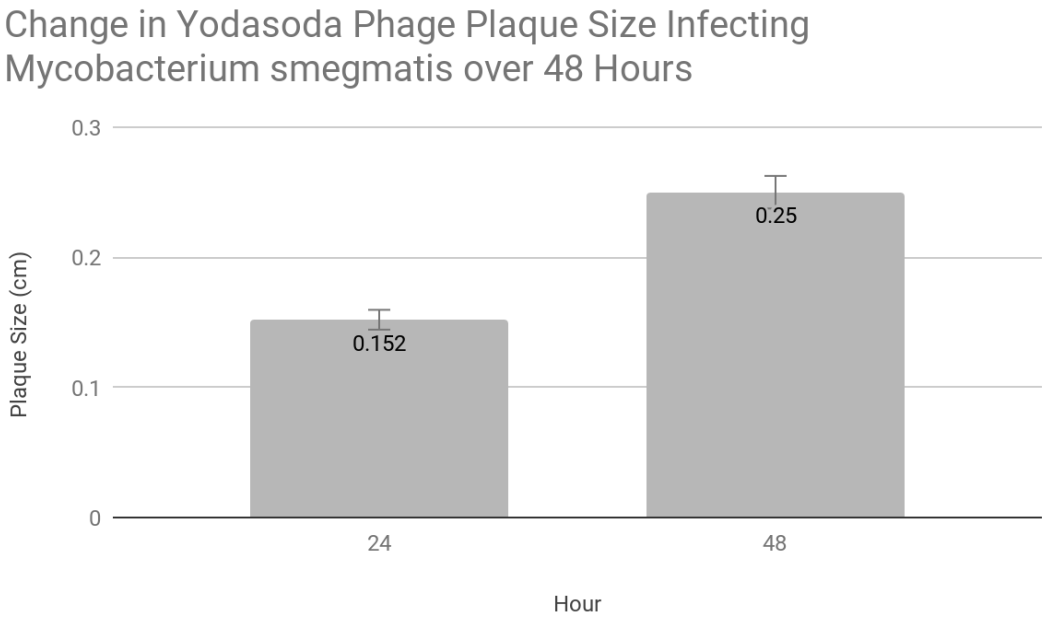

Figure 29. Plaque size in *M. smegmatis* infected with Yodasoda phage over 48 hours. Bars indicate standard error.

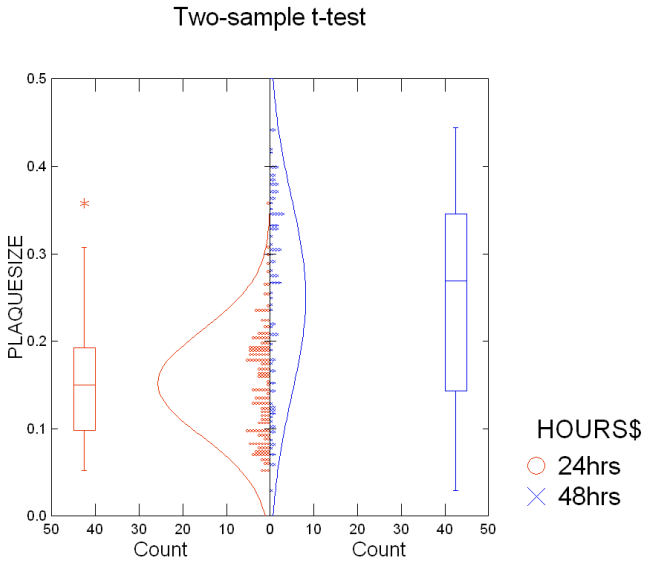

Figure 30. Results of two-sample t-test comparing plaque size in *M. smegmatis* infected with Yodasoda phage over 48 hours ($p<0.0001$).

Table 10

Results From Two-sample t-test Comparing Plaque Size in M. *smegmatis Infected With Yodasoda Phage Over 48 Hours*

GROUP	N	Mean	Standard Deviation
24hrs	157	0.152	0.061
48hrs	92	0.250	0.113

Separate Variance

Difference in Means	:	-0.098
95.00% Confidence Interval	:	-0.124 to -0.073
t	:	-7.728
df	:	122.577
p-value	:	0.000

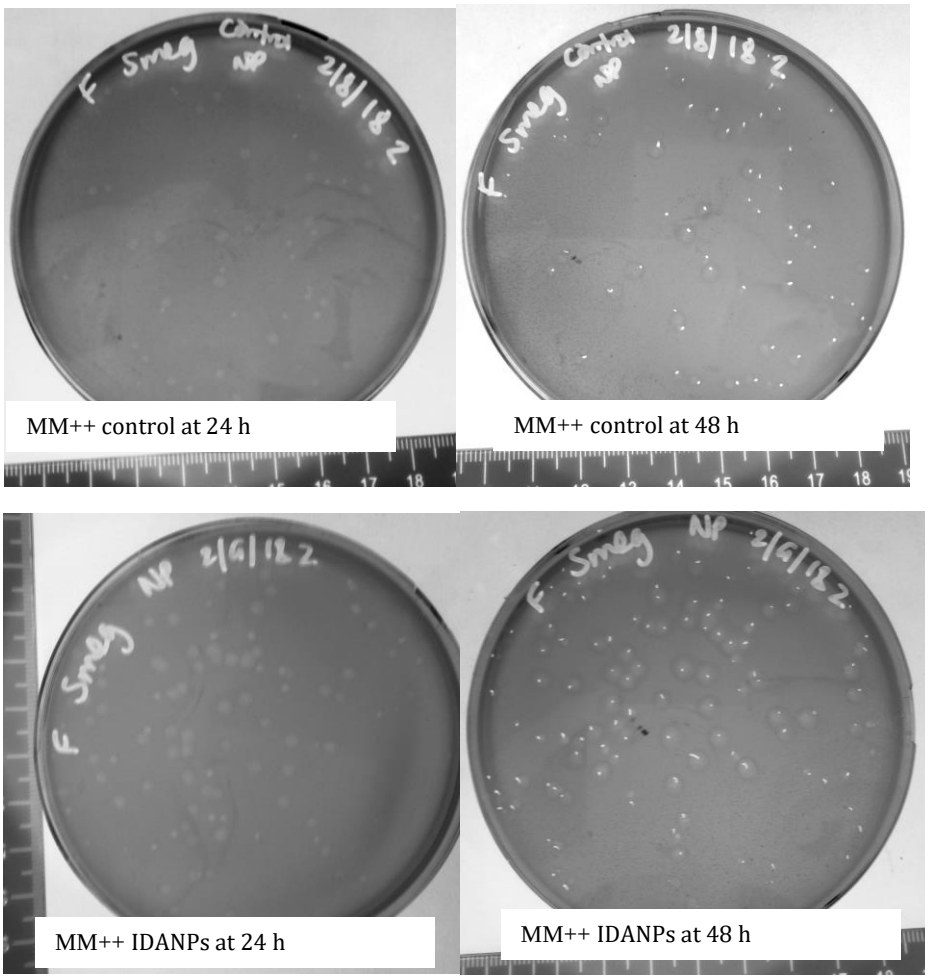

Figure 31. M. smegmatis plaque assays treated with IDANPs. Top row: Control after 24 hrs and 48 hrs. Bottom row: IDANP-treated after 24 hrs and 48 hrs. Pen dots can be seen on the 48 hr pictures, but plaques are below them. Negative effect of photograph shown to emphasize plaques.

Part 5: *S. aureus* cell growth in MM++, Various Iron Treatments and with IDANPs

Cells were grown in MM++, after a 24 hour the TSB++ culture, distributed into test tubes and half were treated with IDANPs. Colony forming units were determined using serial dilutions. For example, if an average of 6.5 colonies were counted at the 10^{-6} concentration in 10 µL, that number was multiplied by 1,000,000 to determine CFU/10 µL. Then, that number was multiplied by 1000 to determine CFU/mL. Average cell count

in the control was $3.33X10^6$ CFU/mL, and $3.92X10^6$ CFU/mL in the IDANP treatment (Figure 32). These results were not significantly statistically significant (p=0.513) (Figure 33; Table 11).

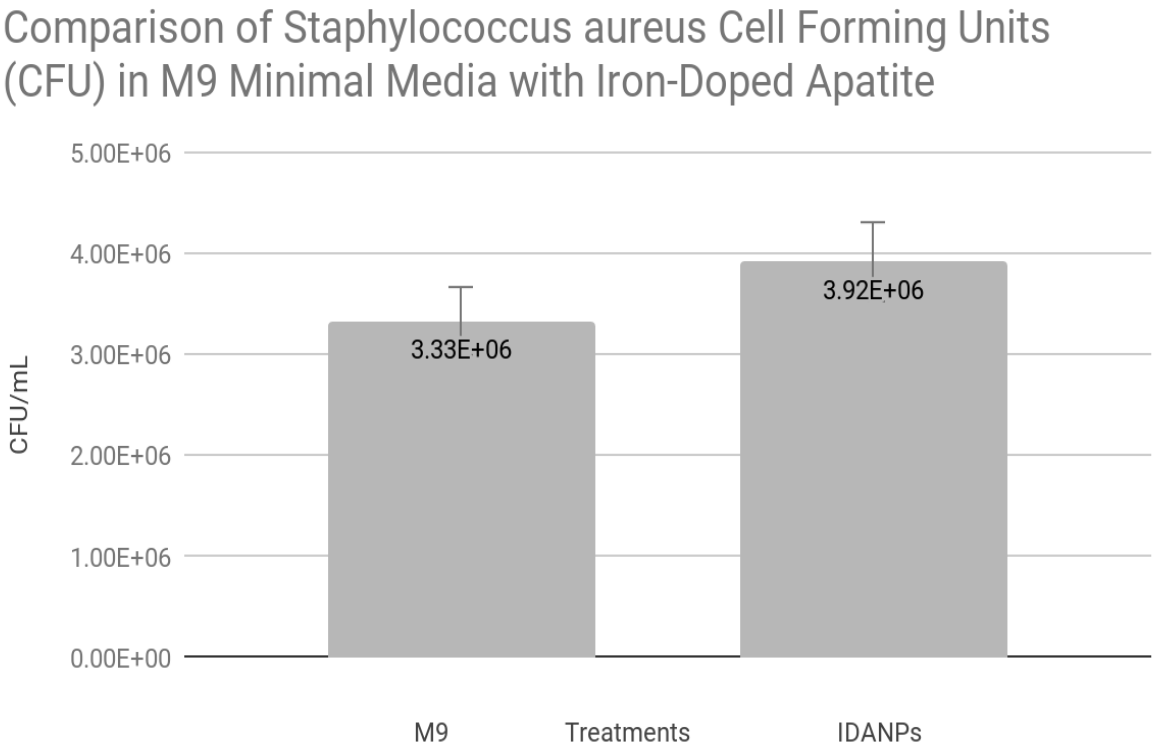

Figure 32. Colony forming units (CFU) of *S. aureus* grown in MM++ and IDANPs. Bars indicate standard error.

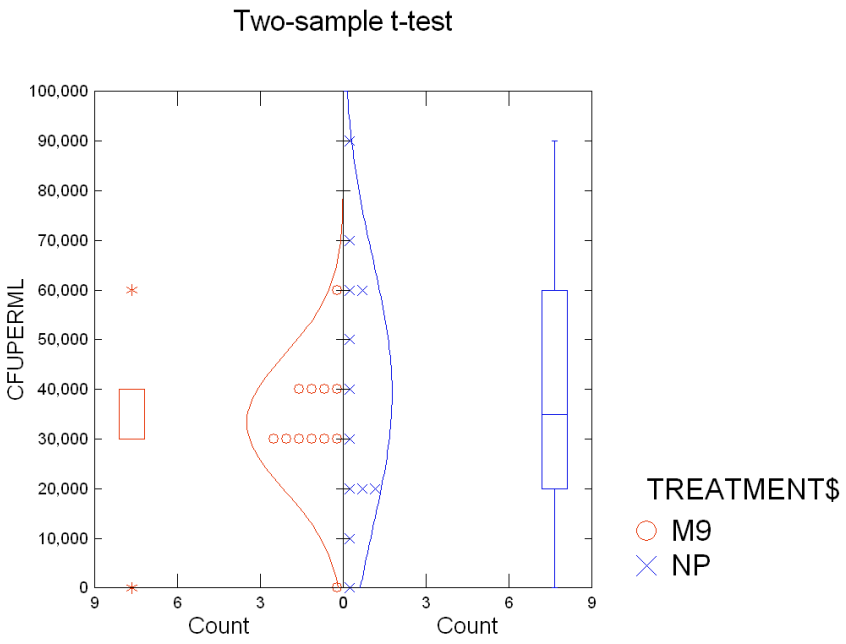

Figure 33. Two-sample t-test comparing colony forming units (CFU) of *S. aureus* in MM++ and IDANP treatment (p=0.513).

Table 11
Results From Two-sample t-test Comparing Colony Forming Units (CFU) of S. *aureus In MM++ and IDANP Treatment*

GROUP	N	Mean	Standard Deviation
M9	12	3,333,333.333	1,370,688.834
NP	12	3,916,666.667	2,712,205.856

Separate Variance

Difference in Means	:	-583,333.333
95.00% Confidence Interval	:	-2,440,474.777 to 1,273,808.110
t	:	-0.665
df	:	16.275
p-value	:	0.515

Colony forming units were compared between *S. aureus* cells grown in MM++ compared to cells treated with IDANPs. A 1:10 dilution in MM++ was cultured from an overnight culture of MM++, after an initial overnight culture in TSB++. The 1:10 dilution was the same as used for the MM++ iron treatment experiments. Serial dilutions were performed at 0.5 hr, 1hr, 2hr and 3hr, and used to determine CFU. CFU measurements

varied from 2.67X10^6 CFU/mL at 0.5 hr for both the MM++ and the IDANP treatment, to 4.00X10^6 CFU/mL and 7.00X10^6 CFU/mL at 1 hr for the M9 and IDANP treatment, respectively, with 3.67X10^6 CFU/mL and 2.00X10^6 CFU /mL at 2 hr and 3.67X10^6 CFU/mL and 4.00X10^6 CFU/mL at 3 hr (Figure 34). A one-way analysis of variance was performed on the MM++ and IDANP treatment, separately, and results showed there was not a significant difference between the times of sampling (p=0.295 for MM++ and p=0.083 for IDANPs) (Figures 35 & 36; Tables 12 & 13). It was determined that it did not matter when serial dilutions were performed, in terms of determining the effect of the IDANPs on cell growth. The IDANPs did not affect cell growth at 0.5 hr, 1hr, 2hr or 3hr.

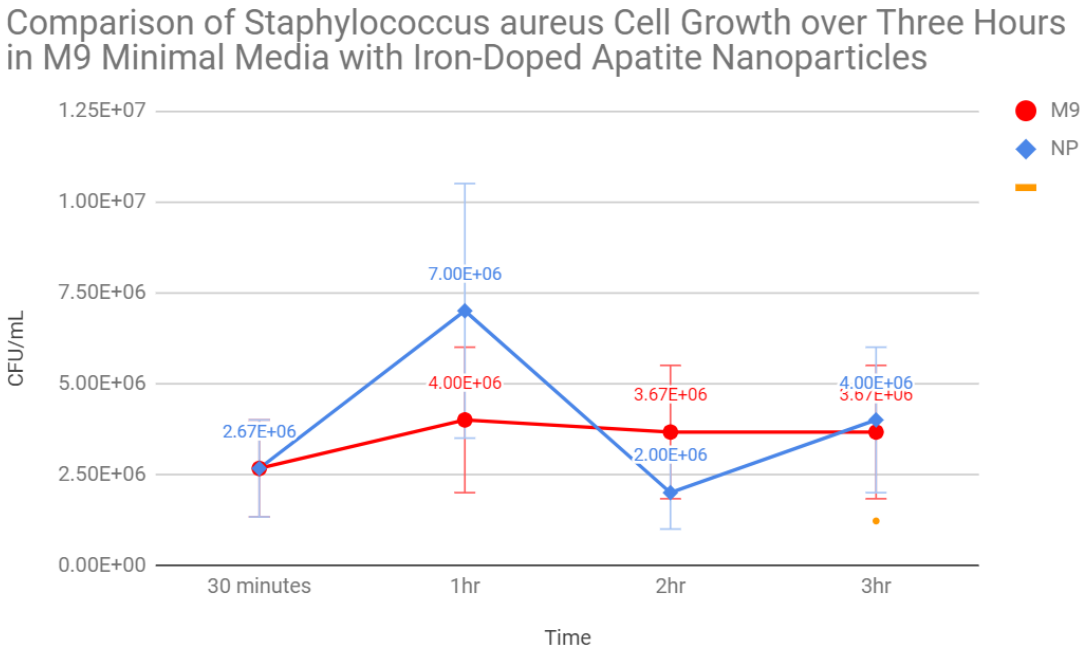

Figure 34. Colony forming units of *S. aureus* in MM++ and IDANP treatments over a three-hour period. Bars indicate standard error.

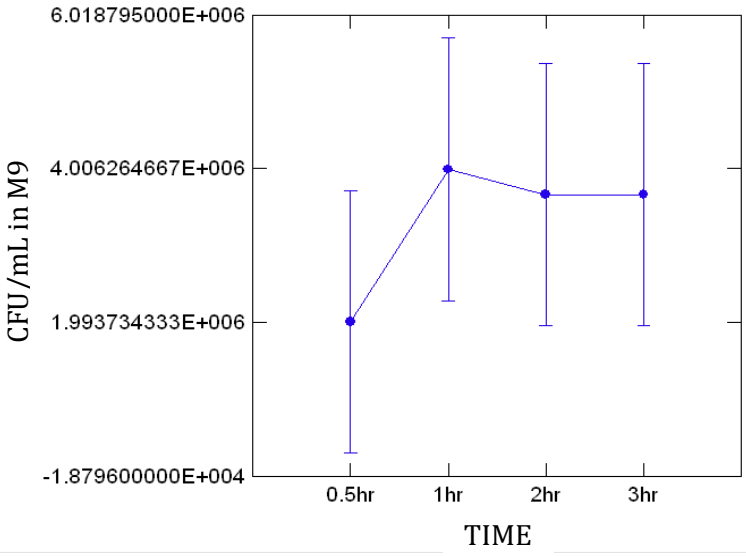

Figure 35. Results of one-way analysis of variance comparing CFU measurements at various times in MM++ in *S. aureus* cells. Bars indicate standard error.

Table 12

Results From Analysis of Variance Comparing CFU Measurements At Various Times in MM++ in S. *aureus Cells*

Source	Type III SS	df	Mean Squares	F-ratio	p-value
TIME$	7.333E+012	3	2.444E+012	1.467	0.295
Error	1.333E+013	8	1.667E+012		

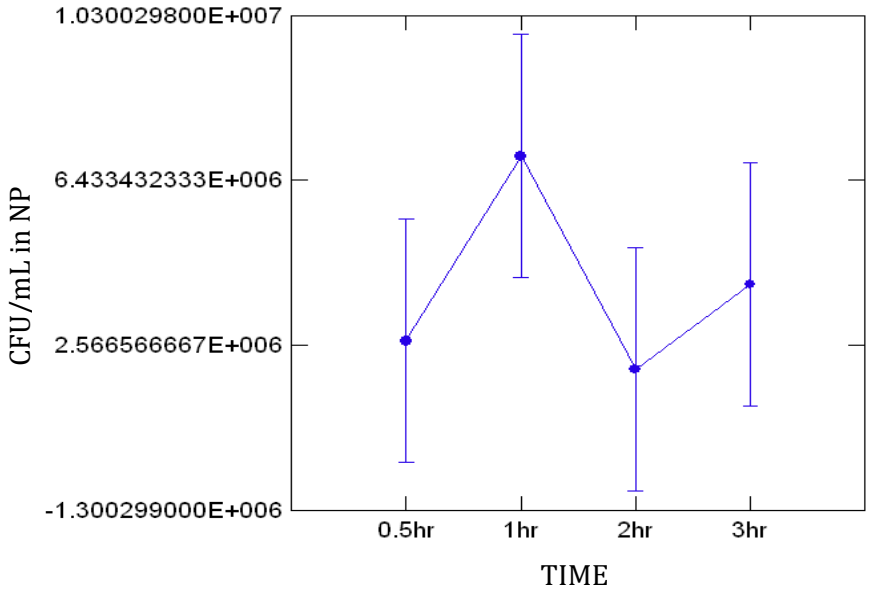

Figure 36. Results of one-way analysis of variance comparing CFU measurements at various times in MM++ in *S. aureus* cells treated with IDANPs. Bars indicate standard error.

Table 13

Results From Analysis of Variance Comparing CFU Measurements At Various Times In MM++ in S. *aureus Cells Treated With IDANPs*

Source	Type III SS	df	Mean Squares	F-ratio	p-value
TIME$	4.425E+013	3	1.475E+013	3.218	0.083
Error	3.667E+013	8	4.583E+012		

Cell growth in the various iron treatments was determined by performing serial dilutions three hours after cells were treated with the different iron treatments. A 1:33 dilution of MM++ was cultured from an overnight culture of MM++, from an overnight culture of TSB++. Half of the treatments were also treated to IDANPs to determine the combined effect of iron treatments and nanoparticle treatment. Cell growth at the lowest iron concentration (0.0004 g/L) was $1.67X10^5$ CFU/mL for IDANPs and $4.00X10^5$ CFU/mL for MM++. At the 0.0008g/L iron concentration, cell growth was $2.33X10^5$ CFU/mL for IDANPs and $2.00X10^5$ CFU/mL for MM++. The two higher concentrations

of iron (0.0016g/L and 0.0032g/L) both showed the same cell growth with $3.33X10^4$ CFU/mL for IDANPs at both concentrations, and $6.67X10^4$ CFU/mL for MM++, also for both concentrations of iron (Figures 37, 41 & 42). It is evident that cell growth decreased with increased iron concentrations. A two-way analysis of variance was performed (Table 14) and showed that there was no significant difference between the different iron treatments (p=0.08). There was no significant difference in cell growth between the MM++ treatments and the IDANP-treated cells (p=0.87), as previous experiments also showed. Further, there was no interaction between iron treatments and IDANP treatments (p=0.17).

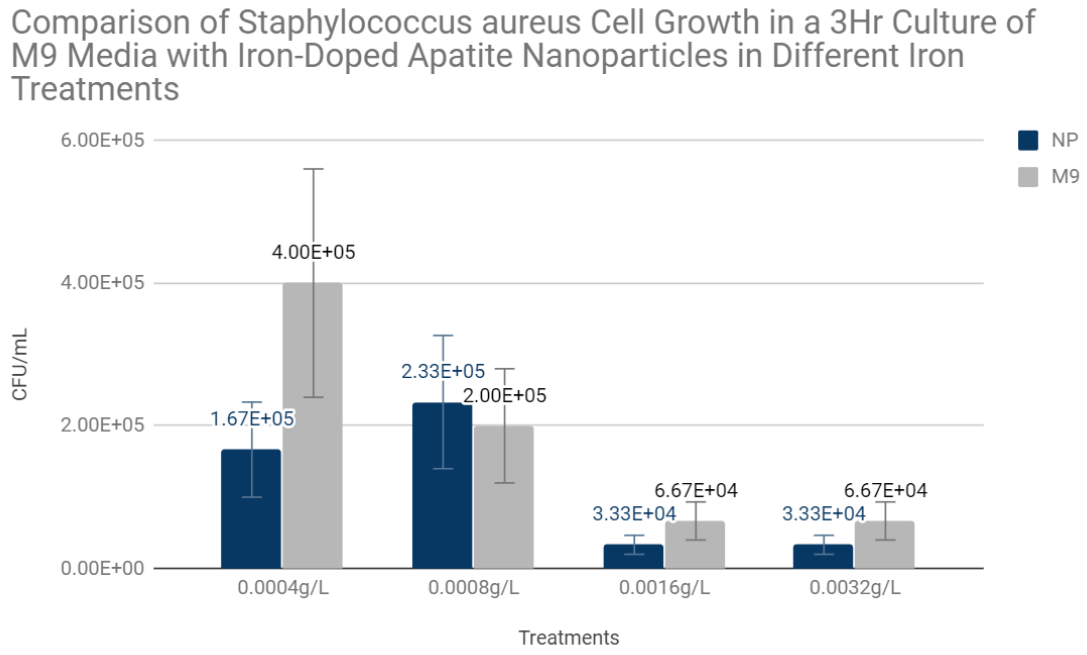

Figure 37. Colony forming units of *S. aureus* in MM++ and IDANP treatment with various iron treatments over a three-hour period. Bars indicate standard error.

Table 14
Two-way Analysis of Variance Comparing Colony Forming Units Grown in MM++ and IDANP Treatment With Various Iron Treatments of S. *aureus*

Source of Variation	*SS*	*df*	*MS*		*F*	*P-value*	*F cr*
Sample (Fe Levels)	138000000000	4	34500000000		2.48	0.08	2
Columns (MM++ vs NP)	382653061.2	1	382653061.2		0.03	0.87	4.
Interaction	101260204082	4	25315051020		1.82	0.17	2
Within	250000000000	18	13888888889				
Total	489642857143	27					

Cell growth was observed in all the iron treatments used for the other experiments, as well as an iron treatment that was two times the highest treatment, at 0.0064 g/L. These cells were sampled from overnight cultures of MM++ in various iron treatments, following an overnight culture of TSB++. This was done to determine the effect of the iron treatments overnight, and if there was a point where the iron treatments had a detrimental effect on the cell growth. The data revealed a pattern in that the lower iron treatments (0.0004 g/L and 0.0008 g/L) had the highest growth at $3.47X10^9$ CFU/mL and $3.27X10^9$ CFU/mL, respectively (Figures 38 and 40). The control growth was $3.00X10^9$ CFU/mL. There was a decline in growth at the medium iron concentration of 0.0016 g/L, with a cell growth of $2.40X10^9$ CFU/mL. Then there was a marked decline in the two highest iron concentrations (0.0032 g/L and 0.0064 g/L) at $1.33X10^9$ CFU/mL and $1.43X10^9$ CFU/mL, respectively. Cells were also grown in TSB++ and the cell growth was $2.45X10^9$ CFU/mL. A one-way analysis of variance was performed to determine significance among these iron treatments. The results showed a significant difference between treatments (p=0.005) (Figure 39; Table 15). These results show the

same pattern of cell growth as the previous experiments, in terms of iron treatments, so it is evident that iron concentrations do affect cell growth, but IDANP treatments do not.

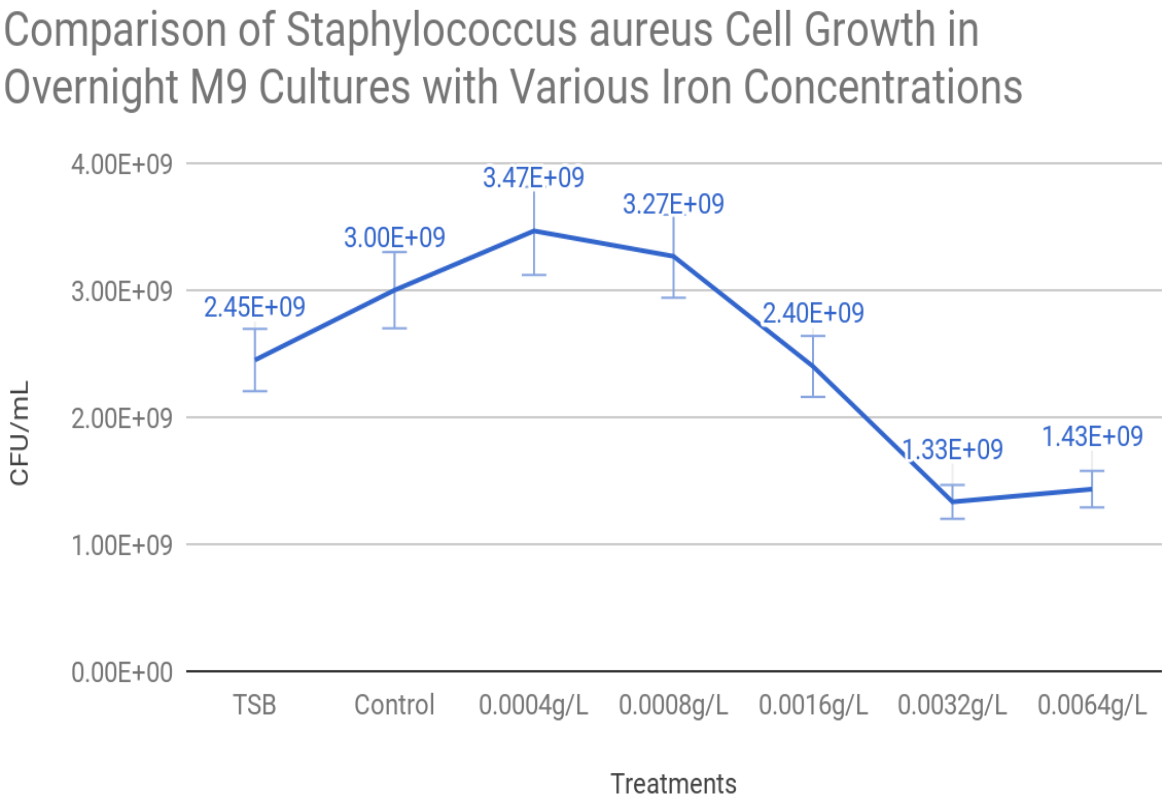

Figure 38. Cell growth in various iron treatments of *S. aureus* cells grown in MM++ overnight.

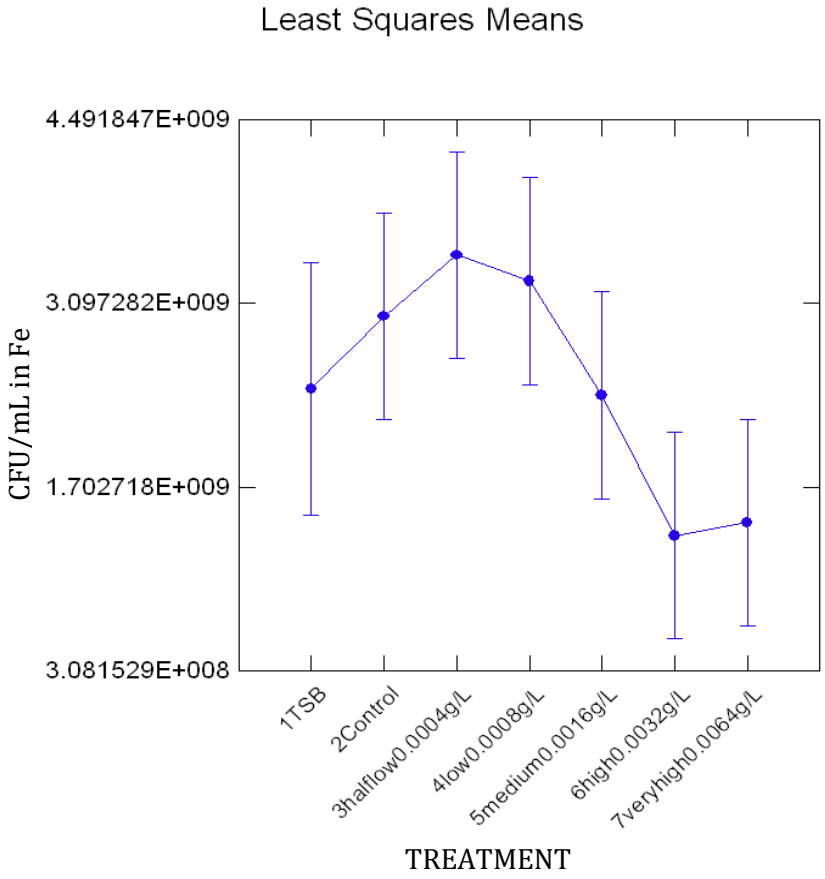

Figure 39. Results from analysis of variance comparing cell growth in various iron treatments of *S. aureus* cells grown in MM++ (p=0.005).

Table 15

Results From Analysis of Variance Comparing Cell Growth in Various Iron Treatments of S. *aureus Cells Grown in MM++*

Source	Type III SS	df	Mean Squares	F-ratio	p-value
TREATMENT$	1.284E+019	6	2.140E+018	5.400	0.005
Error	5.152E+018	13	3.963E+017		

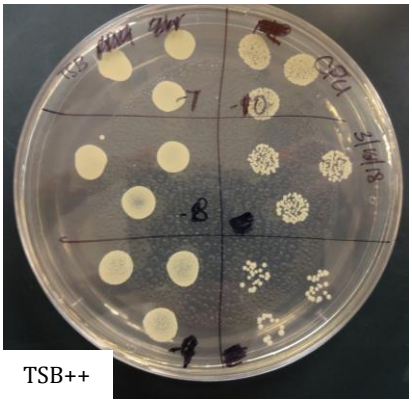

TSB++

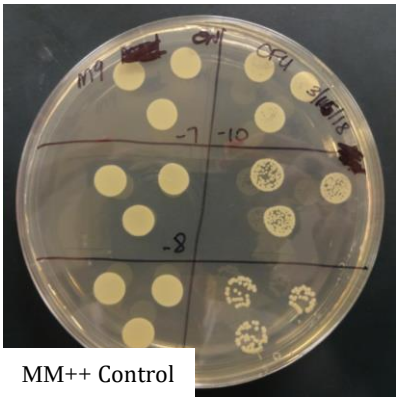

MM++ Control

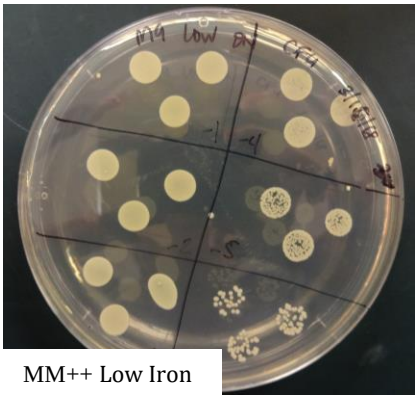

MM++ Low Iron

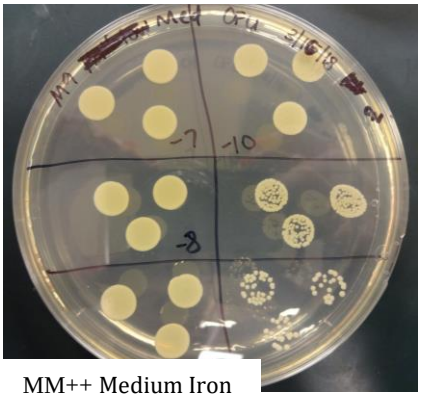

MM++ Medium Iron

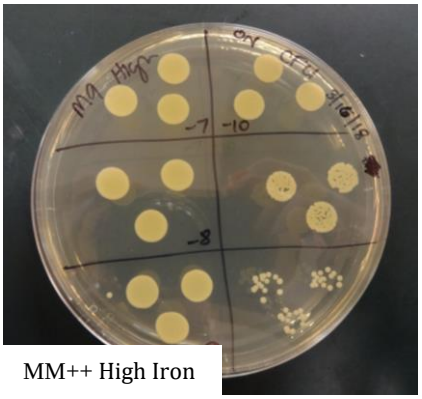

MM++ High Iron

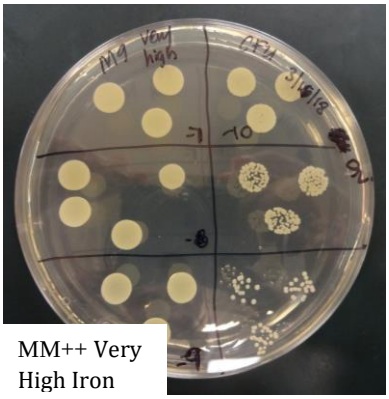

MM++ Very High Iron

Figure 40. S. aureus growth in overnight iron treatments. Top left to bottom right: TSB, MM++, low iron (0.0008g/L), medium iron (0.0016g/L), high iron (0.0032g/L), very high iron (0.0064g/L).

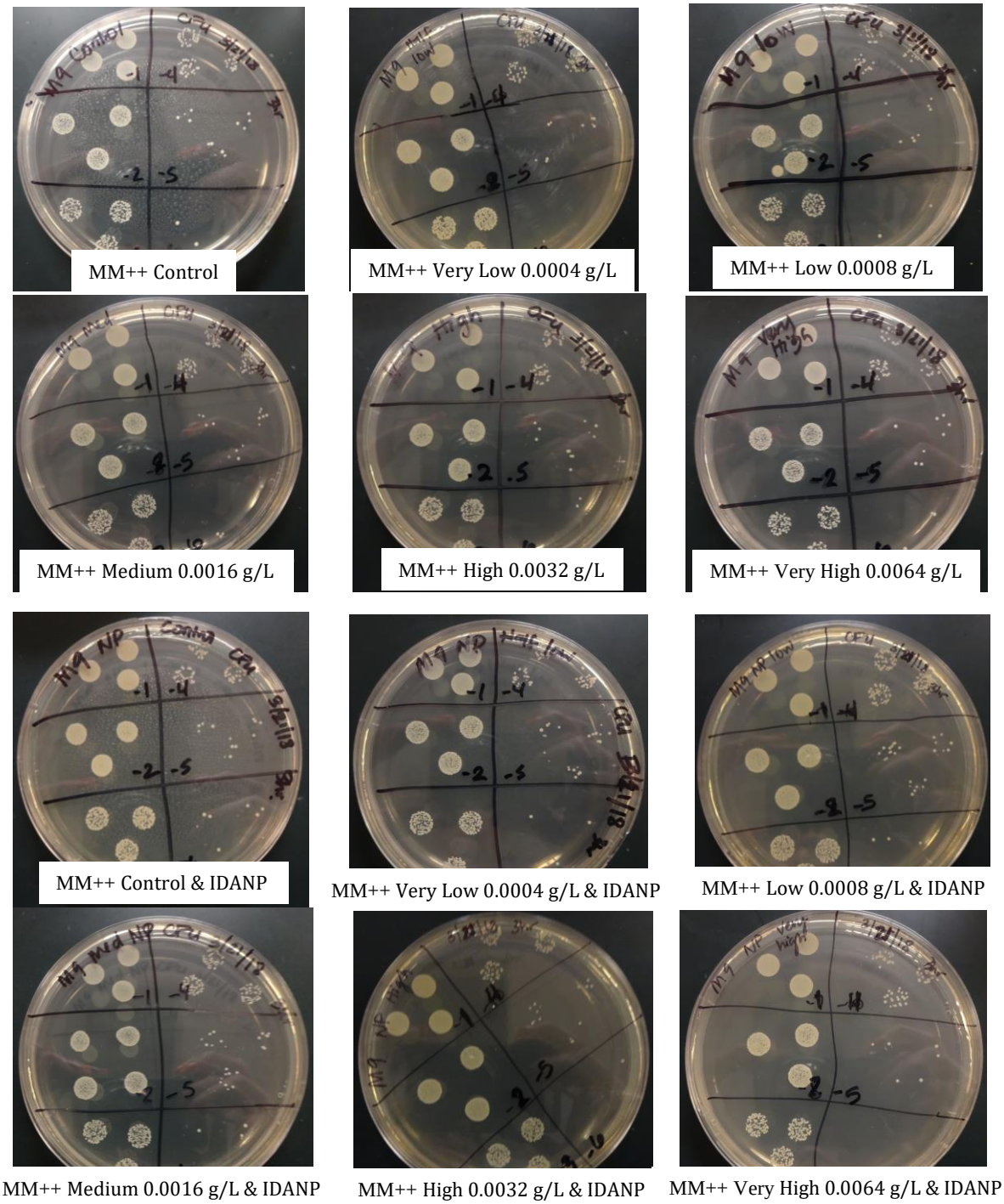

Figure 41. *S. aureus* growth in 3hr iron treatments with and without nanoparticles. Top left to bottom right: No IDANPs - MM++, half low (0.0004g/L), low iron (0.0008g/L), medium iron (0.0016g/L), high iron (0.0016g/L), very high iron (0.0032/L); with IDANPs - MM++, half low (0.0004g/L), low iron (0.0008g/L), medium iron (0.0016g/L), high iron (0.0016g/L), very high iron (0.0032/L).

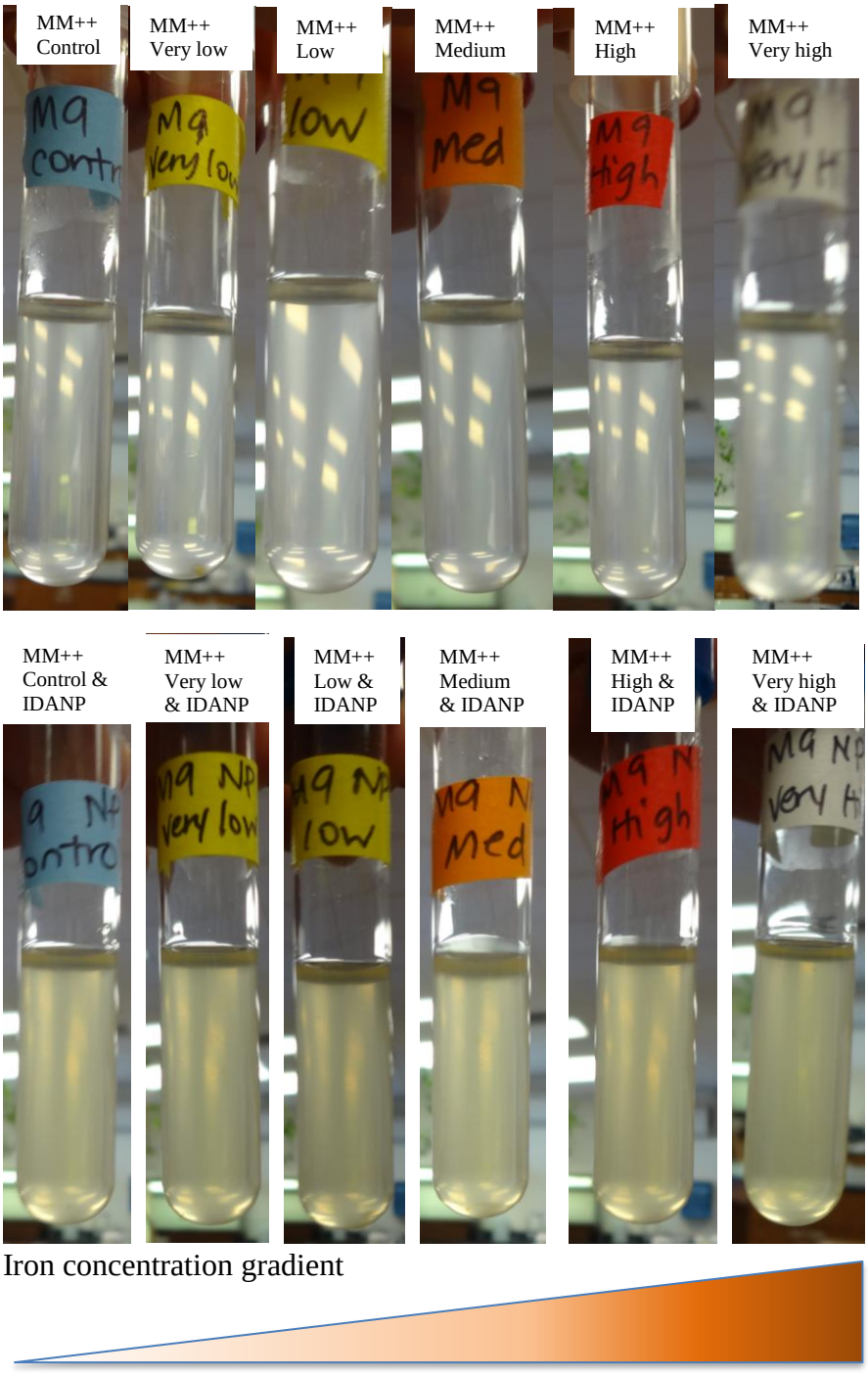

Figure 42. *S. aureus* growth in overnight iron treatments with and without nanoparticles. Top left to bottom right: No IDANPs - MM++, half low (0.0004g/L), low iron (0.0008g/L), medium iron (0.0016g/L), high iron (0.0016g/L), very high iron (0.0032/L); with IDANPs - MM++, half low (0.0004g/L), low iron (0.0008g/L), medium iron (0.0016g/L), high iron (0.0016g/L), very high iron (0.0032/L).

Part 6: Scanning Electron Microscopy of *S. aureus* in MM++, Grown in Various Iron Treatments

To determine whether the presence of iron in the growth media had a resulting effect on cell size or shape, untreated and treated cells in various iron concentrations were imaged using a MIRA 3 TESCAN scanning electron microscope (Figure 43). The results did not show any discernable differences in morphology between the control, low iron (0.0008 g/L), medium iron (0.0016 g/L), high iron (0.0032 g/L) or very high iron (0.0064 g/L). Cells in all treatments had a typical coccus morphology and were usually arranged in clumps.

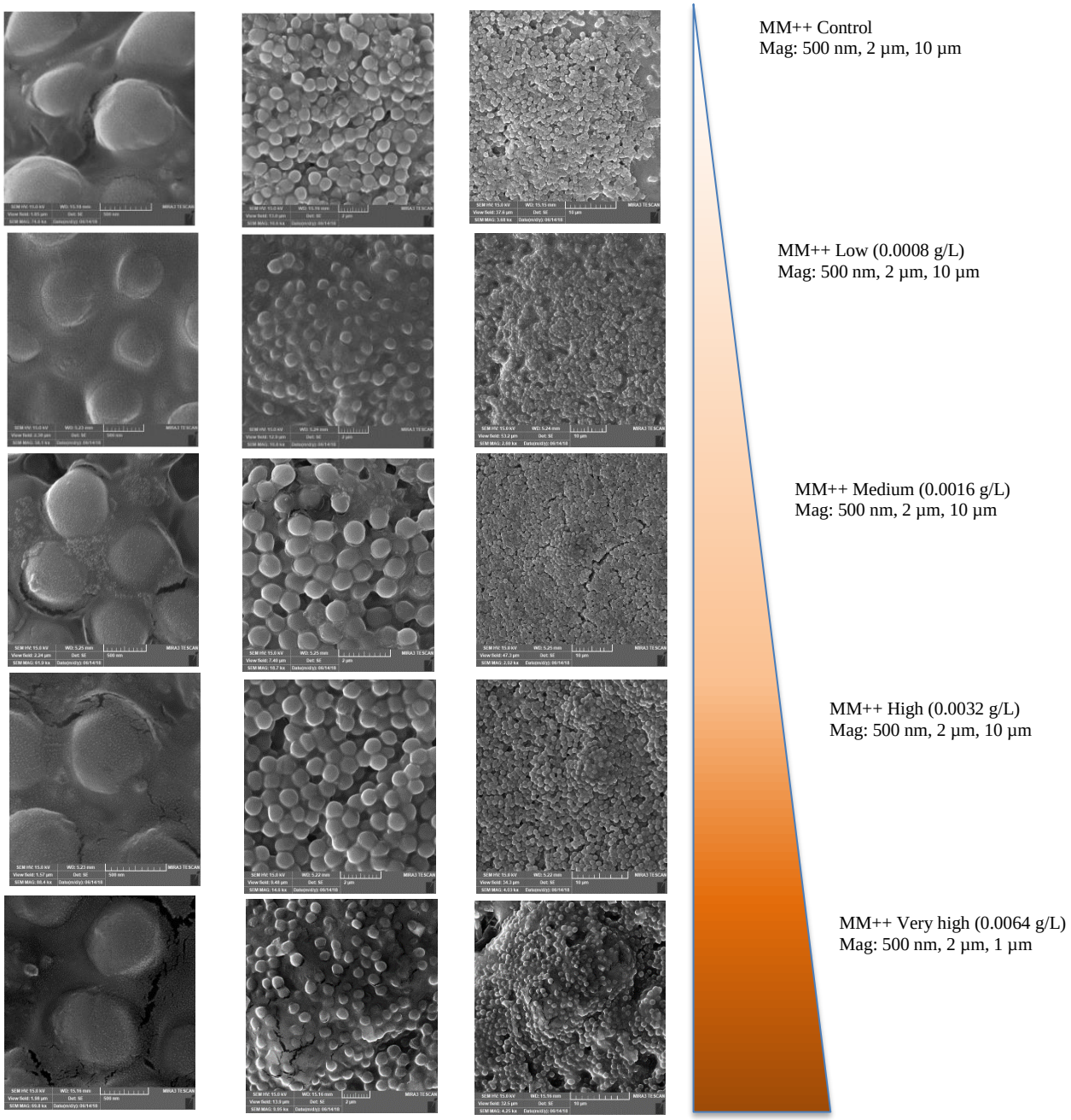

Figure 43. Scanning electron microscopy of *S. aureus* growth in 3hr iron treatments in minimal media. Top to bottom: Control, low iron (0.0008g/L), medium iron (0.0016g/L), high iron (0.0016g/L), very high iron (0.0032/L). Inclusions are the small white dots on the higher resolution images.

Nanoscale inclusions were observed on the cell surfaces and in the interspace between cells. This indicated that the placement of the inclusions was not specific to bacterial surfaces. Energy dispersive spectroscopy was used to identify the nanoscale inclusions. The results revealed that the inclusions were composed of carbon, sodium, nitrogen, phosphorus, sulfur, chloride, oxygen and potassium, which were all components of the MM++. Iron was not identified in these inclusions. These materials mostly likely precipitated out of the minimal media.

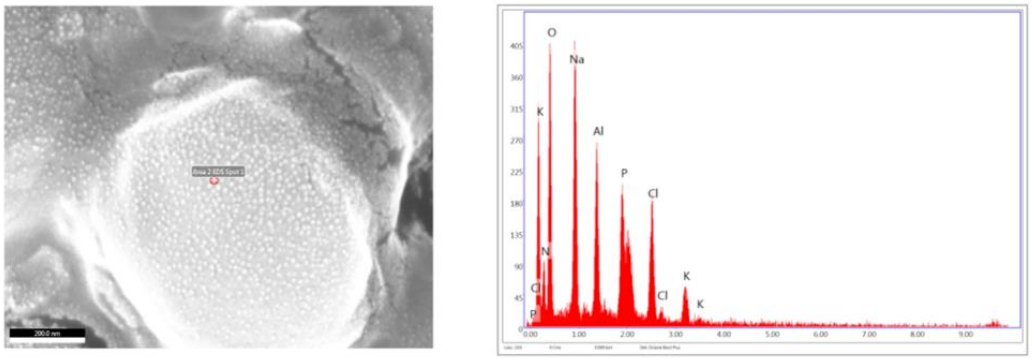

Element	Weight %	Atomic %	Net.-Inten.	Error %	K-ratio
N K	10.1	15.2	40	20.6	20.57786
O K	30.5	40.2	252.5	11.5	11.51989
NaK	20.9	19.2	309.3	8.2	8.16673
AlK	10	7.8	202.4	8.1	8.10558
P K	12.3	8.3	214.8	5.1	5.12871
ClK	11.4	6.8	174.6	7.6	7.60014
K K	4.8	2.6	59	15.5	15.53699

Figure 44. Scanning electron microscopy and energy dispersive spectroscopy identifying composition of nanoscale inclusions of *S. aureus* growth in 3hr iron treatments in minimal media.

Table 16
Summary of Results

Part		**Results**
1 - Iron treatments in MM++ *S. aureus* - JB Phage		Positive, strong linear correlatio and plaque counts: No iron = 1.00; 0.0004g/L iron = 1.34; 0.0016g/L = 1.60; 0.0032g
2 - IDANP -JB Phage- *S. aureus* plaque size	a.	b. Plaque size 15% larger over control c. Plaques size 9.2% larger fro IDANP d. Plaque size 7.8% smaller fr control e. Plaque size 50.8% larger ov f. Plaque size 39% larger over
3 - Medium (0.0016g/L) Iron treatment in MM++ *S. aureus* - JB Phage with IDANPs		Plaque counts with iron and IDA Plaque counts with only IDANP
4 - IDANP - Yodasoda Phage - *M. smegmatis* plaque size	a.	b. Plaque size 25% larger over control c. Plaques size 57.4% larger fr IDANP d. Plaque size 64% larger from control
5 - *S. aureus* cell growth in MM++ with iron treatments and IDANPs	a.	b. M9 Control: $3.33X10^6$; IDA c. No difference in cell counts both M9 and IDANP d. No difference in cells grown various iron treatments over in high iron treatments. e. Difference in cells grown in treatments. Decreased grow

INTERPRETATION, DISCUSSION AND VALUE

Part 1: MM++ *S. aureus* with JB Phage Plaque Assays in Various Iron Treatments

When *S. aureus* cells were grown in MM++ in various iron treatments, the number of plaque counts increased with increased iron. These results were significantly different ($p < 0.05$). The Ferrojan Horse Hypothesis (Bonnain, Breitbart & Buck, 2016) states that the phages may be in competition with iron. It is possible that the increased iron aids in phage infection, or they provide conditions that indirectly facilitate phage infection.

More siderophores are produced when cell are in low iron environments (Hammer & Skaar, 2011). These molecules seek out and bind to iron, then bring it into the cell via iron uptake receptors. In high iron environments, fewer siderophores would be produced and therefore fewer iron uptake receptors would be bound to siderophore-iron complexes. It is possible that the phage is then binding to these vacant iron uptake receptors since the iron requirements of the cell have been met or surpassed.

To test this interaction between the phage and the iron uptake receptors, knockout cells could be used, in which a genetic modification yields the iron receptor genes inactive. Similarly, methods could be used to disable the iron uptake receptors in the cell. If phage infection was reduced in these cells, that would be evidence that the phages are using these receptors to infect cells, shedding light on the mechanism of infection in this system.

Part 2: Effect of IDANP Treatment in *S. aureus* Phage in MM++

S. aureus cells treated with IDANPs and infected with JB phage had 15% larger plaque sizes compared to untreated cells. Additionally, the plaque sizes in IDANP-treated cells continued to increase over time when plates were left to incubate for 48 and 96 hours. Plaque sizes in untreated cells did not change over 48 hours and increased over 96 hours, but to a lesser amount than the treated cells.

There are several factors that can cause increased plaque size (Gallet, Kannoly & Wang, 2011), including adsorption rate, the timing of cell lysis and phage morphology. The IDANPs could be influencing the first two. Since IDANPs also increase plaque count (Gregory, 2017), it is likely that adsorption rate is increased. Further, the IDANPs could be providing some of the raw materials to produce more phages.

Larger plaque sizes and a prolonged effect of phage infections with IDANPs could be important when using phages for phage therapy. These effects could extend and amplify the effects of phage therapy in treating bacterial infections.

Part 3: MM++ *S. aureus* with JB Phage Plaque Assays in Iron Treatments Treated with IDANPs

Cells were grown in the medium iron treatment 0.0016 g/L and then treated with IDANPs to determine the combined effect of both treatments. There was an increase in plaque counts in cells grown in iron treatments and treated with IDANPs. Further, the increase in plaque counts was similar to that of cells grown in the same concentration of iron, but not treated with nanoparticles, compared to no iron. Therefore, the addition of

iron has a predictable effect on the increase of phage infections, and the effect is additive when combined with IDANPs.

Part 4: Effect of IDANP Treatment in *M. smegmatis* with Yodasoda Phage

M. smegmatis showed an increase in plaque sizes when infected with Yodasoda and treated with IDANPs, compared to untreated cells. There was a 20% increase over 24 hours. Plates were also incubated over a 48 hours period to determine if there were prolonged effects of plaque size. Both the IDANP-treated and control cells showed an increase in plaque sizes over time.

This gram-positive host cell/phage biological system also showed the same effect of increased plaque size in cells treated with IDANPs. This could be beneficial when using phages in conjunction with IDANPs in phage therapy in various biological systems. Both systems also showed prolonged effects of IDANPs over time, extending phage infections, and the control group also showed this effect in varying amounts in the two systems.

Part 5: *S. aureus* cell growth in MM++, Various Iron Treatments and with IDANPs

Cell growth was also measured to determine if the iron treatments or IDANPs had any negative effects on the *S. aureus.* In terms of cell growth in MM++, there were no significant differences between the IDANP-treated cells and the untreated cells, which is consistent with previous research (Gregory, 2017). In another experiment, cells were sampled over a three hour period, and there was no significant difference in cell counts in IDANP-treated and untreated cells at the different time periods.

Cells were also grown in the various iron treatments, and treated with IDANPs, compared to an untreated group of iron treatments, for three hours. There was no significant difference between the iron treatments in the IDANP-treated or untreated cells, analyzed separately, although the high iron treatment levels did show a decrease in cell counts, compared to no iron or low iron, which was too low to achieve a lawn on a plate. This can provide an explanation as to why it was difficult to perform plaque assays in the high concentrations of iron. The half low iron treatment (0.0004 g/L) showed the highest growth.

Finally, cells were grown overnight in the various iron treatments to determine if an extended treatment would affect cell growth. Cell counts showed the same pattern of cell growth as the three-hour experiment, with lower cell counts in the two highest iron treatments, and optimal growth in the medium treatment.

These results explain why plaque assays in the higher iron treatments were quite difficult to perform because cell growth was lower than other treatments. The concentration of cells was too low to grow a lawn, so plaques could not be formed.

Additionally, the IDANPs did not negatively affect cell growth, which shows that the mechanism of IDANPs does not involve an overall decrease in cell health but rather an increase in productive phage infections.

Part 6: Scanning Electron Microscopy of *S. aureus* in MM++, Grown in Various Iron Treatments

Scanning electron microscopy showed that there were no morphological differences in the cells that were treated with various concentrations of iron over three hours. Images showed nanoscale inclusions, which were determined to be precipitates

from the MM++. Energy dispersive spectroscopy was performed and showed they were composed of carbon, oxygen, sodium, nitrogen, phosphorus, sulfur, chloride, and potassium. No iron was present in the inclusions. Inclusions appeared uniformly across the cell surfaces and stub surface, indicating that the placement was not specific to bacterial surfaces. The components of the minimal media may have precipitated out during the ethanol drying process.

Summary

IDANPs were found to increase plaque counts and plaque size in various prokaryotic biological systems. These phenomena are both important in terms of medical applications, but also to provide insight on the mechanism of action of these nanoparticles. The mechanism of phage infection is likely related to how these IDANPs interact with the cells. This mechanism likely involves the iron uptake system in the cell, since phage infections are influenced by iron availability in the cell.

One possible explanation for these results is that high iron environments cause the cell to produce less siderophores, which would bind to fewer iron uptake receptors. These receptors may then be available to the phage, which they might be using for infection. However, if the IDANPs are binding to the receptors as an iron-bound siderophore would, this mechanism would not explain the increase in plaque counts in cells treated with IDANPs. Further, an additional supply of iron may provide more raw materials to produce more phage.

Understanding the mechanism of phage infection, and of IDANP-cell interaction can help to develop medical applications and advance phage therapy for a variety of bacterial infections.

REFERENCES CITED

Abedon, S.T. (2011). Bacteriophages and biofilms: ecology, phage therapy, plaques. New York: Nova Science Publishers. 1-131.

Abedon, S.T. & Thomas-Abedon, C. (2010). Phage therapy pharmacology. *Current Pharmacology Biotechnology, 11,* 28-47.

Abedon, S.T., Thomas-Abedon, C., Thomas, A., & Mazure, H. (2011). Bacteriophage prehistory. *Bacteriophage, 1*(3): 174-178.

Abedon S.T. & Yin, J. (2009). Bacteriophage Plaques: Theory and Analysis. In: Clokie M.R., Kropinski A.M. (eds) Bacteriophages. *Methods in Molecular Biology 501*: 161-174.

Akala, R.O., Mazandu, G.K., & Mulder, N.J. (2013). A systems level comparison of *Mycobacterium tuberculosis, Mycobacterium leprae* and *Mycobacterium smegmatis* based on functional interaction network analysis. *Journal of Bacteriology and Parasitology, 4:*173.

Alisky, J., Iczkowski, K., Rapoport, A., & Troitsky, N. (1998) Bacteriophages show promise as antimicrobial agents. *Journal of Infection, 36,* 5-15.

Andrade, M.A., Ciccarelli, F.D., Perez-Iratxeta, C., & Bork, P. (2002). NEAT: a domain duplicated in genes near the components of a putative Fe3+ siderophore transporter from Gram-positive pathogenic bacteria. *Genome Biology, 3,* RESEARCH 0047.

Andriolo, J.M., Hensleigh, R.M., McConnell, C.A., Pedulla, M., Hailer, K., Kasinath, R., Wyss, G., Gleason, W., & Skinner, J.L. (2014). Iron-doped apatite nanoparticles for improvement of phage therapy. *Journal of Vacuum Science and Technology B, 32,* 06FD01.

Andriolo, J.M., Rossi, R.J., McConnell, C.A., Connors, B.I., Trout, K.L., Hailer, K., Pedulla, M. & Skinner, J.L. (2016). Influence of iron-doped apatite nanoparticles on viral infection examined in bacterial versus algal systems. *Institute of Electrical and Electronics Engineers Transactions on Nanobioscience, 15* (8), 908-916.

Antibiotic/Antimicrobial resistance. (2017). *Centers for Disease Control and Prevention.* Retrieved February 4, 2017 from https://www.cdc.gov/drugresistance/.

Antimicrobial resistance. (2017). *World Health Organization Fact Sheets.* Retrieved February 4, 2017 from http://www.who.int/mediacentre/factsheets/fs194/en/.

Beasley, F.C., Vines, E.D., Grigg J.C., Zheng, Q., Liu, S, Lajoie, G.A., Murphy, M.E., & Heinrichs, D.E. (2009). Characterization of staphyloferrin A biosynthetic and transport mutants in *Staphylococcus aureus*. *Molecular Microbiology, 72,* 947-963.

Bonnain, C., Breitbart, M. & Buck, K.N. (2016). The ferrojan horse hypothesis: Iron-virus interactions in the ocean. *Frontiers of Marine Science, 3,* (82).

Capparelli, R., Nocerino, N., Iannaccone, M., Ercolini, D., Parlato, M., Chiara, M., & Iannelli, D. (2010). Bacteriophage therapy of *Salmonella enterica*: a fresh appraisal of bacteriophage therapy. *Journal of Infectious Disease, 201,* 52–61.

Carlton, R.M. (1999). Phage therapy: past history and future prospects. *Archivum Immunologiae et Therapia Experimentalis 47,* 267-274.

Coico, R. (2005). Gram staining. *Current Protocols in Microbiology*. Appendix 3: Appendix 3C.

Corpe, W.A., (1970). Attachment of marine bacteria to solid surfaces. *In* R.s. Manly (ed.), *Adhesion in biological systems.* Academic Press, Inc., New York. pp. 73-87.

Courcol, R.J., Trivier, D., Bissinger, M.C., Martin, G.R., & Brown, M.R. (1997). Siderophore production by *Staphylococcus aureus* and identification of iron-regulated proteins. *Infectious Immunity, 65,* 1944-1948.

Dale, S.E., Sebulsky, M.T., & Heinrichs, D.E. (2004). Involvement of SirABC in iron-siderophore import in *Staphylococcus aureus*. *Journal of Bacteriology, 186,* 8356-8362.

Damo, S.M., Kehl-Fie, T.E., Sugitani, N., Holt, M.E., Rathi, S., Murphy, W., Zhang, Y., Betz, C., Hench, L., Fritz, G., Skaar, E.P., & Chazin, W.J. (2013). Molecular basis for manganese sequestration by calprotectin and roles in the innate immune response for invading bacterial pathogens. *Proceedings of the National Academy of Sciences of the United States of America, 110:*10, 3841-3846.

Danilcauk, M., Lund, A., Saldo, J., Yamado, H., Michalik, J. (2006). Conduction of electron spin resonance of small silver particles. *Spectrochimaca.* Acta Part A *63*: 189-191.

Dar, M.A., Ingle, A., & Rai, M. (2013). Enhanced antimicrobial activity of silver nanoparticles synthesized by *Cryphonectria* sp. Evaluated by singly and in combination with antibiotics. *Nanomedicine: Nanotechnology, Biology, and Medicine, 9,* 105-110.

Drabkin, D. (1951). Metabolism of Hemim Chromoproteins. *Physiological Reviews, 31,* 345-431.

Dryla, A., Gelbmann, D., Von Gabain, A., & Nagy, E., (2003). Identification of a novel iron regulated staphylococcal surface protein with haptoglobin-haemoglobin binding activity. *Molecular Microbiology, 49,* 37-53.

Dryla, A., Hoffmann, B., Gelmann D., Giefing, C., & Hanner, M, et al. (2007). High-affinity binding of the staphylococcal HarA protein to haptoglobin and hemoglobin involves a domain with an antiparallel eight-stranded beta-barrel fold. *Journal of Bacteriology, 189,* 254-264.

Feng, Q.L., Wu, J., Chen, G.Q., Cui, F.Z., Kim, T.N., Kim, J.O. (2008). A mechanistis study of the antibacterial effect of silver ions on *Escherichia coli* and *Staphylococcus aureus. Journal of Biomedical Material Research. 52*: 662-668.

Fischbach, M.A. & Walsh, C.T. (2009). Antibiotics for emerging pathogens. *Science, 325,* 1089-1093.

Friedman, D.B., Stauff, D.L., Pishchany, G., Whitwell, C.W., Torres, V.J., & Skaar, E.P. (2006). *Staphylococcus aureus* redirects central metabolism to increase iron availability. *PLoS Pathology, 2.*

Gallet, R., Kannoly, S., & Wang, I.N. (2011). Effects of bacteriophage traits on plaque formation. *BioMed Central Microbiology, 11:*181.

Gregory, J.M. (2017). Doped apatite nanoparticles: Characterization and biomedical relevance (Doctoral dissertation). Retrieved from ProQuest (ProQuest Number 10285728).

Grigg, J.C., Cheung, J., Heinrichs, D.E., & Murphy, M.E. (2010). Specificity of staphyloferrin B recognition by the SirA receptor from *Staphylococcus aureus*. *Journal of Biological Chemistry, 285,* 34579-34588.

Hajipour, M.J., Fromm, K.M., Ashkarran, A.A., Jimenez de Aberasturi, D., Ruiz de Larramendi, I., Rojo, T., Serpooshan, V., Prak, W.J., & Mahmoudi, M. (2012). Antibacterial properties of nanoparticles. *Trends in Biotechnology, 30* (10), 499-511.

Hammer N.D. & Skaar, E.P. (2011). Molecular mechanisms of *Staphylococcus aureus* in iron acquisition. *Annual Review of Microbiology, 65,* 129-147.

Hatchett, D.W. & Henry, S. (1996). Electrochemistry of sulfur adlayers on low-index faces of silver. *Journal of Physical Chemistry. 100:* 9854-9859.

Hoffmann, C., Leis, A., Niederweis, M., Plitzko, J.M., & Engelhardt, H. (2008). Disclosure of the mycobacterial outer membrane: Cryo-electron tomography and vitreous
sections reveal the lipid bilayer structure. *Proceedings of the National Academy of Sciences of the United States of America, 105:* 10, 3963-3967.

Hwang, I., Hwang, J.H., Choi, H., Kim, K., & Lee, D.G. (2012). Synergistic effects between silver nanoparticles and antibiotics and the mechanisms involved. *Journal of Medical Microbiology, 61,* 1719-1726.

Hyman, P. & Abedon, S.T. (2010). Bacteriophage host range and bacterial resistance. *Advances in Applied Microbiology, 70,* 217-248.

Jones, C.M. & Niederweis, M. (2010). Role of porins in iron uptake of *Mycobacterium smegmatis. Journal of Bacteriology, 192,* (24): 6411-6417.

Jones, CM. & Niederweis, M. (2012). Mycobacterial iron acquisition systems (Doctoral dissertation). University of Alabama at Birmingham.

Kasineth, R.K., McConnell, C., Voyich, J., & Pedulla, M. (2013). On the possibility of modulating bacteriophage virulence employing iron-doped hydroxyapatite biomaterials. *Biological Materials Science Symposium, 2013 The Minerals, Metals and Materials Society Annual Meeting and Exhibition*. San Antonio, TX.

Kim, J.S., Kuk, E., Yu, K. Kim, J.H., Park, S.J. Lee, H.J., Kim, S.H., Park, Y.K., Parkj Y.H., Hwang, C-Y., Kim, Y.K., Lee, Y.S., Jeong, D.H., Cho, M.H. (2007). Microbial effects of silver nanoparticles. *Nanomedicine. 3*: 95-101.

Koch, A.L. (1964). The growth of viral plaques during the enlargement phase. *Journal of Theoretical Biology, 6:* 413-431.

Kohanski, M.A., Dwyer, D.J. & J.J. Collins. (2010). How antibiotics kills bacteria: From targets to networks. *Nature Reviews Microbiology*. *8*(6): 423-435.

Konetschny-Rapp, S., Jung, G., Meiwes., J., & Zahner, H. (1990). Staphyloferrin A: a structurally new siderophore from staphylococci. *European Journal of Biochemistry, 191,* 65-74.

Kuehnert, M.J., Kruszon-Moran D., Hill, H.A., McQuillan, G., McAllister, S.K., Fosheim, G., McDougal, L.K., Chaitram, J., Jensen, B., Fridkin, S.K., Killgore, G., & Tenover, F.C. (2006). Prevalence of *Staphylococcus aureus* nasal colonization in the United States, 2001-2002. *Journal of Infectious Disease, 193*: 172-179.

Loc-Carrillo, C. & Abedon, S.T. (2011). Pros and cons of phage therapy. *Bacteriophage*, 1(2), 111-114.

Matsumara, Y., Yoshikata, K., Kunisaki, S., Tsuchido, T. (2003). Mode of bacterial action of silver zeolite and its comparison with that of silver nitrate. *Applied Environmental Microbiology. 69,* 4278-4281.

Messenger, A.J. & Ratledge, C. (1982). Iron transport in *Mycobacterium smegmatis*: uptake of iron from ferric citrate. *Journal of Bacteriology, 149:* 131-135.

Middlebrook, G., Cohn, M.L. & Schaefer, W.B. (1954). Studies on isoniazid and tubercle bacilli. III. The isolation, drug-susceptibility, and catalase-testing of tubercle bacilli from isoniazid-treated patients. *American Review of Tuberculosis, 70*: 852-872.

Moody, A., (2014). The effects of bacteriophage and nanoparticles on microbial processes. (Masters Thesis). Retrieved from ProQuest (ProQuest Number 1565306).

Neilands, J.B. (1995). Siderophores: Structure and function of microbial iron transport compounds. *The Journal of Biological Chemistry, 270* (45), 26723-26726.

Nickel, A., Pedulla, M., & Kasinath, R. (2010). The effect of nanoparticles on bacteriophage infections. *Nano Science and Technology Institute-Nanotech, 3,* 546-549.

Nickel, A. L. (2010). Synthesis of nanoparticles and their effects on microbial processes. M.S.Thesis, Montana Tech.

Noble, W.C., Valkenburg, H.A., & Wolters C.H. (1967). Carriage of *Staphylococcus aureus* random samples of a normal population. *The Journal of Hygiene, 65,* 567-573.

Pilpa, R.M., Robson, S.A., Villareal, V.A., Wong, M.L., Phillips, M., & Clubb, R.T. (2009). Functionally distinct NEAT (NEAr Transporter) domains within the *Staphylococcus aureus* IsdH/HarA protein extract heme from methemoglobin. *Journal of Biological Chemistry, 284,* 1166-1176.

Pinto-Alphandary, H., Andremont, A., & Couvreur, P. (2000). Targeted delivery of antibiotics using liposomes and nanoparticles: research and applications. *International Journal of Antimicrobial Agents, 13,* 155-168.

Prabhu, S. & Poulose, E.K. (2012). Silver nanoparticles: mechanism of antimicrobial action, synthesis, medical applications, and toxicity effects. *International Nano Letters, 2* (32).

Puck, T.T. & Lee, H.H. (1954). Mechanism of cell wall penetration by viruses: An increase in host cell permeability induced by bacteriophage infections. *Journal of Experimental Medicine, 99* (5): 481-494.

Rakhuba, D.V., Kolomiets, E.I., Szwajcer Dey, E., & Novik, G.I. (2010). Bacteriophage receptors, mechanisms of phage adsorption and penetration into host cell. *Polish Journal of Microbiology, 59* (3), 145-155.

Ramazanov, M.A., Ahmadov, I.S., Ramanzanli, V.N., & Agayeva, N.J. (2016). Effect of nanoparticles on the activity of the electrone ion pumps in plasmatic membrane of plants cells. *Trends in Nanotechnology & Materials Science, (1),* 1-5.

Ratledge, C. & Dover, L.G. (2000). Iron metabolism in pathogenic bacteria. *Annual Review of Microbiology, 54*, 881-941.

Ratledge, C. & Ewing, M. (1996). The occurrence of carboxymycobactin, the siderophore of pathogenic mycobacteria, as a second extracellular siderophore in *Mycobacterium smegmatis. Microbiology, 142* (Pt 8): 2207-2212.

Ratledge, C., Patel, P.V., & Mundy, J. (1982). Iron transport in *Mycobacterium smegmatis:* The location of Mycobactin by electron microscopy. *Microbiology, 128*: 1559-1565.

Ratledge, C. & Marshall, B.J. (1972). Iron transport in *Mycobacterium smegmatis*: the role of mycobactin. *Biochimica et Biophysica Acta, 279:* 58-74.

Sebulsky, M.T., Hothstein, D., Hunter, M.D., & Heinrichs, D.E. (2000). Identification and characterization of a membrane permease involved in iron-hydroxamate transport in *Staphylococcus aureus*. *Journal of Bacteriology, 182*, 4394-4400.

Sebulsky, M.T., Shilton, B.H., Speziali, C.D., & Heinrichs, D.E. (2003). The role of FhuD2 in iron(III)-hydroxamate transport in *Staphylococcus aureus. Journal of Biological Chemistry. 278* (50): 49890-900.

Sebulsky, M.T., Speziali, C.D., Shilton, B.H., Edgell, D.R., & Heinrichs, D.E. (2004). FhuD1, a ferric hydroxamate-binding lipoprotein in *Staphylococcus aureus*: a case of gene duplication and lateral transfer. *Journal of Biological Chemistry, 279*, 53152-53159.

Serwer, P. & Hayes, S.J. (1982). Agarose gel electrophoresis of bacteriophages and related particles. I. Avoidance of binding to the gel and recognizing of particles with packaged DNA. *Electrophoresis, 3*: 76-80.

Shahverdi, A.R., Fakhimi, A., Shahverdi, H.R., & Minaian, S. (2007). Synthesis and effect of silver nanoparticles on the antibacterial activity of different antibiotics against *Staphylococcus aureus* and *Escherichia coli*. *Nanomedicine: Nanotechnology, Biology and Medicine, 3*, 168-171.

Skaar, E.P., Humayun, M., Bae, T., DeBord, K.L., & Schneewind, O. Iron-source preference of *Staphylococcus aureus* infections. *Science, 305,* 1626-1628.

Skurnik, M., Pajunen, M., & Kiljunen, S. (2007). Biotechnology challenges of phage therapy. *Biotechnology Letters, 29,* 995-1003.

Sondi, I., Salopek-Sondi, B. (2004). Silver nanoparticles as antimicrobial agent: A case study on *E. coli* as a model for Gram-negative bacteria. *Journal of Colloid and Interface Science. 275,* 177-182.

Stratton, C.W. (2003). Dead bugs don't mutate: susceptibility issues in the emergence of bacterial resistance. *Emerging Infectious Disease, 9,* 10-16.

Tan, S.Y. & Y. Tatsumura. (2015). Alexander Fleming (1881-1955): Discoverer of penicillin. *Singapore Medical Journal. (56)*7: 366-367.

Tolosano, E. & Altruda, F. (2002). Hemopexin: structure, function, and regulation. *DNA Cell Biology, 21,* 297-306.

Torres V., Pishchany, G., Humayan, M., Schneewind, O., & Skaar, E. (2006) *Staphylococcus aureus* IsdB is a hemoglobin receptor required for heme iron utilization. *Journal of Bacteriology, 188,* 8421-8429.

Wittebole, X., De Roock, S., & Opal, S.M. (2014). A historical overview of bacteriophage therapy as an alternative to antibiotics for the treatment of bacterial pathogens. *Virulence, 5* (1), 226-235.

Yu, S., Fiss, E., & Jacobs, W.R. (1998). Analysis of the exochelin locus in *Mycobacterium smegmatis:* Biosynthesis genes have homology with genes of the peptide synthetase family. *Journal of Bacteriology, 180* (17): 4676-4685.

Zhang, W., Ma, J., Zang, C., Song, Y., & Lui, P. (2011). The Fur transcription regulator and Fur-regulated genes in *Clostridium botulinum* A ATCC 3502. *Journal of Biomedicine and Biotechnology, 2011.*

APPENDICES

APPENDIX A

PART 1 RAW DATA

Table 17

Raw Data of Half Low Iron Concentration (0.0004 g/L)

Experiment T	11/16/17	2.5X10^5 titer	Plaques really hard to see. Probably not valid :(. Used the M9 Media with excess MgSO4... bad idea.					
	Control	Treatment	Standardized to c	control std to control				
1	4	7	1.842105263	1.052631579				
2	5			1.315789474				
3	5	4	1.052631579	1.315789474	ANOVA	p=0.164		
4	2	4	1.052631579	0.5263157895	Kruskal Wallis	p=0.211		
5	3	6	1.578947368	0.7894736842				
negative control	0	0						
Average	3.8	Standardized Av	1.381578947	1				
Experiment U	11/17/17	2.5X10^5 titer	Plaques really hard to see. Probably not valid :(. Used the M9 Media with excess MgSO4... bad idea.					
	Control	Treatment	Standardized to c	control std to control				
1	4	6	1.5	1				
2	5	4	1	1.25				
3	4	6	1.5	1	ANOVA	p=0.368		
4	6	6	1.5	1.5	Kruskal Wallis	p=0.382		
5	1	3	0.75	0.25				
Average	4	Standardized Av	1.25	1				
Overall through Experiment U								
p=0.041								
KW p=0.102								
Average = 1.315								
Experiment X	12/11/17	5X10^5 titer	1:5 dilution. Too high but plaques evident and lawn thick.					
	Control	Treatment	Standardized to c	control std to control				
1	1	2	1	0.5				
2	3	3	1.5	1.5				
3	2	3	1.5	1	ANOVA	0.437		
4		2	1		Kruskal Wallis	0.445		
Average	2	Standardized Av	1.25	1				
Overall through experiment X								
p=0.002								
p=0.034								
Average = 1.2933								

Table 18

Raw Data of Low Iron Concentration (0.0008 g/L)

Experiment A	9/28/17	10^-5 titer				Overall low treatments: p=0.131; not significant			Overall low Average
	Control	Treatment	Treatment Standardized to Control		Control	Control Standardized to Control Mean			1.514149914
1	105	92	1.281337047		105	1.462395543			
2	71	81	1.128133705		71	0.9888579387			
3	64	91	1.267409471		64	0.8913649025		p=0.254	
4	63	66	0.9192200557		63	0.8774373259	Kruskal Wallis nonparametric p=0.175		
5	56	90	1.253481894		56	0.7799442897			
negative control	0	0							
Average	71.8	Standardized Aw	1.169916435						
Standard deviatic	19.30543965	10.9772492							
Experiment D	10/1/17	10^-5 titer							
	Control	Treatment	Treatment Standardized to Control						
1	no growth	22	0.8979591837		28	1.142857143			
2	28	22	0.8979591837		29	1.183673469		p=0.583	
3	29	31	1.265306122		17	0.693877551	Kruskal Wallis nonparametric p=0.561		
4	17	low growth			24	0.9795918367			
5	24	12	0.4897959184						
negative control	0	0							
Average	24.5	Standardized Aw	0.887755102						
Standard deviatic	5.446711546	7.762087348							
Experiment H	10/6/17	10^-5 titer							
	Control	Treatment	Treatment Standardized to Control						
1	7	1	0.2272727273		7	1.590909091			
2	3	6	1.363636364		3	0.6818181818			
3	5	6	1.363636364		5	1.136363636		p=0.752	
4	4	6	1.363636364		4	0.9090909091	Kruskal Wallis nonparametric p=0.523		
5	3	5	1.136363636		3	0.6818181818			
negative control	0	0							
Average	4.4	Standardized Aw	1.090909091						
Standard deviatic	1.673320053	2.167948339							
Experiment L	10/13/17	5X10^-4 titer							
	Control	Treatment	Treatment Standardized to Control						
1	44	110	1.724137931		44	0.6896551724			
2	55	108	1.692789969		55	0.8620689655			
3	74	92	1.44200627		74	1.159874608		p=0.001	
4	61	115	1.802507837		61	0.9561128527	Kruskal Wallis nonparametric p=0.009		
5	85	138	2.163009404		85	1.332288401			
negative control	0	0							
Average	63.8	Standardized Aw	1.764890282						
Standard deviatic	16.0530371	16.60722734							
Experiment M	10/14/17	5X10^-4 titer							
	Control	Treatment	Treatment Standardized to Control						
1	169	202	0.9950738916		169	0.8325123153			
2	213	223	1.098522167		213	1.049261084		p=0.270	
3	223	230	1.133004926		223	1.098522167	Kruskal Wallis nonparametric p=0.009		
4	192	226	1.113300493		192	0.9458128079			
5	218	203	1		218	1.073891626			
negative control	0	0							
Average	203	Standardized Aw	1.067980296						
Standard deviatic	22.37185732	13.29285522							
Experiment R	11/10/17	2.5*10^-5 titer							
	Control	Treatment	Treatment Standardized to Control						
1	clumped agar	clumped agar							
2	35	91	1.459900855	0.5615003289					
3	88	82	1.315515056	1.411772255	p=-0.149				
4	64	138	2.213915582	1.026743459	KW p=0.0127				
negative control	0	0							
Average	62.33333333	Standardized Aw	1.663110498						
Standard deviatic	26.53927907	30.0721355							
Experiment S	11/11/17	2.5*10^-5 titer							
	Control	Treatment	Treatment Standardized to Control						
1	63	105	1.485850458	0.8915178445					
2	49	125	1.768884612	0.693402768					
3	100	127	1.797168964	1.41510769	p=-0.017				
4		135	1.910376457		KW p=0.034				
negative control		123							
Average	70.66666667	Standardized Aw	1.740570123	1.000009434					
Standard deviatic	36.06244584	5.291502622							

Table 19

Raw Data of Medium Iron Concentration (0.0016 g/L)

Experiment B	9/29/17	10^-5 titer			
	Control	Treatment	Standardized to Control		
1	8	24	2.4		
2	17	13	1.3		
3	7	27	2.7		
4	10	20	2		
5	8		0		
negative control	0	0			
Average	10	Standardized Ave	1.68		Average
Experiment N	10/27/17	5X10^4 titer			
	Control	Treatment	Standardized to (	control std to control	
1	203	284	1.584379358	1.132496513	
2	tip not in	268	1.49511855		
3	119	242	1.350069735	0.6638772664	ANOVA
4	220	257	1.433751743	1.227336123	Kruskal Wallis
5	175	259	1.444909344	0.9762900976	
negative control	0	0			
Average	179.25	Standardized Ave	1.461645746	1	
Experiment O	10/28/17	5X10^4 titer			
	Control	Treatment	Standardized to (	control std to control	
1	425	476	1.043859649	0.9320175439	
2	412	542	1.188596491	0.9035087719	ANOVA
3	469	543	1.190789474	1.028508772	Kruskal Wallis
4	453	559	1.225877193	0.9934210526	
5	521	525	1.151315789	1.14254386	
negative control	0	0			
Average	456	Standardized Ave	1.160087719		
Experiment P	10/28/17	titer 10^-5			
	Control	Treatment	Standardized to (	control std to control	
1		43	1.954545455	0	
2		31	1.409090909	0	
3	22	39	1.772727273	1	
4	24	34	1.545454545	1.090909091	
5	20	56	2.545454545	0.9090909091	
negative control	0	0			
Average	22	Standardized Ave	1.845454545		
Experiment Q	10/28/17	titer 1.67 x 10^-5			
	Control	Treatment	Standardized to (	control std to control	
1	56	119	2.07860262	0.9781659389	
2	52	112	1.956331878	0.9082969432	
3	73	114	1.991266376	1.27510917	
4	48	106	1.851528384	0.8384279476	
5		83	1.449781659		
negative control	0	0			
Average	57.25	Standardized Ave	1.865502183		
OVERALL AVERAGE SO FAR					
Control	1				
Medium	1.602538039				

Table 20

Raw Data of High Iron Concentration (0.0032 g/L)

Experiment C	9/1/17	10^-5 titer					
	Control	Treatment	Treatment Stand	Control	Control Standardized to Control Mean		
1	59	49	1.725352113	59	2.077464789		
2	22	46	1.61971831	22	0.7746478873		
3	14	45	1.584507042	14	0.4929577465		
4	29	67	2.35915493	29	1.021126761		p<0.05
5	18	80	2.816901408	18	0.6338028169		
negative control	0	0		Control Average	1		
Average	28.4	Standardized Av	2.021126761				
Experiment I	10/10/17	10^-4 titer					
	Control	Treatment	Treatment Standardized to Control				
1	108	186	1.036789298	108	0.602006689		
2	140	316	1.761426979	140	0.7803790412		
3	171	310	1.727982163	171	0.9531772575		
4	157	343	1.911928651	157	0.8751393534		
5	321	251	1.399108138	321	1.789297659		p=0.06
negative control	0	0		Control Average	1		
Average	179.4	Standardized Av	1.567447046				
Standard deviatic	82.57299801	62.91820086					
Experiment J	10/10/17	5X10^-5 titer					
	Control	Treatment	Treatment Standardized to Control				
1	47	166	1.482142857	47	0.4196428571		
2	46	176	1.571428571	46	0.4107142857		
3	63	209	1.866071429	63	0.5625		p=0.05
4	171	226	2.017857143	171	1.526785714		
5	233	280	2.5	233	2.080357143		
negative control	0	0					
Average	112	Standardized Av	1.8875				
Standard deviatic	85.29947245	45.38501955					

APPENDIX B

PART 2 RAW DATA

Table 21

Raw Data IDANP – JB Phage – S. *aureus plaque size*

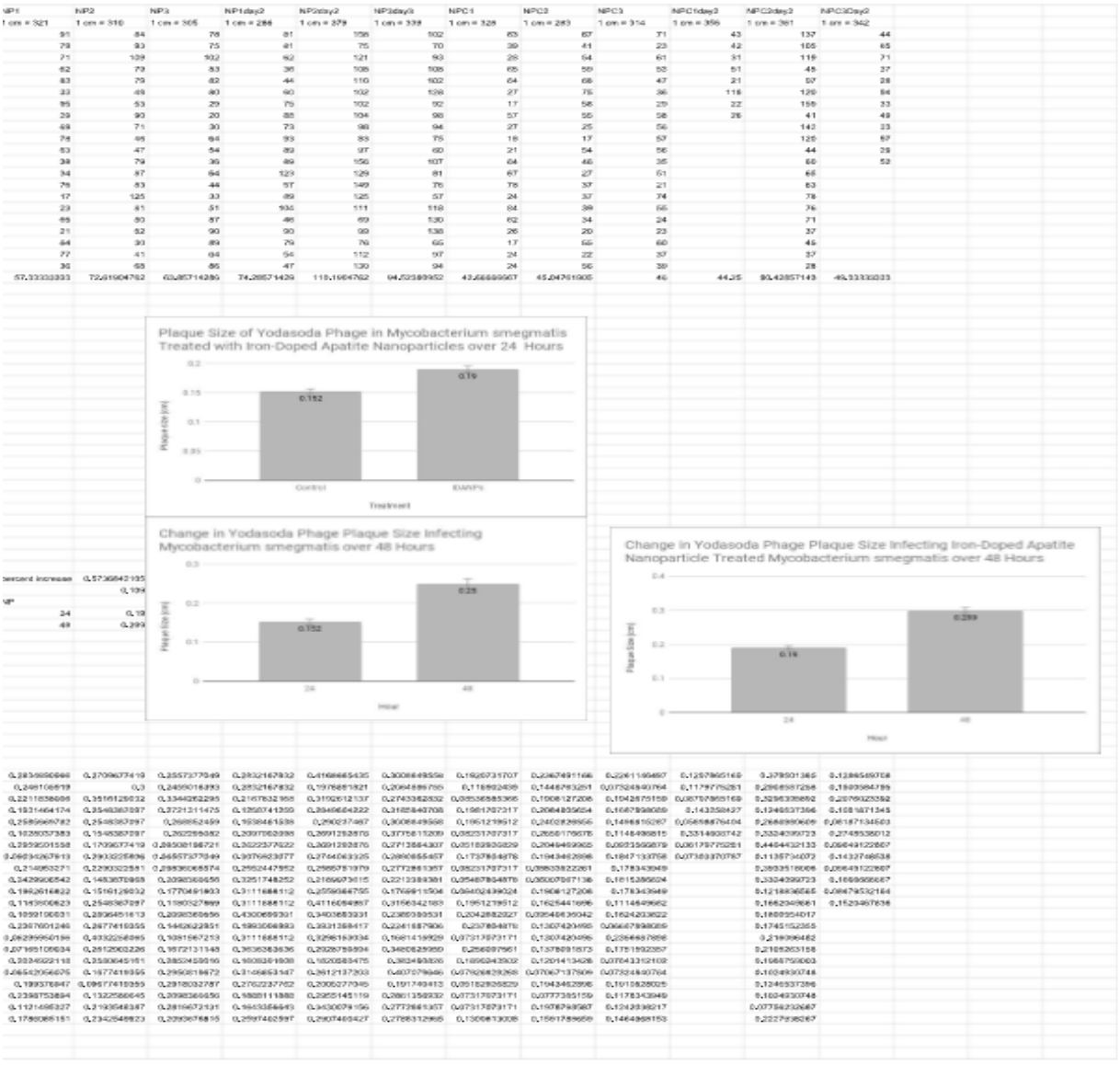

NP 1	NP 2	NP1 day 2	NP2 day 2	NPC1	NPC2	NPC1 day 2	NPC2 Day 2
1 cm = 333	1 cm = 321	1 cm = 341	1 cm = 315	1 cm = 358	1 cm = 319	1 cm = 341	1 cm = 356
71	67	145	142	73	75	125	117
93	44	115	131	65	67	40	125
82	46	76	107	23	51	105	114
62	53	117	96	39	66	124	143
51	46	63	99	75	49	61	123
72	50	94	102	64	27	91	99
46	34	85	86	57	31	127	132
51	54	123	104	36	46	92	136
72	68	91	121	66	47	104	132
57	41	91	107	80	28	133	123
48	60	118	101	25	65	102	137
94	55	112	94	30	57	137	142
79	64	82	112	69	92	118	124
66	63	57	142	57	59	10	138
25	67	89	90	52	43	106	123
53	66	92	100	67	35	94	118
23	91	105	97	85	39	85	138
66	55	102	120	69	44	122	148
83	30	95	120	50	46	143	100
30	45	109	120	65	56	24	86
41	53	128	147	36	81	91	158
56	59	109	112	38	62	75	109
42	41	90	143	42	59	53	109
33	51	86	110	72	30	100	84
48	65	83	96	47	44	71	91
51	51	105	123	81	54		
57	99	134	83	46	69		
56	120	127	100	61	61		
59	71	81	99	107	52		
57	60	86	85	65	52		
44	56	137	75	39	30		
60	85	109	99	110	85		
66	52		36	128	65		
60	68		80	67	34		
73	74		83	44	42		
59	101		98	66	34		
60	63		141	60	70		
33	88		116	35	38		
24	79		114	29	44		
89	83		85	100			
102	68		112	35			
75	93		96	35			
57	57		109	30			
30	49		131	30			
42	73		121	75			
53	52		56	35			
79	49			26			
72	78			27			
47	26			23			
52	57			25			
95	57			27			
52	59			35			
61	53						
59	56						
19	24						
14	50						
30	66						
74							
56,96275862	61,14035088	101,125	105,2391304	54,28846154	52,02564103	93,32	121,84

Control	0,152
IDANPs	0,19
	-0,038
Percent higher N	-0,2

0,2132132132	0,2087227414	0,4252199413	0,4507936508	0,2039106145	0,2351097179	0,366568915	0,3286516854
0,2792792793	0,1370716511	0,3372434018	0,4158730159	0,1815642458	0,210031348	0,1173020528	0,3511235955
0,2462462462	0,1433021807	0,2228739003	0,3396825397	0,06424581006	0,1598746082	0,3079178886	0,3202247191
0,1861861862	0,1651090343	0,3431085044	0,3047619048	0,1089385475	0,2068965517	0,3636363636	0,4016853933
0,1531531532	0,1433021807	0,1847507331	0,3142857143	0,2094972067	0,1536050157	0,1788856305	0,345505618
0,2162162162	0,1557632399	0,275659824	0,3238095238	0,1787709497	0,08463949843	0,2668621701	0,2780898876
0,1381381381	0,1059190031	0,2492668622	0,273015873	0,1592178771	0,09717868339	0,3724340176	0,3707865169
0,1531531532	0,1682242991	0,3607038123	0,3301587302	0,1005586592	0,144200627	0,2697947214	0,3820224719
0,2162162162	0,2118380062	0,2668621701	0,3841269841	0,1843575419	0,1473354232	0,3049853372	0,3707865169
0,1711711712	0,1277258567	0,2668621701	0,3396825397	0,2234636872	0,08777429467	0,3900293255	0,345505618
0,1441441441	0,1869158879	0,3460410557	0,3206349206	0,06983240223	0,2037617555	0,2991202346	0,3848314607
0,2822822823	0,1713395639	0,3284457478	0,2984126984	0,08379888268	0,1786833856	0,4017595308	0,3988764045
0,2372372372	0,199376947	0,2404692082	0,3555555556	0,1927374302	0,2884012539	0,3460410557	0,3483146067
0,1981981982	0,1962616822	0,1671554252	0,4507936508	0,1592178771	0,1849529781	0,0293255132	0,3876404494
0,07507507508	0,2087227414	0,2609970674	0,2857142857	0,1452513966	0,1347962382	0,3108504399	0,345505618
0,1591591592	0,2056074766	0,2697947214	0,3174603175	0,187150838	0,1097178683	0,275659824	0,3314606742
0,06906906907	0,2834890966	0,3079178886	0,3079365079	0,2374301676	0,1222570533	0,2492668622	0,3876404494
0,1981981982	0,1713395639	0,2991202346	0,380952381	0,1927374302	0,1379310345	0,357771261	0,4157303371
0,2492492492	0,09345794393	0,2785923754	0,380952381	0,1396648045	0,144200627	0,4193548387	0,2808988764
0,09009009009	0,1401869159	0,3196480938	0,380952381	0,1815642458	0,1755485893	0,07038123167	0,2415730337
0,1231231231	0,1651090343	0,3753665689	0,4666666667	0,1005586592	0,2539184953	0,2668621701	0,4438202247
0,1681681682	0,1838006231	0,3196480938	0,3555555556	0,1061452514	0,1943573668	0,219941349	0,3061797753
0,1261261261	0,1277258567	0,2639296188	0,453968254	0,1173184358	0,1849529781	0,1554252199	0,3061797753
0,0990990991	0,1588785047	0,2521994135	0,3492063492	0,2011173184	0,09404388715	0,293255132	0,2359550562
0,1441441441	0,2024922118	0,2434017595	0,3047619048	0,1312849162	0,1379310345	0,2082111437	0,2556179775
0,1531531532	0,1588785047	0,3079178886	0,3904761905	0,2262569832	0,1692789969		
0,1711711712	0,308411215	0,3929618768	0,2634920635	0,1284916201	0,2163009404		
0,1681681682	0,3738317757	0,3724340176	0,3174603175	0,1703910615	0,1912225705		
0,1771771772	0,2211838006	0,2375366569	0,3142857143	0,2988826816	0,1630094044		
0,1711711712	0,1869158879	0,2521994135	0,2698412698	0,1815642458	0,1630094044		
0,1321321321	0,1744548287	0,4017595308	0,2380952381	0,1089385475	0,09404388715		
0,1801801802	0,2647975078	0,3196480938	0,3142857143	0,3072625698	0,2664576803		
0,1981981982	0,1619937695		0,1142857143	0,3575418994	0,2037617555		
0,1801801802	0,2118380062		0,253968254	0,187150838	0,1065830721		
0,2192192192	0,230529595		0,2634920635	0,1229050279	0,131661442		
0,1771771772	0,3146417445		0,3111111111	0,1843575419	0,1065830721		
0,1801801802	0,1962616822		0,4476190476	0,1675977654	0,2194357367		
0,0990990991	0,2741433022		0,3682539683	0,09776536313	0,1191222571		
0,07207207207	0,246105919		0,3619047619	0,08100558659	0,1379310345		
0,2672672673	0,2585669782		0,2698412698	0,2793296089			
0,3063063063	0,2118380062		0,3555555556	0,09776536313			
0,2252252252	0,2897196262		0,3047619048	0,09776536313			
0,1711711712	0,1775700935		0,346031746	0,08379888268			
0,09009009009	0,1526479751		0,4158730159	0,08379888268			
0,1261261261	0,2274143302		0,3841269841	0,2094972067			
0,1591591592	0,1619937695		0,1777777778	0,09776536313			
0,2372372372	0,1526479751			0,07262569832			
0,2162162162	0,2429906542			0,07541899441			
0,1411411411	0,08099688474			0,06424581006			
0,1561561562	0,1775700935			0,06983240223			
0,2852852853	0,1775700935			0,07541899441			
0,1561561562	0,1838006231			0,09776536313			
0,1831831832	0,1651090343						
0,1771771772	0,1744548287						
0,05705705706	0,07476635514						
0,04204204204	0,1557632399						
0,09009009009	0,2056074766						
0,2222222222							

APPENDIX C

PART 3 RAW DATA

Table 22

Raw Data of Medium (0.0016 g/L) Iron Treatment in M9 Minimal Media with S. *aureus JB Phage in IDANPs*

ControlFe	28	1.12	Experiment C	1						
ControlFe	23	0.92	4/12/18	1		NP	Control		NP	Control
ControlFe	40	1.6	Medium Fe (90%)	1						
ControlFe	9	0.36		1	1.2	1.2	1.12		1.2	1.12
NPFe	30			1.2	2.12	2.12	0.92		2.12	0.92
NPFe	53			2.12	3.56	3.56	1.6		3.56	1.6
NPFe	89			3.56	1.32	1.32	0.36		1.32	0.36
NPFe	33			1.32	1.25	1.25	0		1.25	0
				2.05	1.5625	1.5625	0.625		1.5625	0.625
					2.5	2.5	0.9375		2.5	0.9375
					1.25	1.25	1.5625		1.25	1.5625
					1.5625	1.5625	1.875		1.5625	1.875
					1.813888889	1.151560178	0.7726597325		1.151560178	0.7726597325
ControlFe	0	0	Experiment D			1.515601783	1.069836553		1.515601783	1.069836553
ControlFe	2	0.625	4/13/18			1.716196137	0.5943536404		1.716196137	0.5943536404
ControlFe	3	0.9375	Medium Fe 90%			1.857355126	1.500742942		1.857355126	1.500742942
ControlFe	5	1.5625	Full titer			1.567607727	1.062407132		1.567607727	1.062407132
ControlFe	6	1.875	Left for weekend...			1.723808639			0.880952381	1
	3.2								1.071428571	1
						p=0.003			2.19047619	1
NPFe	4	1.25							1.44	1
NPFe	5	1.5625							1.00	1.650898783
NPFe	8	2.5								
NPFe	4	1.25								
NPFe	5	1.5625							p=0.001	
		1.625								
ControlFe	104	0.7726597325	Experiment E							
ControlFe	144	1.069836553	4/18/18							
ControlFe	80	0.5943536404	Medium Fe 90%							
ControlFe	202	1.500742942	Full titer Looks great!							
ControlFe	143	1.062407132								
	134.6									
NPFe	155	1.151560178								
NPFe	204	1.515601783								
NPFe	231	1.716196137								
NPFe	250	1.857355126								
NPFe	211	1.567607727								
		1.56166419								
ControlFe	1440		Experiment F							
ControlFe	x		4/20/18							
ControlFe	3		Medium Fe 90%							
ControlFe	192		Good! Two different TA							
ControlFe	42									
	42									
NPFe	2076									
NPFe	x									
NPFe	37	0.880952381								
NPFe	45	1.071428571								
NPFe	92	2.19047619								
		1.380952381								
	1,441666667									

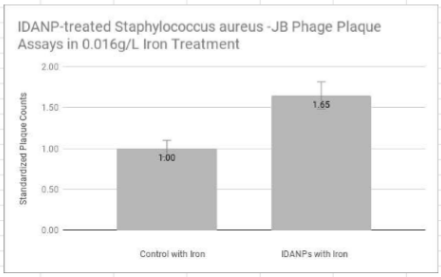

APPENDIX D

PART 4 RAW DATA

Table 23

Raw Data of IDANP – Yodasoda phage – M. *smegmatis Plaque Size*

NP1	NP2	NP3	NP1day2	NP2day2	NP3day3	NPC1	NPC2	NPC3	NPC1day2	NPC2day2	NPC3Day2
1 cm = 321	1 cm = 310	1 cm = 305	1 cm = 286	1 cm = 379	1 cm = 339	1 cm = 328	1 cm = 283	1 cm = 314	1 cm = 356	1 cm = 361	1 cm = 342
91	84	78	81	158	102	63	67	71	43	137	44
79	93	75	81	75	70	39	41	23	42	105	65
71	109	102	62	121	93	28	54	61	31	119	71
62	79	83	36	108	108	65	59	53	51	45	37
83	79	82	44	110	102	64	68	47	21	97	28
33	48	80	60	102	128	27	75	36	118	120	94
95	53	29	75	102	92	17	58	29	22	159	33
29	90	20	88	104	98	57	55	58	26	41	49
69	71	30	73	98	94	27	25	55		142	33
78	46	64	93	83	75	18	17	57		120	57
63	47	54	89	97	60	21	54	56		44	29
38	79	36	89	156	107	64	46	35		60	52
34	87	64	123	129	81	67	27	51		65	
76	83	44	57	149	76	78	37	21		63	
17	125	33	89	125	57	24	37	74		78	
23	81	51	104	111	116	84	39	55		76	
65	80	87	46	69	130	62	34	24		71	
21	52	90	90	99	138	26	20	23		37	
64	30	89	79	76	65	17	55	60		45	
77	41	64	54	112	97	24	22	37		37	
36	68	86	47	130	94	24	56	39		28	
57.33333333	72.61904762	63.85714286	74.28571429	110.1904762	94.52380952	42.66666667	45.04761905	40	44.25	80.42857143	49.33333333

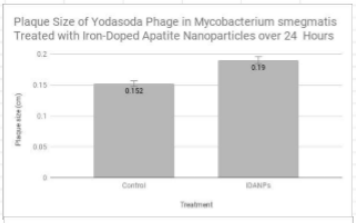

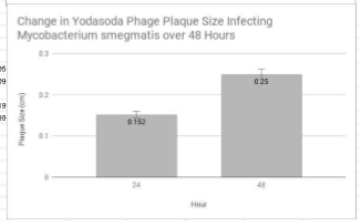

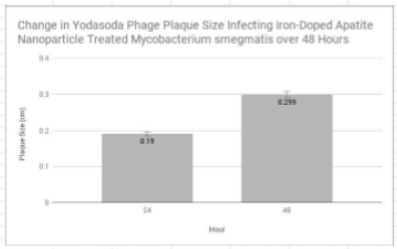

percent increase	0.573684211
	0.109
NP	
24	0.19
48	0.299

0.283490966	0.2709677419	0.2557377049	0.2832167832	0.4168865435	0.3008849558	0.192073707	0.2367491166	0.2261146497	0.1207865169	0.379501385	0.1298549708
0.246100919	0.3	0.2459016393	0.2832167832	0.1978891821	0.2064896755	0.119902439	0.1448763251	0.07324840764	0.1179775281	0.2908587258	0.1900584795
0.2211838006	0.3516129032	0.3344262295	0.2167832168	0.3192612137	0.2743362832	0.08536585366	0.1908127208	0.1942675159	0.08707865169	0.3296398892	0.2376023392
0.1931464174	0.2548387097	0.2721311475	0.1258741259	0.2849604222	0.3185840708	0.1981707317	0.2084805654	0.1687898089	0.143258427	0.1246537396	0.1081871345
0.2585669782	0.2548387097	0.268852459	0.1538461538	0.290237467	0.3008849558	0.1951219512	0.2402826855	0.1496815287	0.05898876404	0.2686980609	0.08187134503
0.1028037383	0.1548387097	0.262295082	0.2097902098	0.2691292876	0.3775811209	0.08231707317	0.2650176678	0.1146496815	0.3314606742	0.3324099723	0.2748538012
0.2959501558	0.1709677419	0.09508196721	0.2622377622	0.2691292876	0.2713864307	0.05182926829	0.2049469965	0.0923566879	0.06179775281	0.4404432133	0.09649122807
0.09034267913	0.2903225806	0.06557377049	0.3076923077	0.2744063325	0.2600855457	0.1737804878	0.1943462898	0.1847133758	0.07303370787	0.1135734072	0.1432748538
0.214953271	0.2290322581	0.09836065574	0.2552447552	0.2585751979	0.2772861357	0.08231707317	0.08833922261	0.178343949		0.3933518006	0.09649122807
0.2479906542	0.1483870968	0.2098360656	0.3251748252	0.2189973615	0.2212389381	0.05487804878	0.06007067138	0.1615286624		0.3324099723	0.1666666667
0.1962616822	0.1516129032	0.1770491803	0.3111888112	0.2559366755	0.1769911504	0.06402439024	0.1908127208	0.178343949		0.1218836565	0.08479532164
0.1183800623	0.2548387097	0.1180327869	0.3111888112	0.4116094987	0.3156342183	0.1951219512	0.1625441696	0.1114649682		0.1662049861	0.1520467836
0.1059190031	0.2806451613	0.2098360656	0.4300699301	0.3403693931	0.2369380531	0.2042682927	0.09540636042	0.1624203822		0.1800554017	
0.2367601246	0.2677419355	0.1442622951	0.1993006993	0.3931398417	0.2241857906	0.237804878	0.1307420495	0.06687898089		0.1745152355	
0.08299950166	0.4032258065	0.1081967213	0.3111888112	0.3298153034	0.1681415929	0.07317073171	0.1307420495	0.2356687898		0.216066482	
0.07165109034	0.2612903226	0.1672131148	0.2636363636	0.2928759894	0.3480825959	0.256097561	0.1379061873	0.1751592357		0.2105263158	
0.2024922118	0.2580645161	0.2852459016	0.1608391608	0.1820580475	0.383480826	0.1890243902	0.1201413428	0.07643312102		0.1966759003	
0.06542056075	0.1677419355	0.2950819672	0.2146853147	0.2612137203	0.407079646	0.07926829268	0.07067137809	0.07324840764		0.1024930748	
0.199376947	0.09677419355	0.2918032787	0.2762237762	0.2005277045	0.191740413	0.05182926829	0.1943462898	0.1910828025		0.1246537396	
0.2398753894	0.1322580645	0.2098360656	0.1888111888	0.2955145119	0.2861356932	0.07317073171	0.0777385159	0.1178343949		0.1024930748	
0.1121495327	0.2193548387	0.2819672131	0.1643356643	0.3430079156	0.2772861357	0.07317073171	0.1978798587	0.1242038217		0.07756232687	
0.1786085151	0.2342549923	0.2093768815	0.2597402597	0.2907400427	0.2788312965	0.1300813008	0.1591788659	0.1464968153		0.2227938267	

NP 1	NP 2	NP1 day 2	NP2 day 2	NPC1	NPC2	NPC1 day 2	NPC2 Day 2		F	h
1 cm = 333	1 cm = 321	1 cm = 341	1 cm = 315	1 cm = 358	1 cm = 319	1 cm = 341	1 cm = 356			1
71	67	145	142	73	75	125	117			
93	44	115	131	65	67	49	125			
82	46	76	107	23	51	105	114			
62	53	117	96	39	66	124	143			
51	46	63	99	75	49	61	123			
72	50	94	102	64	27	91	99			
46	34	85	86	57	31	127	132			
51	54	123	104	36	46	92	136			
72	68	91	121	66	47	104	132			
57	41	91	107	80	28	133	123			
48	60	118	101	25	65	102	137			
94	55	112	94	30	57	137	142			
79	64	82	112	69	92	118	124			
66	63	57	142	57	59	10	135			
25	67	89	90	52	43	106	123			
53	66	92	100	67	35	94	118			
23	91	105	97	85	39	85	138			
66	55	102	120	69	44	122	148			
83	30	95	120	50	46	143	100			
30	45	109	120	65	56	24	86			
41	53	128	147	36	81	91	158			
56	59	109	112	38	62	75	109			
42	41	90	143	42	59	53	109			
33	51	86	110	72	30	109	84			
48	65	83	96	47	44	71	91			
51	51	105	123	81	54					
57	99	134	83	46	69					
56	120	127	109	61	61					
59	71	81	99	107	52					
57	60	86	85	65	52					
44	56	137	75	39	30					
60	85	109	99	110	85					
66	52		36	128	65					
60	68		80	67	34					
73	74		83	44	42					
59	101		98	66	34					
60	63		141	60	70					
33	88		116	35	38					
24	79		114	29	44					
89	83		85	100						
102	68		112	35						
75	93		96	35				Control	0.152	
57	57		109	30				IDANPs	0.19	
30	49		131	30						
42	73		121	75					-0,038	
53	52		56	35				Percent higher N	-0,2	
79	49			26						
72	78			27						p
47	26			23						
52	57			25						h
95	57			27						
52	59			35						
61	53									
59	56									
19	24									
14	50									
30	66									
74										
56.98275862	61.14035088	101.125	105.2391304	54.28846154	52.02564103	93.32	121.84			
0,2132132132	0,2087227414	0,4252199413	0,4507936508	0,2039106145	0,2351097179	0,366568915	0,3286516854			
0,2792792793	0,1370716511	0,3372434018	0,4158730159	0,1815642458	0,219031348	0,1173020528	0,3511235955			
0,2462462462	0,1433021807	0,2228739003	0,3396825397	0,06424581006	0,1598746082	0,3079178886	0,3202247191			
0,1861861862	0,1651090343	0,3431085044	0,3047619048	0,1089385475	0,2068965517	0,3636363636	0,4016853933			
0,1531531532	0,1433021807	0,1847507331	0,3142857143	0,2094972067	0,1536050157	0,1788856305	0,345505618			
0,2162162162	0,1557632399	0,275659824	0,3238095238	0,1787709497	0,08463949843	0,2668621701	0,2780898876			
0,1381381381	0,1059190031	0,2492668622	0,273015873	0,1592178771	0,06717668339	0,3724340176	0,3707865169			
0,1531531532	0,1682242991	0,3607038123	0,3301587302	0,1005586592	0,144200627	0,2697947214	0,3820224719			
0,2162162162	0,2118380062	0,2668621701	0,3841269841	0,1843575419	0,1473354232	0,3049853372	0,3707865169			
0,1711711712	0,127258567	0,2668621701	0,3396825397	0,2234636872	0,0877429467	0,3900293255	0,345505618			
0,1441441441	0,1869158879	0,3460410557	0,3206349206	0,06983240223	0,2037617555	0,2991202346	0,3848314607			
0,2822822823	0,1713395639	0,3284457478	0,2854126984	0,06379888268	0,1786333856	0,4017595308	0,3988764045			
0,2372372372	0,199376947	0,2404692082	0,3555555556	0,1927374302	0,2884012539	0,3466410557	0,3483146067			
0,1981981982	0,1962616822	0,1671554252	0,4507936508	0,1592178771	0,1849529781	0,2932551132	0,3792134831			
0,2750750751	0,2087227414	0,2609970674	0,2857142857	0,1452513966	0,1347962382	0,3108504399	0,345505618			
0,1591591592	0,2056074766	0,2697947214	0,3174603175	0,187150838	0,1097178683	0,279658624	0,3314606742			
0,2690690691	0,2834890966	0,3079178886	0,3079365079	0,2374301676	0,1222570533	0,2492668622	0,3876404494			
0,1981981982	0,1713395639	0,2991202346	0,380952381	0,1927374302	0,1379310345	0,357771261	0,4157303371			
0,2492492492	0,09345794393	0,2785923754	0,380952381	0,1396648045	0,144200627	0,4193548387	0,2808988764			
0,09009009009	0,1401869159	0,3196480938	0,380952381	0,1815642458	0,1755485893	0,07038123167	0,2415730337			
0,1231231231	0,1651090343	0,3753665689	0,4666666667	0,1005586592	0,2539184953	0,2668621701	0,4438202247			
0,1681681682	0,1838006231	0,3196480938	0,3555555556	0,1061452514	0,1943573668	0,219941349	0,3061797753			
0,1261261261	0,127258567	0,2639296188	0,453968254	0,1173184358	0,1849529781	0,1554252199	0,3061797753			
0,0990990991	0,1588785047	0,2521994135	0,3492063492	0,2011173184	0,09404388715	0,293255132	0,2359550562			
0,1441441441	0,2024922118	0,2434017595	0,3047619048	0,1312849162	0,1379310345	0,2082111437	0,2556179775			
0,1531531532	0,1588785047	0,3079178886	0,3904761905	0,2262569832	0,1692789969					
0,1711711712	0,308411215	0,3929618768	0,2634920635	0,1284916201	0,2163009404					
0,1681681682	0,3738317757	0,3724340176	0,3174603175	0,1703910615	0,1912225705					
0,1771771772	0,2211838006	0,2375366569	0,3142857143	0,2988826816	0,1630094044					
0,1711711712	0,1869158879	0,2521994135	0,2698412698	0,1815642458	0,1630094044					
0,1321321321	0,1744548287	0,4017595308	0,2380952381	0,1089385475	0,09404388715					
0,1801801802	0,2647975078	0,3196480938	0,3142857143	0,3072625698	0,2684576803					
0,1981981982	0,1619937695		0,1142857143	0,3575418994	0,2037617555					
0,1801801802	0,2118380062		0,253968254	0,187150838	0,1065830721					
0,2192192192	0,230529595		0,2634920635	0,1229050279	0,131661442					
0,1771771772	0,3146417445		0,3111111111	0,1843575419	0,1065830721					
0,1801801802	0,1962616822		0,4476190476	0,1675977654	0,2194357367					
0,0990990991	0,2741433022		0,3682539683	0,09776536313	0,1191222571					
0,07207207207	0,246105919		0,3619047619	0,08100558659	0,1379310345					
0,2672672673	0,2585669782		0,2698412698	0,2793296089						
0,3063063063	0,2118380062		0,3555555556	0,09776536313						
0,2252252252	0,2897196262		0,3047619048	0,09776536313						
0,1711711712	0,1775700935		0,346031746	0,08379888268						
0,0900900901	0,1526479751		0,4158730159	0,08379888268						
0,1261261261	0,2274143302		0,3841269841	0,2094972067						
0,1591591592	0,1619937695		0,1777777778	0,09776536313						
0,2372372372	0,1526479751			0,07262569832						
0,2162162162	0,2429906542			0,07541899441						
0,1411411411	0,08099688474			0,06424581006						
0,1561561562	0,1775700935			0,06983240223						
0,2852852853	0,1775700935			0,07541899441						
0,1561561562	0,1838006231			0,09776536313						
0,1831831832	0,1651090343									
0,1771771772	0,1744548287									
0,06705705706	0,07476635514									
0,04204204204	0,1557632399									
0,0900900900	0,2056074766									
0,2222222222										

APPENDIX E

PART 5 RAW DATA

Table 24

Raw Data of S. *aureus Cell Growth (CFU) in MM++ and With IDANPs Over Three-hour Period*

		M9	NP		30 minutes	1hr	2hr	3hr
	30 min	3,000,000.00	6,000,000.00		3,000,000.00	3,000,000.00	4,000,000.00	3,000,000.00
	30 min	3,000,000.00	2,000,000.00		3,000,000.00	3,000,000.00	4,000,000.00	4,000,000.00
	30 min	0	0		0	6,000,000.00	3,000,000.00	4,000,000.00
	1 hr	3,000,000.00	7,000,000.00	M9	2,000,000.00	4,000,000.00	3,666,666.67	3,666,666.67
	1 hr	3,000,000.00	5,000,000.00		6,000,000.00	7,000,000.00	3,000,000.00	4,000,000.00
	1 hr	6,000,000.00	9,000,000.00		2,000,000.00	5,000,000.00	2,000,000.00	2,000,000.00
	2 hr	4,000,000.00	3,000,000.00		0	9,000,000.00	1,000,000.00	6,000,000.00
	2 hr	4,000,000.00	2,000,000.00	NP	2,666,666.67	7,000,000.00	2,000,000.00	4,000,000.00
	2 hr	3,000,000.00	1,000,000.00					
	3 hr	3,000,000.00	4,000,000.00		30 minutes	1hr	2hr	3hr
	3 hr	4,000,000.00	2,000,000.00	M9	2.67E+06	4.00E+06	3.67E+06	3.67E+06
	3 hr	4,000,000.00	6,000,000.00	NP	2.67E+06	7.00E+06	2.00E+06	4.00E+06
		3.33E+06	3.92E+06					1.22E+06
		-4	-4					
		comparing times... no difference						
		p=0.295	p=0.083					

Table 25

Raw Data of Cell Growth (CFU) of S. *aureus in 3hr Culture in MM++ With Iron Treatments and IDANPs*

		NP	M9		
	Control	1212120	909000	4,000,000.00	3,000,000.00
	Control	606000	1212100	2,000,000.00	4,000,000.00
	Control	1818100	1212100	6,000,000.00	4,000,000.00
	0.5low	100000	400000		
	0.5low	200000	300000		
	0.5low	200000	500000		
	low	200000	300000		
	low	200000	200000		
	low	300000	100000		
	medium	0	0		
	medium	0	100000		
	medium	100000	100000		
	high	100000	200000		
	high	0	0		
	high	0	0		
	veryhigh	400000	200000		
	veryhigh	200000	100000		
	veryhigh	300000	0		

		NP	M9
half low	0.0004g/L	1.67E+05	4.00E+05
low	0.0008g/L	2.33E+05	2.00E+05
medium	0.0016g/L	3.33E+04	6.67E+04
high	0.0032g/L	3.33E+04	6.67E+04
very high	0.0064g/L	3.33E+04	1.00E+05

Table 26
Raw Data of Cell Growth (CFU) of S. aureus *In Different Iron Treatments Overnight*

TSB	2300000000
TSB	2600000000
Control	3000000000
Control	2600000000
Control	3400000000
0.5low	3200000000
0.5low	2800000000
0.5low	4400000000
low	2200000000
low	4300000000
low	3300000000
medium	1900000000
medium	3200000000
medium	2100000000
high	1500000000
high	1200000000
high	1300000000
veryhigh	1100000000
veryhigh	1600000000
veryhigh	1600000000

TSB	2.45E+09
Control	3.00E+09
0.0004g/L	3.47E+09
0.0008g/L	3.27E+09
0.0016g/L	2.40E+09
0.0032g/L	1.33E+09
0.0064g/L	1.43E+09